





**AVE SARAPUU**

Electrochemical reduction of oxygen  
on quinone-modified carbon electrodes  
and on thin films of platinum and gold



TARTU UNIVERSITY  
PRESS

Institute of Chemistry, University of Tartu, Estonia

Dissertation in Colloid and Environmental Chemistry

Dissertation is accepted for the commencement of the degree of Doctor of Philosophy in Chemistry on April 24, 2008 by the Doctoral Committee of the Institute of Chemistry, University of Tartu.

Doctoral advisor: Dr. Kaido Tammeveski, Institute of Chemistry, University of Tartu.

Opponent: Prof. Elisabet Ahlberg, Department of Chemistry, Göteborg University, Sweden.

Commencement: 15<sup>00</sup> June 18, 2008 in Tartu, 18 Ülikooli Str., room 204.

ISSN 1406–0299

ISBN 978–9949–11–876–2 (trükis)

ISBN 978–9949–11–877–9 (PDF)

Autoriõigus Ave Sarapuu, 2008

Tartu Ülikooli Kirjastus

[www.tyk.ee](http://www.tyk.ee)

Tellimus nr 184

# TABLE OF CONTENTS

1. LIST OF ORIGINAL PUBLICATIONS .....	6
2. ABBREVIATIONS AND SYMBOLS .....	7
3. INTRODUCTION .....	9
4. LITERATURE OVERVIEW .....	10
4.1. The general scheme of oxygen reduction .....	10
4.2. Oxygen reduction on carbon materials and on quinone-modified electrodes .....	11
4.3. Oxygen reduction on gold electrodes .....	15
4.4. Oxygen reduction on platinum electrodes .....	18
5. EXPERIMENTAL .....	22
6. RESULTS AND DISCUSSION .....	23
6.1 Oxygen reduction on quinone-modified carbon electrodes .....	23
6.1.1. Preparation and characterization of quinone-modified electrodes .....	23
6.1.2. Oxygen reduction on AQ-modified glassy carbon electrodes .....	24
6.1.3. Oxygen reduction on AQ- and PQ-modified BDD and HOPG electrodes .....	29
6.2. Oxygen reduction on nanostructured Au electrodes .....	32
6.2.1. Surface morphology of thin Au films .....	32
6.2.2. Cyclic voltammetry of thin Au films .....	33
6.2.3. Oxygen reduction on thin Au films in 0.5 M H <sub>2</sub> SO <sub>4</sub> .....	33
6.2.4. Oxygen reduction on thin Au films in 0.1 M KOH .....	37
6.3. Oxygen reduction on nanostructured Pt electrodes .....	39
6.3.1. Surface morphology of thin Pt films .....	40
6.3.2. Cyclic voltammetry of thin Pt films .....	40
6.3.3. Oxygen reduction on thin Pt films .....	41
7. SUMMARY .....	49
8. REFERENCES .....	51
9. SUMMARY IN ESTONIAN .....	58
10. ACKNOWLEDGEMENTS .....	60
11. PUBLICATIONS .....	61

## I. LIST OF ORIGINAL PUBLICATIONS

- I** A. Sarapuu, K. Vaik, D.J. Schiffrin, K. Tammeveski, Electrochemical reduction of oxygen on anthraquinone-modified glassy carbon electrodes in alkaline solution, *Journal of Electroanalytical Chemistry* 541 (2003) 23–29.
- II** A. Sarapuu, K. Helstein, D.J. Schiffrin, K. Tammeveski, Kinetics of Oxygen Reduction on Quinone-Modified HOPG and BDD Electrodes in Alkaline Solution, *Electrochemical and Solid State Letters* 8 (2005) E30–E33.
- III** A. Sarapuu, K. Tammeveski, T.T. Tenno, V. Sammelselg, K. Kontturi, D.J. Schiffrin, Electrochemical reduction of oxygen on thin-film Au electrodes in acid solution, *Electrochemistry Communications* 3 (2001) 446–450.
- IV** A. Sarapuu, M. Nurmik, H. Mändar, A. Rosental, T. Laaksonen, K. Kontturi, D.J. Schiffrin, K. Tammeveski, Electrochemical reduction of oxygen on nanostructured gold electrodes, *Journal of Electroanalytical Chemistry* 612 (2008) 78–86.
- V** A. Sarapuu, A. Kasikov, T. Laaksonen, K. Kontturi, K. Tammeveski, Electrochemical reduction of oxygen on thin-film Pt electrodes in acid solutions, *Electrochimica Acta* (2008, in press) (doi:10.1016/j.electacta.2008.04.003).
- VI** A. Sarapuu, A. Kasikov, L. Matisen, K. Tammeveski, Electroreduction of oxygen on gold-supported thin Pt films in acid solutions, *Journal of Electroanalytical Chemistry*, submitted (JELECHEM-D-08-00120)

### Author's contribution

The author has performed all electrochemical measurements and calculations for [I–III,V,VI] and participated in [IV]. The author is responsible for the interpretations and writing the papers [I,II,IV–VI] and participated in [III].

## 2. ABBREVIATIONS AND SYMBOLS

$A$	geometric surface area of an electrode
AFM	atomic force microscopy
AQ	9,10-anthraquinone
$A_r$	real surface area of the catalyst
AuNPs	gold nanoparticles
BDD	boron-doped diamond
$c_{O_2}^b$	concentration of oxygen in the bulk solution
CV	cyclic voltammetry
$d$	particle diameter
$D_{O_2}$	diffusion coefficient of oxygen
DFT	density functional theory
$E$	electrode potential
$E^0$	standard potential
$E_{(i)}^0$	standard potential of surface Q/Q <sup>2-</sup> couple
$E_{Q/Q^{2-}}^0$	standard potential of surface Q/Q <sup>2-</sup> couple
$E_{1/2}$	half-wave potential
EC	electrochemical-chemical
EC-NMR	electrochemical nuclear magnetic resonance
$E_f$	redox potential
$F$	Faraday constant
GC	glassy carbon
GIXRD	glancing incidence angle X-ray diffraction
$h$	nominal film thickness
HOPG	highly oriented pyrolytic graphite
$I$	current
$I_D$	disk current
$I_k$	kinetic current
$I_R$	ring current
$j$	current density
$j_{dl}$	diffusion-limited current density
$j_k$	kinetic current density
$k$	heterogeneous electron transfer rate constant
$k^{0'}$	the apparent electrochemical rate constant for O <sub>2</sub> reduction
$k_c$	rate constant of the reaction between quinone radical anion and O <sub>2</sub>
$k_i$	rate constant of the reaction between quinone radical anion and O <sub>2</sub>

$k_i \Gamma_i$	chemical rate parameter
K-L	Koutecky-Levich
MA	mass activity
MEA	membrane-electrode assembly
MWCNTs	multi-walled carbon nanotubes
$N$	collection efficiency
$n$	number of electrons transferred per O <sub>2</sub> molecule
ORR	oxygen reduction reaction
PQ	9,10-phenanthrenequinone
PtNPs	platinum nanoparticles
Q	quinone
$R$	universal gas constant
r.d.s.	rate-determining step
RDE	rotating disk electrode
RRDE	rotating ring-disk electrode
SA	specific activity
SCE	saturated calomel electrode
SHE	standard hydrogen electrode
$T$	temperature
TEM	transmission electron microscopy
$v$	potential scan rate
XAS	X-ray absorption spectroscopy
XPS	X-ray photoelectron spectroscopy
$\alpha$	transfer coefficient
$\Gamma_i$	surface concentration of quinone species
$\Gamma_Q$	surface concentration of quinone species
$\Delta E_{(i)}$	difference between the standard potentials of the Q <sup>•-</sup> /Q <sup>2-</sup> and Q/Q <sup>•-</sup> couples
$\nu$	kinematic viscosity of the solution
$\Phi$	percentage of peroxide formation on the disk
$\omega$	electrode rotation rate



### 3. INTRODUCTION

The oxygen reduction reaction (ORR) is an important process in fuel cells and other electrochemical technologies and its kinetics has been widely studied [1–4]. The reaction proceeds either as a four-electron process or a two-electron process, depending on the electrode material as well as on the reaction conditions, such as the solution pH [1–3]. Platinum has been the electrode material of choice for fuel cells, as it supports the four-electron reduction of  $O_2$  at relatively low overpotentials [1–3], but its high cost has led to researches for other catalytically active materials. Still, for the low-temperature fuel cells the platinum group metals and alloys have displayed the best characteristics and using these catalysts in a highly dispersed form on high surface area carbon support allows to reduce the loading of this costly metal. However, it has been found that the electrocatalytic properties of nanoparticles can differ from those of the bulk metal and the catalyst activity may decrease as the particle size decreases down to a few nanometres, thus counterbalancing the effect of reducing the metal loading by decreasing the particle size [5]. The particle size effect and the adsorption of reduction intermediates and spectator species are the key issues of the electrocatalysis of  $O_2$  reduction on platinum [2,6].

Gold has long been regarded as an inactive metal, however, in the last decade gold nanoparticles have gained attention for unique catalytic properties for several reactions, such as low temperature CO oxidation [7]. Therefore, it is of particular importance to study the particle size effect of gold for  $O_2$  reduction.

Hydrogen peroxide is produced commercially *via* a chemical route using the anthraquinone process [8]. Alternatively, peroxide can be generated by electrochemical reduction of oxygen, employing electrocatalysts that support only two-electron reduction of oxygen, such as carbon materials [2]. Their low cost and high surface area makes them suitable for commercial applications. The carbon surface can be easily modified, for example, by grafting with quinones, thereby further enhancing its electrocatalytic activity for oxygen reduction. Electrochemical generation of peroxide has several advantages over the chemical route [9].

In the present work, oxygen reduction has been studied on various electrocatalysts. 9,10-anthraquinone (AQ) [I,II] and 9,10-phenanthrenequinone (PQ) [II] have been grafted onto glassy carbon (GC) [I], boron-doped diamond (BDD) [II] and highly-oriented pyrolytic graphite (HOPG) [II] surface and the kinetic parameters of oxygen reduction have been determined. In the second part of the work, thin gold films have been prepared by vacuum evaporation onto the GC electrodes and the dependence of the oxygen reduction kinetics on the film thickness has been studied in acidic and alkaline solution [III, IV]. In the third part, thin platinum films on GC [V] and gold substrates [VI] were prepared by the same method and the kinetic parameters of oxygen reduction as a function of the film thickness were determined in  $HClO_4$  and  $H_2SO_4$  solutions.

## 4. LITERATURE OVERVIEW

### 4.1. The general scheme of oxygen reduction

The oxygen reduction reaction (ORR) is a multielectron reaction that involves a number of elementary steps and various reaction intermediates. The reaction proceeds by either a direct four-electron pathway, where the final product is water:



or by two-electron pathway yielding hydrogen peroxide:



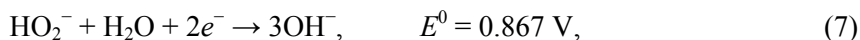
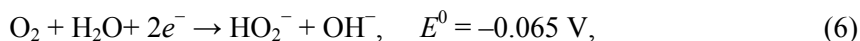
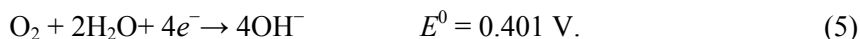
Peroxide can be further reduced:



or catalytically decomposed (disproportionated):

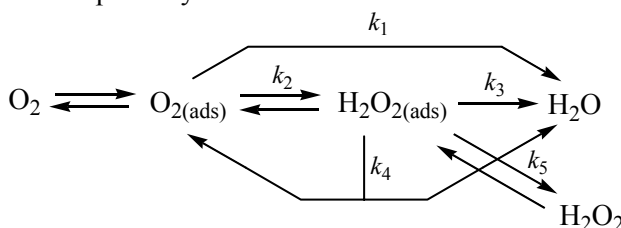


In alkaline solution, the corresponding reactions are:



[1–4].

The simplified reaction pathway is shown in Scheme 1.

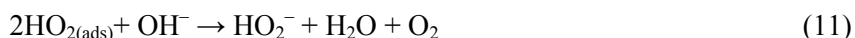
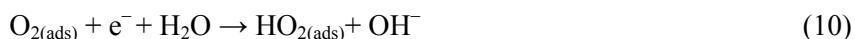


**Scheme 1.** Simplified mechanism of oxygen reduction in acid solutions. The rate constants for the different steps in the scheme are indicated in the figure ( $k_i$ ). (ads) denotes the species in their adsorbed state.

Despite the apparent simplicity, these overall reactions represent a complex electrocatalytic network and involve many elementary steps. The dominating pathway depends on several factors, for example, on the electrode material, solution pH and on electrode potential [1,4].

## 4.2. Oxygen reduction on carbon materials and on quinone-modified electrodes

Oxygen reduction on carbon materials has been extensively investigated [2–4,9–22], because it is a cheap and widely available support for the other, more expensive catalysts such as Pt. In alkaline solution, the high surface area carbon itself is a rather active catalyst for ORR [9]. However, there is still no general agreement on the ORR mechanism on carbon surfaces and several mechanisms have been proposed [10–19]. For example, Morcos and Yeager suggested a mechanistic scheme where the reduction of adsorbed  $O_2$  (Reaction (10)) is the rate-determining step (r.d.s), which is followed by disproportionation [10]:



Xu et al. have considered the following pathway [16]:



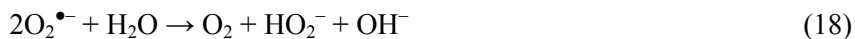
or



They proposed that adsorption of  $O_2^{\bullet-}$  on a carbon surface makes this species more basic and therefore accelerates its protonation (Reaction (13)), which is the rate determining step at  $pH > 12$ . At  $pH < 10$ , the first electron transfer (Reaction (12)) becomes rate-determining. At lower pH, adsorbed  $HO_2^{\bullet}$  blocks the adsorption centres of  $O_2$  and the reduction proceeds by the outer sphere route.

The electrocatalytic properties of bulk carbon materials are highly dependent on their structure. Glassy carbon (GC) and graphite are rather active catalysts for ORR, but on boron doped diamond (BDD) and on the basal plane of highly oriented pyrolytic graphite (HOPG) this process is extremely inhibited also in alkaline solution. Tryk et al. have studied the reduction of  $O_2$  on these materials and suggested that there are two distinct types of reduction processes [19]. In the first process, the first electron transfer (Reaction (12)) is rate-determining. The second process is considered to be electrocatalytically mediated by the quinone radical anions that are formed from the native quinone-type functionalities on carbon surface at certain potentials [12]:





or



where Q is the surface quinone species. Reaction (17) has been proposed as the r.d.s. [12]. At more negative potentials, the quinone radical anions are reduced to dianions (Reaction (20)) that are not electrocatalytically active towards  $O_2$  reduction:



The native quinone functionalities are present on GC surface, but their surface concentration is very low on BDD and on basal plane of HOPG. This explains why the pre-wave of  $O_2$  reduction is observed on GC, but not on BDD and HOPG and three orders of magnitude larger electron transfer rate constants for  $O_2$  reduction on GC [19]. Depending on the  $E^0$  values for Reactions (16) and (20), there is a small range of potentials where the surface concentration of semiquinone is high and this leads to a peak shape for  $O_2$  reduction  $I$ - $E$  curve. The more positive the redox potential of surface quinones the lower the  $O_2$  reduction overpotential would be.

To improve the catalytic activity of carbon electrodes towards  $O_2$  reduction, the surface pre-treatment by electrochemical and chemical oxidation has been employed [14–16,20]. Pre-treatment may increase the electrode roughness and number of active sites and it can introduce more oxygen-containing (quinone-type) functional groups, serving as mediators [16,20]. Oxidised carbon surfaces may also catalyse the further reduction of hydrogen peroxide in alkaline solutions [14,16,20].

The electrocatalytic activity of carbon electrodes towards  $O_2$  reduction can be further increased by surface modification with quinones [3,11,12,20–39]. Several methods have been proposed for attaching the quinones on carbon. For instance, adsorptive attachment provides an easy preparation procedure for the study of the kinetics of  $O_2$  reduction [3,11,12,24–27,33–36]. A disadvantage of this modification method is that quinones tend to desorb from the surface during long-term operation, especially in alkaline solutions [25,34]. An alternative strategy is to attach the quinones covalently to the surface [12,21,23,29,30–32,37–39]. The most convenient method for the covalent modification of carbon electrodes was developed by Allongue et al. and this is based on the electrochemical reduction of diazonium salts [40]. In the first step the aryl diazonium cation ( $R-N_2^+$ ) is electrochemically reduced yielding an aryl radical ( $R^\bullet$ ):



In the second step the radical reacts with a carbon surface and a strong covalent (C–C) bond is formed:



This procedure has been employed for the modification of the electrodes with quinones [21,29,30,38]. Besides carbon materials the electrografting by diazonium reduction can be used for the covalent modification of metals and semiconductors with aryl group [41]. An advantage of the diazonium reduction method is that it can be carried out in an aprotic media as well as in aqueous acidic solutions. Alternatively, the covalent modification can be achieved by anodic oxidation of carboxylate substituents [31,37].

The reduction of oxygen on quinone-modified carbon surfaces has been extensively investigated [3,11,20,21–39]. The reaction is believed to follow the mechanism of electrocatalytic redox mediation *via* semiquinones (Reactions (16–19)). The reduction rate is proportional to the surface concentration of the semiquinone radical formed by the electrochemical reduction of quinone groups [21]. Various quinones have been employed: 9,10-phenanthrenequinone (PQ) [12,29,36,38], 1,2-naphthoquinone [36], 1,4-naphthoquinone and its derivatives [3,11,23,24,27,32,33] and most frequently, 9,10-anthraquinone (AQ) and its derivatives [11,12,21,25,26,34–38,42–45]. The main factor determining the O<sub>2</sub> reduction activity of a surface-confined quinone is its redox potential, but it is also influenced by the rate constant of the reaction between the semiquinone and O<sub>2</sub> [29]. For instance, the redox potential of PQ in 0.1 M KOH is about 300 mV more positive than that of AQ and therefore, the PQ modified electrode has considerably higher electrocatalytic activity towards O<sub>2</sub> reduction than AQ-modified electrode [29]. The standard potentials of the reduction of quinones to corresponding neutral semiquinones and quinols have been found using the quantum chemical calculations and the results obtained were in a good agreement with experimental data [46]. Introducing the substituents into the quinone molecule may stabilise the semiquinone radical intermediate and therefore, increase the activity of the quinone towards O<sub>2</sub> reduction [30].

The O<sub>2</sub> reduction activity of quinone-modified electrodes has been found to significantly depend on the solution pH [24,26,38,45]. It has been shown that the protonated semiquinones that prevail at low pH (pH < pK<sub>a</sub> of the protonation equilibrium of the semiquinone radical anion) are much less reactive than the radical anion at high pH [24,45]. This observation has also been rationalised by the results of quantum chemical calculations [47].

It is of special importance to determine the intrinsic catalytic activity of surface-bound quinones for the reduction of oxygen. On quinone-modified GC electrodes, both the native quinone groups and attached AQ are electrocatalytically active towards O<sub>2</sub> reduction and give their contribution to overall reaction. To analyse the *I-E* curves of the O<sub>2</sub> reduction of quinone-modified electrodes, a surface redox catalytic cycle model has been proposed [21]. According to this model, O<sub>2</sub> reduction proceeds in parallel on three different surface sites: at native quinone groups on the substrate, at surface-confined AQ and at a heterogeneous electrode surface. The kinetic parameters of O<sub>2</sub> reduction were found by non-linear regression analysis of the *I-E* curves [21].

The model clearly shows that it is possible to control the electrocatalytic properties of the surface in two ways: by controlling the quinone redox potential with appropriate substituents and by altering the reactivity of the radical intermediate towards oxygen [21]. A further proof for the validity of this model is provided by Kullapere et al. by studying the reduction of O<sub>2</sub> on a mixed film of AQ and phenyl groups on GC [48]. The current peak related to the native quinone groups on GC was absent on this modified electrode and it was attributed to blocking effect of the attached phenyl groups. The values of the kinetic parameters related to surface-bound AQ were in a good agreement with those determined for GC/AQ electrodes [I].

The rate constant of the reaction between O<sub>2</sub> and quinone radical anion ( $k_c$ ) has been shown to depend on the nature of the quinone, however, the variation between the different quinones is not very large. For instance, the  $k_c$  values calculated for PQ and AQ on GC were similar [38]. The values of  $k_c$  for sulfur-containing derivatives of anthraquinone in 0.1 M KOH [30] were of the same order of magnitude as that of AQ [I]. It has been shown that the  $k_c$  value may also depend on the electrode substrate, for instance, four times higher value of  $k_c$  was found for PQ-modified edge plane pyrolytic graphite, as compared to GC/PQ electrode at pH = 10 [35].

It is expected that the protonation of the semiquinone results in a decrease in the rate constant of the chemical step of over four orders of magnitude, as predicted by quantum chemical calculations for pH  $\ll$  pK<sub>a</sub> (pK<sub>a</sub> of the protonation equilibrium of the quinone radical anion) [47]. This is supported by experimental data: for GC/AQ and GC/PQ electrodes the  $k_c$  value considerably decreases with decreasing pH and is less than  $1 \times 10^8 \text{ cm}^3 \text{ mol}^{-1} \text{ s}^{-1}$  for pH < 8. Complete inactivation of quinones is expected in acidic solution [47]. However, the reports by Compton and co-workers show that quinones retain considerable activity even at low pH. At pH = 3, the  $k_c$  values for 1,2-dihydroxyanthraquinone between  $2.1 \times 10^6$  and  $2.2 \times 10^7 \text{ cm}^3 \text{ mol}^{-1} \text{ s}^{-1}$  depending on the surface coverage were obtained [26]. In addition, very high  $k_c$  value has been found at pH = 2.5 for AQ covalently attached to multi-walled carbon nanotubes (MWCNTs) ( $k_c = 8.6 \times 10^8 \text{ cm}^3 \text{ mol}^{-1} \text{ s}^{-1}$ ) [49]. For AQs-incorporated clay modified electrodes [43] and carbon paste electrodes [42], the optimum pH for O<sub>2</sub> reduction has been found close to neutral.

Due to the native oxygen-containing groups on the GC surface, this material is rather active towards oxygen reduction in alkaline solution and it may be difficult to distinguish between the contributions of surface-bound quinone and native quinone groups. As compared to GC, the oxygen reduction overpotential on bare BDD [50,19] and HOPG [10,15,16,19] electrodes in alkaline solution is considerably higher. Therefore, using these materials as electrode substrates enables one to observe the effect of the quinone directly and to determine the kinetic parameters more precisely.

### 4.3. Oxygen reduction on gold electrodes

Gold is a rather inactive electrocatalyst for ORR in acid media and a two-electron reduction of oxygen takes place on Au electrodes, the first electron transfer being the r.d.s. [51–56]. In alkaline solutions, the electrocatalytic activity of Au for O<sub>2</sub> reduction is considerably higher and this reaction has been extensively studied on polycrystalline gold electrodes [57–62] as well as on single crystal surfaces [56,63–70]. Considerable efforts have been directed at establishing the oxygen reduction mechanism on gold [56,58,62–76]. In both acid and alkaline solutions the reaction has been found to be structure sensitive. In acid solutions, the order of activity increases in the sequence: Au(111) < Au(110) < Au(100) [1,53,56]. In alkaline solution, Au(100) has much higher activity than the other low-index surfaces [63,64] and it has been reported to be even more active than polycrystalline Pt [1], however, the reason for this effect still remains unclear. On the Au(111) and Au(110) plane at low overpotentials, hydrogen peroxide is the main product of O<sub>2</sub> reduction, but Au(100) supports its further reduction to OH<sup>−</sup> in a limited potential region at low overpotentials [63–70]. McIntyre and Peck attributed the activity of Au(100) for 4e<sup>−</sup> reduction to its four-fold symmetry and the transfer to 2e<sup>−</sup> reduction at more negative potentials to the reconstruction of the Au surface to “hex” surface with hexagonal overlayer, which is likely to behave similarly to the Au(111) surface [76]. However, it was confirmed later using *in-situ* X-ray diffraction that the reconstruction cannot be the dominant mechanism for the change of reaction pathway [70]. Another explanation that was given to the unique catalytic properties of Au(100) is related to its four-fold symmetry that is suitable for a strong chemisorption of OH<sup>−</sup> in this potential region, which in turn enables the dissociative adsorption of O<sub>2</sub> [63,69,70]. Studies of the stepped Au surfaces have shown that the surfaces vicinal to Au(100) support the 4e<sup>−</sup> reduction only if they are composed of very long (100) oriented terraces [53]. At elevated temperatures, significantly more peroxide is further reduced to H<sub>2</sub>O on all crystal faces [65]. The O<sub>2</sub> reduction pathway can also be influenced by adsorbed inert species. For instance, oxygen reduction on fullerene-modified gold electrodes produces hydrogen peroxide selectively [77].

More recently, the role of adsorbed OH in the exceptional activity of Au(100) has been disputed, as the OH adsorption takes place also on the other crystal faces and the reaction order for OH<sup>−</sup> is close to zero, which indicates that OH<sup>−</sup> is not involved in the reaction mechanism. The 4e<sup>−</sup> reduction pathway on the Au(100) electrode was attributed to adsorbed HO<sub>2</sub><sup>−</sup> that has a specific interaction with the Au(100) but not with the other crystal faces. At potentials negative to the potential of zero charge it desorbs from the surface and the reduction proceeds by 2e<sup>−</sup> route [67]. The presence of adsorbed HO<sub>2</sub><sup>−</sup> on Au in certain potential range in alkaline solution was confirmed by surface enhanced infrared reflection-absorption spectroscopy. It was proposed that in acid solution, protonation of HO<sub>2</sub><sup>−</sup> is fast and H<sub>2</sub>O<sub>2</sub> diffuses into the solution, therefore,

the  $2e^-$  mechanism prevails [73]. An alternative hypothesis has been recently proposed that on the Au(100) surface the peroxide is further decomposed by disproportionation process catalysed by base [74]. The role of interaction between OOH and Au(*hkl*) surface in determining O<sub>2</sub> reduction activity and pathway has also been emphasised by the recent quantum chemical calculations [75].

In the last decade Au nanoparticles (AuNPs) have received an increasing attention, especially for unique catalytic properties for low temperature CO oxidation [7]. During the last five years, several authors have also studied O<sub>2</sub> reduction on AuNPs supported on bulk carbon materials, such as glassy carbon [78–87], highly oriented pyrolytic graphite [86,87] and boron-doped diamond [88–92]. Various methods have been used to prepare the nanostructured gold electrodes and thin Au films, for example vacuum evaporation and sputter deposition [71,89–91,93], attachment of colloidal Au nanoparticles on self-assembled monolayers [94,95] and most often, electrodeposition [82–88,92]. The morphology, particle size and also the crystallographic orientation of the electrodeposited AuNPs are markedly influenced by the nature of the underlying substrate as well as by the electrodeposition conditions [85,87]. It is particularly attractive to attach AuNPs to carbon nanotubes, as these hybrid materials have shown excellent electrocatalytic properties for O<sub>2</sub> reduction in 0.5 M H<sub>2</sub>SO<sub>4</sub> [96].

The electrocatalytic activity of nanostructured Au electrodes for O<sub>2</sub> reduction can differ from that of the bulk polycrystalline gold. El-Deab et al. observed increased ORR activity and enhanced further reduction of H<sub>2</sub>O<sub>2</sub> on AuNPs electrodeposited on Au electrodes as compared with bulk gold in acid solution, which was attributed to the enrichment of Au surface by steps [97,98]. The same authors also found that the oxygen reduction wave at a Au/GC electrode prepared by electrodeposition in the presence of cysteine showed a positive shift compared to that for bare polycrystalline Au [85]. The increased ORR activity has also been observed on AuNPs deposited on a BDD support as compared to bulk gold [88–91]. Previous works have mainly employed relatively large Au particles, with particle diameter  $d > 15$  nm [85,88–90,97,98]. Only Yagi et al. have studied smaller Au particles ( $d > 2$  nm), which have displayed a positive shift of the O<sub>2</sub> reduction potential and increased current efficiency for the  $4e^-$  reduction. Heat treatment improved the electrocatalytic activity of the electrodes, probably due to the shape change and the thermal facetting of the particles [91]. However, the specific activity of O<sub>2</sub> reduction for the Au catalyst has not been determined in these works [85,88–91,97,98]; therefore, no conclusions about the particle size effect can be made. A moderate increase in O<sub>2</sub> reduction specific activity has been observed for Cu particles coated by Au. This was attributed to particulate, nano-sized nature of the catalyst, however, the size of the particles was 200–300 nm, which is too large for true particle size effect [99].



By contrast, a rapid decrease of the O<sub>2</sub> reduction specific activity with decreasing Au particle size for particle diameters below ~3.0 nm has recently been observed by Guerin et al. for vacuum deposited Au thin films in acid media. They carried out a combinatorial study using an electrode array that allowed simultaneously obtain 19 data points with different Au particle dimensions, the rotating disk electrode (RDE) experiments were performed for comparison purposes. The loss in activity at small Au centers was observed on both TiO<sub>x</sub> and carbon substrates. As a result, the maximum in the mass normalised catalyst activity was at around 3 nm particle size [100].

The structure sensitivity of the ORR on gold in alkaline solutions is more evident than in acid media and this reaction has been used as an indirect means for characterising the crystallographic orientation of nanostructured Au electrodes [78,79,83,84,86,87]. El-Deab et al. have studied O<sub>2</sub> reduction in 0.1 M KOH on AuNPs with different distribution of surface sites prepared by electrodeposition on GC and/or HOPG in the presence of L-cysteine or I<sup>-</sup> as additives. The Au nanostructures prepared in the presence of cysteine were enriched in the Au(100) orientation and supported 4e<sup>-</sup> reduction of O<sub>2</sub> at low overpotentials [84,86,87]. The presence of I<sup>-</sup> at the electrodeposition decreases the size of Au particles formed [86]. For HOPG substrate, the electro-oxidative pre-treatment resulted in deposition of smaller Au particles with increased O<sub>2</sub> reduction activity, as compared to the AuNPs electrodeposited onto the untreated HOPG substrate [86]. However, the particle size effect cannot be evaluated in these works, as the electroactive Au surface area has not been determined.

The effect of particle surface structure has also been investigated by Hernandez et al., who synthesized AuNPs using the water-in-oil microemulsion method in the presence of I<sup>-</sup> or S<sup>2-</sup> as additives. The rotating ring-disk electrode (RRDE) studies of O<sub>2</sub> reduction revealed a high number of electrons ( $n = 3.5$ ) transferred per O<sub>2</sub> molecule at low overpotentials. The nanoparticles synthesized at the presence of I<sup>-</sup> had the highest ratio of Au(100) crystal facets and the highest electrocatalytic activity towards O<sub>2</sub> reduction [78]. They have also prepared gold nanorods with only (111) and (110) surface domains [79] and cubic Au nanoparticles with high amount of (100) sites [80] and showed that at low overpotentials, the nanorods catalyse 2e<sup>-</sup> reduction and cubic AuNPs 4e<sup>-</sup> reduction of O<sub>2</sub>.

There are many reports on the unique catalytic activity of Au nanoparticles for various reactions, as reviewed by Meyer et al. [7]. Their exceptional activity towards CO oxidation has been attributed to increased adsorption strength of CO and oxygen at low coordinated Au atoms at the particle edges and corners, as shown by DFT calculations [101]. The binding energy of O<sub>2</sub> and reaction intermediates with the metal catalyst also displays an important role in O<sub>2</sub> electroreduction; therefore, the particle size effect is expected for this reaction.

## 4.4. Oxygen reduction on platinum electrodes

The electrochemical reduction of oxygen on platinum in acid media has been extensively investigated, as it finds application in the fuel cell technology [1,2]. The structure sensitivity of the ORR on Pt(*hkl*) surfaces is well established and is due to the structure sensitive adsorption of spectator species, such as OH<sub>ads</sub> [102], HSO<sub>4(ads)</sub> [103], Cl<sub>ads</sub> [104], Br<sub>ads</sub> [105], and H<sub>upd</sub> [103]. For example, in H<sub>2</sub>SO<sub>4</sub> solution the ORR activity increases in the sequence Pt(111) < Pt(100) < Pt(110) [103,106–108]. Very strong inhibition of the ORR has been found on Pt(111) and it has been attributed to strong adsorption of the (bi)sulfate anions because of the symmetry match between geometries of the Pt(111) face and oxygen atoms of the sulfate anion [103,108]. The adsorbed anions apparently block the centres for initial O<sub>2</sub> adsorption, therefore hindering the ORR, but the reaction pathway is not affected, as no H<sub>2</sub>O<sub>2</sub> is produced in the kinetically controlled potential region [108]. In the solution of HClO<sub>4</sub> where no strongly adsorbing anions are present, the activity of Pt single crystal faces for ORR increases in the sequence Pt(100) < Pt(111) < Pt(110) [102,106,107]. In this solution, the oxygen reduction kinetics is affected by the adsorption of oxygen-containing species (OH<sub>ads</sub>). The ORR is most strongly inhibited by OH<sub>ads</sub> on Pt(100), which is possibly related to high affinity of Pt(100) sites for the adsorption of oxygen-containing species that block the centres of O<sub>2</sub> adsorption. More recently, it has been found that in addition to the site blocking effect, the adsorbed OH and sulfate ions have a strong negative electronic effect on the kinetics of the ORR on Pt(111). The change of the coverage of OH<sub>ad</sub> in the mixed kinetic-diffusion controlled region has been suggested as the reason why the apparent Tafel slope deviates from its intrinsic value in HClO<sub>4</sub> but not in H<sub>2</sub>SO<sub>4</sub> [109].

Considerable efforts have been directed towards improving the catalyst efficiency of energy conversion and lowering the content of costly Pt in electrocatalysts [110]. In practical electrodes, Pt nanoparticles (PtNPs) dispersed on high surface area carbon supports are used, but it has been found that if the size of these particles is in the range of a few nanometres, their electrocatalytic properties can differ from those of the bulk polycrystalline platinum [5]. To evaluate these size effects, numerous investigations have been carried out using PtNPs supported on porous carbon [111–127]. As the testing of membrane-electrode assemblies (MEAs) in fuel cells is often complicated, an alternative technique was developed on the basis of the RDE method, where the supported catalyst is deposited onto a GC disk and can be readily tested in an ordinary electrochemical cell [128]. This method was complicated by a strong diffusion resistance of O<sub>2</sub> through the Nafion film and mathematical modelling was necessary to extract the kinetic parameters [129]. By attaching the catalyst layer to the GC support via an only sub-micrometer thick Nafion film placed on top of the dried catalyst layer, Schmidt et al. [130] were able to minimize the film diffusion resistance and to determine the kinetic current densities directly from

the RDE data. Later this method was also applied in the RRDE configuration [131].

Thin Pt films on flat carbon substrates consisting of small Pt islands can also be regarded as a model system for studying the particle size effects, therefore, the ORR on the vacuum-evaporated thin Pt films on glassy carbon [132] and on sputter-deposited thin films on graphite [133] has been studied. The model catalyst approach has also been used for the study of electrocatalytic properties of Pt/GC electrodes for O<sub>2</sub> reduction in alkaline solution [134].

Despite the numerous researches on Pt particle size effects, the results are still contradictory. In most of these studies, a decrease in the catalytic activity of oxygen reduction with decreasing the particle size has been observed [112–124,132,135]. However, some authors have found no effect of particle size on the kinetics of O<sub>2</sub> reduction [111,125,126]. For example, recent EC-NMR studies have indicated that the difference in the surface electronic properties of the PtNPs of different sizes is negligible and therefore, the ORR activity is independent of particle size [126]. Watanabe et al. proposed that the O<sub>2</sub> reduction activity depends on the intercrystallite distances, not on crystallite sizes [125], but this hypothesis was opposed by Giordano et al. [116]. The recent studies on the uniform arrays of Pt particles of the same size have also shown that ORR activity is independent of the interparticle spacing [136]. However, it was shown very recently using the planar model Pt/GC electrodes with low Pt loading that the mass transport effects depend on Pt loading and may affect the ORR activity and increase H<sub>2</sub>O<sub>2</sub> production [137].

The particle-size effect has been attributed to the geometric factors, associated with the distribution of the crystal facets on the particle surface [138], or to the change in the electronic structure of smaller particles that increases the adsorption energy of oxygenated species [124,132,139]. Kinoshita has modelled the changes in the surface fraction of Pt atoms on the (100) and (111) crystal facets, edges and corners as the particle size decreases, and found that the ORR activity decreases at the PtNPs ( $d < 6$  nm) where the fraction of (111) facets on the surface grows rapidly. The maximum of mass activity (MA) should appear at about 3.5 nm grain size for cubo-octahedral Pt particles [138]. This prediction has found experimental evidence [114,115]. In accordance with that, the cubic PtNPs with Pt(100) surface orientation showed higher O<sub>2</sub> reduction activity in H<sub>2</sub>SO<sub>4</sub> solution than polycrystalline Pt particles [140,141]. It has also been noted that Pt surface oxide reduction wave shifts to lower potentials as the particle size decreases, which led to the suggestion that the origin of the size effect is associated with the stronger adsorption of oxygenated intermediate species on the smaller particles that inhibits O<sub>2</sub> reduction [114,123,124]. Stronger adsorption of OH on smaller PtNPs has been confirmed by *in situ* XAS investigation [139]. The results obtained on Pt stepped surfaces in H<sub>2</sub>SO<sub>4</sub> and HClO<sub>4</sub> have suggested stronger adsorption of OH on step sites, as compared to the terraces [142,143]. Decreased O<sub>2</sub> reduction activity of carbon-supported PtNPs in sulfuric acid solutions as compared to the electrolytes

containing only non-adsorbing ions has also been noted [117,118,131]. Chen and Kucernak have studied and modelled the electrochemical reduction of oxygen on single submicrometer-sized Pt particles and found that in addition to the site-blocking, anion adsorption may change the potential near the inner Helmholtz plane and thereby change the effective driving potential for reactants and intermediates [144]. Furthermore, the particle size dependent double-layer effects may affect the O<sub>2</sub> reduction kinetics [144].

Another promising way to further reduce the Pt content in ORR electrocatalysts without losing activity involves using Pt alloys with other metals or very thin Pt layers supported on metal nanoparticles [145,146]. In such bimetallic systems, the activity of Pt can be changed through electronic and/or geometric effects [145–147]. Enhanced O<sub>2</sub> reduction activity has been found in many Pt-M bimetallic systems as compared to pure Pt, for example, on Pt-M alloy nanoparticles where M = V, Cr, Fe, Co, Ni [148]; on Pt<sub>3</sub>M surfaces where M = Ni, Co, Fe, Ti, V [149], on Pt monolayers on Pd [146], etc.

Due to its inertness, gold is the metal of choice to be used in combination with Pt. There are several reports on O<sub>2</sub> reduction studies for Pt catalysts supported on various forms of gold: bulk polycrystalline Au [150–153], Au(111) monocrystal [154–157], Au nanoparticles [156,158,159] and Au sputtered onto BDD [160]. Platinum-plated nanoporous gold has shown good performance and stability in MEAs [161]. Bare gold is a much less active electrocatalyst than platinum for ORR in acid media [53,54]. However, in some cases it has been found that the activity of Au-supported Pt is higher than that of Pt. Van Brussel et al. have studied O<sub>2</sub> reduction on polycrystalline gold electrodes modified by Pt and noted that the electrocatalytic activity of the electrodes was lower than that of the bulk Pt electrode in the negative potential scan, but significantly higher in the positive scan [150,151]. Desic et al. have also found that in the high current density region, Au–Pt electrodes showed higher O<sub>2</sub> reduction activities than pure platinum [152]. On the other hand, Pt monolayer [154,155,157] and Pt islands [154] on Au(111) appeared to be less active than bulk Pt. The activity of Au/Pt core-shell nanoparticles increased with increasing the thickness of Pt shell [159]. In addition, O<sub>2</sub> reduction has been studied on Pt-Au alloy nanoparticles and their catalytic activity increased with increasing the Pt content in alloy in acid media [162,163]. The activity of Pt-Au alloy nanoparticles also depends on the preparation method and may be almost equal to the activity of Pt particles [164]. It was recently demonstrated that modifying PtNPs with Au clusters considerably stabilises these during prolonged potential cycling [165].

The change of the Pt reactivity in the Pt-Au bimetallic systems has also been a subject of theoretical modelling. The calculations have indicated that the oxygen reduction activity of transition metal catalysts is primarily determined by changes in the oxygen binding energy [166]. The ORR electrocatalytic activity of platinum monolayers supported on other metal monocrystals shows a volcano-type dependence on the d-band centre of the platinum monolayer

structures [155]. The differences in the electrocatalytic activity of Pt-Au systems as compared to pure Pt have been attributed to expansive strain of Pt overlayer on Au(111) that increases the metal d-band centre energy and leads to stronger binding of OH [157]. More recently, it was shown by DFT calculations that the adsorption energy of oxygenated intermediates depends also on the electron density near the Fermi level, for instance, Pt pseudomorphic overlayer on Au(111) binds both O and OH more strongly than Pt(111) [167]. Adsorbed OH on Pt is known to inhibit the ORR by site blocking and electronic effects [105,109,124].

The history and prospects for Pt-alloy cathode catalysts have been reviewed by Gasteiger et al. They have pointed out that the reports on the catalytic activity of platinum-based catalysts for the ORR are contradictory and have provided the benchmark oxygen reduction activities to establish the relative merit of candidate catalysts by using two different testing procedures [110]. Mayrhofer et al. have emphasised the significance of the respective experimental parameters for obtaining reliable data and have given some guidelines for the RDE measurements and for the determination of the specific activity of O<sub>2</sub> reduction [168]. These aspects are very important for the development of new electrocatalysts for oxygen reduction to improve the performance of low temperature fuel cells.

## 5. EXPERIMENTAL

GC, BDD, Au and Pt electrodes employed for RDE experiments were prepared by mounting the disks into Teflon holders. The RRDE experiments were carried out on a GC disk-Pt ring electrode, Au disk-Pt ring electrode or GC disk-Au ring electrode (Pine Instruments). The surface of the GC and BDD electrodes was polished to a mirror finish with 1.0 and 0.3  $\mu\text{m}$  alumina slurries (Buehler); the bulk Pt and Au electrodes were finished by polishing with 0.05  $\mu\text{m}$  alumina slurry. The HOPG disks were mounted in a special holder and the fresh surface was prepared prior to each measurement by removing the top layers with adhesive tape.

The covalent attachment of quinones was performed in acetonitrile (Riedel-de Haën) containing 0.1 M tetrabutylammonium tetrafluoroborate, TBABF<sub>4</sub> (Fluka) and 1 mM of the Fast Red AL Salt (Acros Organics) or diazonium tetrafluoroborates of AQ or PQ that were synthesized according to a published procedure [169]. The electrografting by AQ was also performed in 0.05 M H<sub>2</sub>SO<sub>4</sub> containing 10 mM of Fast Red AL Salt.

Thin films of Pt and Au with a nominal thickness ( $h$ ) of 0.25 to 20 nm were prepared by electron beam evaporation or vacuum evaporation. For TEM studies, the Au and Pt films were evaporated onto formvar/carbon-coated copper grids and examined using a Tecnai 12 instrument operated at 120 kV accelerating voltage. The freshly prepared Au thin films were coated with a 0.5  $\mu\text{m}$  thick Nafion film by applying a droplet of 0.5% Nafion solution (Aldrich) in ethanol on the electrode surface and allowing the solvent to evaporate in air.

The electrolyte solutions for studying O<sub>2</sub> reduction were prepared from 70% HClO<sub>4</sub> (Suprapur, Merck) or 96% H<sub>2</sub>SO<sub>4</sub> (Suprapur, Merck) or KOH pellets (AristaR, BDH or pro analysi, Merck) in Milli-Q water; these were saturated with O<sub>2</sub> (99.999%, AGA or 99.95%, AGA) or deaerated with Ar gas (99.999%, AGA). An EDI101 rotator and a CTV101 speed control unit (Radiometer, Copenhagen) were used for the RDE experiments. A Pine Instrument Company AFMSRX rotator and MSRX speed controller were used for the RRDE measurements. A saturated calomel electrode (SCE) was employed as a reference and all the potentials are referred to this electrode. The counter electrode compartment of the three-electrode cell was separated from the main cell compartment by a glass frit and Pt wire served as a counter electrode. The potential was applied with an Autolab potentiostat PGSTAT10 or PGSTAT30 (Eco Chemie B.V., The Netherlands) and the experiments were controlled with General Purpose Electrochemical System (GPES) software. All experiments were carried out at room temperature ( $23 \pm 1^\circ\text{C}$ ).

## **6. RESULTS AND DISCUSSION**

### **6.1. Oxygen reduction on quinone-modified carbon electrodes**

The electrochemical reduction of oxygen reduction was studied on glassy carbon electrodes modified with AQ at various surface concentrations [I] and on HOPG and BDD electrodes modified with AQ and PQ [II].

#### **6.1.1. Preparation and characterization of quinone-modified electrodes**

The carbon electrodes were covalently modified with AQ or PQ, using the electrochemical reduction of the corresponding diazonium salts [21]. The first sweep between 0.65 and  $-0.45$  V showed a high reduction current peak, but very small currents were observed during the second sweep, indicating that the first sweep ensured almost complete monolayer coverage. In order to achieve surface coverages less than a monolayer, a single scan was made and the potential was reversed at less negative values (Figure 1). For comparison purposes, grafting of GC by AQ was also made from an aqueous acidic solution of the AQ diazonium salt.

The stability of covalently attached quinones was characterised by cycling the electrodes 100 times between 0 and  $-1.25$  V in Ar-saturated 0.1 M KOH. The peak current decreased significantly during the initial stages of cycling, indicating desorption of non-covalently attached quinone molecules. Figure 2 shows typical stable cyclic voltammetric responses of GC/AQ electrodes with different surface coverages. The peaks in the voltammograms correspond to the quinone/hydroquinone couple. The surface concentration of quinone ( $\Gamma_0$ ) was determined by the charge integration under the CV peaks of surface-confined quinones.

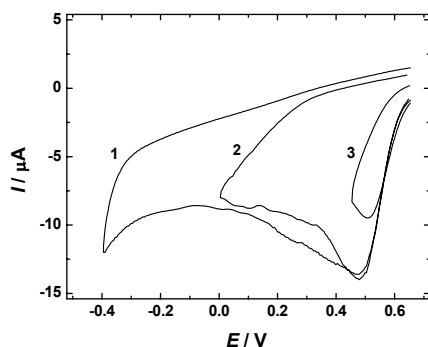


**Figure 1.** Electrochemical grafting of GC with anthraquinone in Ar-saturated acetonitrile containing 1 mM Fast Red AL and 0.1 M TBABF<sub>4</sub>;  $\nu = 50 \text{ mV s}^{-1}$ . Resulting surface concentrations of AQ: (1)  $4.3 \times 10^{-10} \text{ mol cm}^{-2}$ ; (2)  $3.0 \times 10^{-10} \text{ mol cm}^{-2}$ ; (3)  $7.8 \times 10^{-11} \text{ mol cm}^{-2}$ .

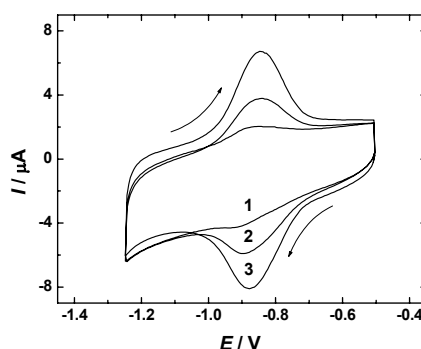
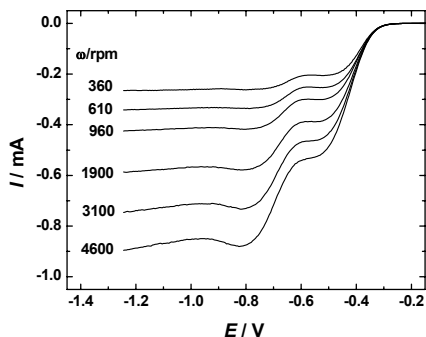


**Figure 2.** Cyclic voltammograms for GC/AQ electrodes in Ar saturated 0.1 M KOH for different surface concentrations  $\Gamma_Q$ : (1)  $5.2 \times 10^{-11}$ ; (2)  $2.3 \times 10^{-10}$ ; (3)  $4.3 \times 10^{-10} \text{ mol cm}^{-2}$ .  $\nu = 50 \text{ mV s}^{-1}$ ,  $A = 0.196 \text{ cm}^2$ .

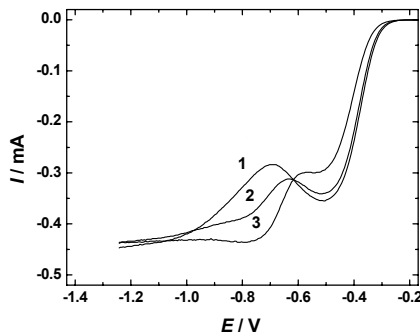
### 6.1.2. Oxygen reduction on AQ-modified glassy carbon electrodes

Figure 3 shows the RDE results for a GC/AQ electrode with  $\Gamma_Q = 2.3 \times 10^{-10} \text{ mol cm}^{-2}$  at different rotation rates. These results are very similar to those previously obtained [21]. Typical oxygen reduction polarisation curves for various AQ surface concentrations are shown in Figure 4 and the results are compared with those for an unmodified GC electrode. For the latter and for the GC/AQ electrodes at low surface coverage a current maximum at *ca*  $-0.5 \text{ V}$  was observed. It has been proposed that at the prewave potentials, oxygen reduction is mediated by semiquinone radicals (Reactions (16–19)) existing on the native GC surface [12,21] and that the surface concentration of semiquinone follows the same potential dependence as the oxygen reduction current [21]. It is notable though (Figure 4), that the pre-wave current is lower for higher surface concentrations of attached AQ, indicating that it is partially blocking the native GC surface sites and therefore suppressing the rate of O<sub>2</sub> reduction at the pre-wave. The chemical nature of these native groups is unclear at present, but these are very good electrocatalysts for oxygen reduction in alkaline solution.





**Figure 3.** RDE voltammetry curves for oxygen reduction in  $O_2$  saturated 0.1 M KOH on a GC/AQ electrode ( $\Gamma_Q = 2.3 \times 10^{-10} \text{ mol cm}^{-2}$ ) at various rotation rates.  $\nu = 20 \text{ mV s}^{-1}$ ,  $A = 0.196 \text{ cm}^2$ .



**Figure 4.** RDE voltammetry curves for oxygen reduction in  $O_2$  saturated 0.1 M KOH on: (1) GC; (2) GC/AQ,  $\Gamma_Q = 7.3 \times 10^{-11} \text{ mol cm}^{-2}$ ; (3) GC/AQ,  $\Gamma_Q = 4.3 \times 10^{-10} \text{ mol cm}^{-2}$ ;  $\nu = 20 \text{ mV s}^{-1}$ ;  $\omega = 960 \text{ rpm}$ ,  $A = 0.196 \text{ cm}^2$ .

At potentials  $E < -0.7 \text{ V}$  oxygen reduction occurs at a heterogeneous electrode surface and therefore the current increases again on a bare GC electrode. The GC/AQ electrodes show a sharp current increase at much more positive potentials, clearly indicating the strong electrocatalytic effect of surface-bound AQ on  $O_2$  reduction. A higher value of  $\Gamma_Q$  causes a sharper current increase close to its diffusion limited value, supporting the assumption that at those potentials the reduction involves the reaction of oxygen with the AQ semiquinone intermediate.

The kinetic parameters of  $O_2$  reduction as a function of AQ surface concentration have been calculated following the surface redox-catalytic cycle model previously proposed [21]. According to this model,  $O_2$  reduction at functionalised GC electrodes proceeds in parallel on two different surface sites, at surface quinone groups (either native or covalently attached) and at the heterogeneous electrode surface. In this model, the current density is given by:

$$\frac{1}{j} = \frac{1}{j_{dl}} - \frac{1}{2Fc_{O_2}^b k^0 e^{-f\alpha(E-E^0)} + \sum_i \frac{2Fc_{O_2}^b k_i \Gamma_i}{1 + e^{f(E-E_{(i)}^0)} e^{(f/2)\Delta E_{(i)}} + e^{-f(E-E_{(i)}^0)} e^{(f/2)\Delta E_{(i)}}}} \quad (23)$$

where  $i = 1$  corresponds to properties of the quinone groups on native GC and  $i = 2$  to those of the attached quinone.  $j_{dl}$  is the diffusionally controlled limiting current density;  $k^0$  is the apparent electrochemical rate constant on the free carbon surface;  $\alpha$  is the transfer coefficient for  $O_2$  reduction on the free GC surface;  $E^0$  is the standard potential of the  $O_2/HO_2^-$  couple ( $-0.065 \text{ V}$  vs. SHE);  $k_i$  is the rate constant for the Reaction (17);  $\Gamma_i$  is the surface concentration of the quinone species;  $E_{(i)}^0$  is the standard potential of surface  $Q/Q^{2-}$  couples;  $\Delta E_{(i)}$  is

the difference between the standard potentials of the  $Q^{\bullet-}/Q^{2-}$  and the  $Q/Q^{\bullet-}$  couples;  $c_{O_2}^b$  is the concentration of oxygen in the bulk ( $1.2 \times 10^{-6}$  mol cm<sup>-3</sup>) [170],  $F$  is the Faraday constant and  $f = F/RT$ .

The rate of the chemical reaction between the semiquinones formed on native GC and molecular oxygen is proportional to the product  $k_1 \Gamma_1$ . Unfortunately, for the bare GC electrodes no clearly defined voltammetric peak was observed on the CV curves recorded in Ar saturated 0.1 M KOH and therefore, it was not possible to determine the surface concentration of native quinones ( $\Gamma_1$ ). For GC/AQ electrodes, the covalently attached anthraquinone molecules act as electrocatalytic sites and the rate of the chemical reaction between  $AQ^{\bullet-}$  and  $O_2$  is given by  $k_2 \Gamma_2 c_{O_2}$ . The increase in current at potentials more negative than  $-0.75$  V was modelled according to the Butler-Volmer formalism [21]. Although the surface is heterogeneous, a single average value of  $k^{0'}$  and  $\alpha$  was used to represent electron transfer reactions occurring on a distribution of surface sites on the native GC surface that become available for electron transfer in this potential region. This is a simple device for parameterising a reaction occurring at multiple sites. The purpose of the present work is not to analyse this potential region but to investigate the kinetics at the quinone centres.

The kinetic parameters for oxygen reduction were calculated by the non-linear regression (NLR) analysis of the current-potential curves at different rotation rates [21]. The values of the diffusion-limited current densities used were calculated from the Koutecky-Levich plots of  $O_2$  reduction and these were fixed during the analysis. Some dependence of the values of the parameters on rotation rate was observed and the averages obtained are listed in Table 1. There was a slight tendency for  $E_{(1)}^0$  to decrease with increasing AQ surface concentration. As previously observed this is most probably related to a change in the adsorption conditions on native GC quinone-type sites, which is due to the influence of AQ attached onto neighbouring sites. The value of  $E_{(2)}^0 = -0.88 \pm 0.01$  V should be independent of  $\Gamma_Q$ , as it is indeed observed, if there is no interaction between the AQ molecules present on the surface. The value of  $E_{(2)}^0$  is very close to the average redox potential ( $E_f$ ) of the GC/AQ electrode in oxygen-free 0.1 M KOH. For instance, for  $\Gamma_Q = 2.3 \times 10^{-10}$  mol cm<sup>-2</sup>,  $E_f = -0.867$  V. This value compares well with that previously determined of  $E_f = -0.860$  V, measured at the same sweep rate [21]. The values of  $\alpha$  ( $\alpha = 0.19 \pm 0.01$ ),  $\Delta E_{(1)}$  ( $\Delta E_{(1)} = -0.23 \pm 0.02$  V) and  $\Delta E_{(2)}$  ( $\Delta E_{(2)} = -0.34 \pm 0.03$  V) showed no dependence on  $\Gamma_Q$ . The values of these kinetic parameters at different coverages are very similar to those previously obtained for  $\Gamma_Q = 2.5 \times 10^{-10}$  mol cm<sup>-2</sup> [21].

**Table 1.** Average values of kinetic parameters for O<sub>2</sub> reduction on AQ-modified GC electrodes as a function of anthraquinone surface concentration  $\Gamma_Q$ . The parameters were calculated by non-linear regression analysis. The O<sub>2</sub> reduction measurements were carried out in 0.1 M KOH.

$10^{10} \times \Gamma_Q$ (mol cm <sup>-2</sup> )	$E_{(1)}^0$ (V)	$E_{(2)}^0$ (V)	$10^4 k^{0s}$ (cm s <sup>-1</sup> )	$\alpha$	$\Delta E_{(1)}$ (V)	$\Delta E_{(2)}$ (V)	$k_1 \Gamma_1$ (cm s <sup>-1</sup> )	$k_2 \Gamma_2$ (cm s <sup>-1</sup> )
0	-0.516 ± 0.004		(7.2 ± 1.9)	0.18 ± 0.01	-0.192 ± 0.004		0.025 ± 0.001	
0.52	-0.53 ± 0.01	-0.875 ± 0.012	(5.0 ± 2.6)	0.19 ± 0.02	-0.21 ± 0.01	-0.37 ± 0.01	0.028 ± 0.002	0.037 ± 0.001
0.73	-0.53 ± 0.01	-0.874 ± 0.013	(4.6 ± 2.5)	0.2 ± 0.03	-0.22 ± 0.01	-0.36 ± 0.02	0.027 ± 0.002	0.040 ± 0.001
1.9	-0.57 ± 0.02	-0.860 ± 0.006	(4.0 ± 2)	0.19 ± 0.02	-0.27 ± 0.02	-0.29 ± 0.01	0.011 ± 0.002	0.072 ± 0.004
2.3	-0.55 ± 0.02	-0.877 ± 0.006	(3.3 ± 1.8)	0.2 ± 0.02	-0.23 ± 0.01	-0.35 ± 0.02	0.019 ± 0.002	0.12 ± 0.01
3	-0.57 ± 0.02	-0.882 ± 0.003	(3.5 ± 2)	0.19 ± 0.02	-0.26 ± 0.02	-0.34 ± 0.03	0.014 ± 0.002	0.13 ± 0.01
3.7	-0.55 ± 0.02	-0.890 ± 0.006	(3.5 ± 2)	0.19 ± 0.01	-0.22 ± 0.02	-0.38 ± 0.03	0.018 ± 0.003	0.14 ± 0.03
4.3	-0.55 ± 0.02	-0.876 ± 0.009	(3.6 ± 2.2)	0.21 ± 0.02	-0.22 ± 0.02	-0.32 ± 0.05	0.018 ± 0.002	0.24 ± 0.02
2.2*	-0.57 ± 0.01	-0.909 ± 0.008	(2.8 ± 1.1)	0.18 ± 0.01	-0.26 ± 0.02	-0.39 ± 0.01	0.008 ± 0.002	0.071 ± 0.003

\* This GC/AQ electrode was modified in an aqueous solution of Fast Red AL Salt.

The constancy of  $\alpha$  indicates that the free GC surface responsible for the reduction following the equivalent of an activated electron transfer step is unaffected by coverage. Also, the constancy of  $\Delta E_{(1)}$  and  $\Delta E_{(2)}$  indicates that the thermodynamic properties of the semiquinone of the grafted AQ are independent of coverage in the range investigated. Although there is some scatter in the data, the rate constant  $k^{0s}$  decreased with increasing  $\Gamma_Q$  and this is most likely due to a site-blocking effect of AQ. There was only a slight tendency for the parameter of  $k_1 \Gamma_1$  to decrease at higher surface concentrations of AQ. Its decrease is expected since the number of native quinone sites on GC should decrease with increasing surface coverage.

The most notable dependence on AQ surface coverage was observed for the chemical rate parameter  $k_2 \Gamma_2$ . According to the proposed EC mechanism (Reactions (16) and (17)) the rate of O<sub>2</sub> reduction is limited by the chemical step when the rate of electron transfer to surface-confined AQ is fast. Therefore, the reduction rate should increase at higher AQ surface concentrations as can be seen in Figure 4. Importantly, the calculated parameter  $k_2 \Gamma_2$  was linearly dependent on  $\Gamma_Q$ , as shown in Figure 5. From the slope of this graph, a value for the rate constant  $k_2 = (4.7 \pm 0.3) \times 10^8 \text{ cm}^3 \text{ mol}^{-1} \text{ s}^{-1}$  was found.

A comparison between surfaces functionalised in aqueous solution and acetonitrile indicated that the conditions under which the electrode was grafted did not affect the properties of the electroactive groups, as both GC/AQ electrodes gave similar responses and there was no significant difference in the kinetic parameters obtained using the NLR analysis. It can be concluded that the grafting procedure is very robust.

The reduction of O<sub>2</sub> on AQ-modified electrodes was also studied using the RRDE method. The percentage of peroxide formation on the disk ( $\Phi$ ) was calculated from [131]:

$$\Phi = \frac{200I_R/N}{I_D + I_R/N} \quad (24)$$

where  $I_R$  and  $I_D$  are the ring and disk currents and  $N$  is the collection efficiency. The percentage yields of H<sub>2</sub>O<sub>2</sub> were in the range from 95 to 100% for all the GC/AQ electrodes studied, showing that O<sub>2</sub> reduction proceeds entirely by a 2-electron pathway (Figure 6). This is in agreement with the results obtained from the analysis of the RDE data using the Koutecky-Levich (K-L) equation:

$$\frac{1}{j} = \frac{1}{j_k} + \frac{1}{j_{dl}} = -\frac{1}{nFkc_{O_2}^b} - \frac{1}{0.62nFD_{O_2}^{2/3}\nu^{-1/6}c_{O_2}^b\omega^{1/2}} \quad (25)$$

where  $j_k$  and  $j_{dl}$  are the kinetic and diffusion-limited current densities, respectively,  $k$  is the rate constant for O<sub>2</sub> reduction,  $D_{O_2}$  is the diffusion coefficient of oxygen ( $1.9 \times 10^{-5} \text{ cm}^2 \text{ s}^{-1}$ ) [170],  $c_{O_2}^b$  is the concentration of oxygen in the bulk ( $1.2 \times 10^{-6} \text{ mol cm}^{-3}$ ) [170] and  $\nu$  is the kinematic viscosity of the solution ( $0.01 \text{ cm}^2 \text{ s}^{-1}$ ) [171].

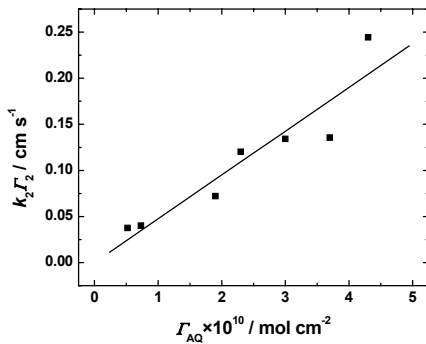


**Figure 5.** Dependence of the calculated chemical rate parameter  $k_2\Gamma_2$  on AQ surface concentration.

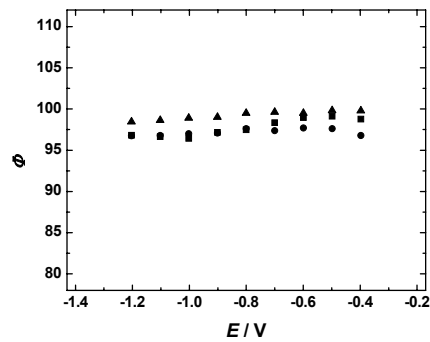


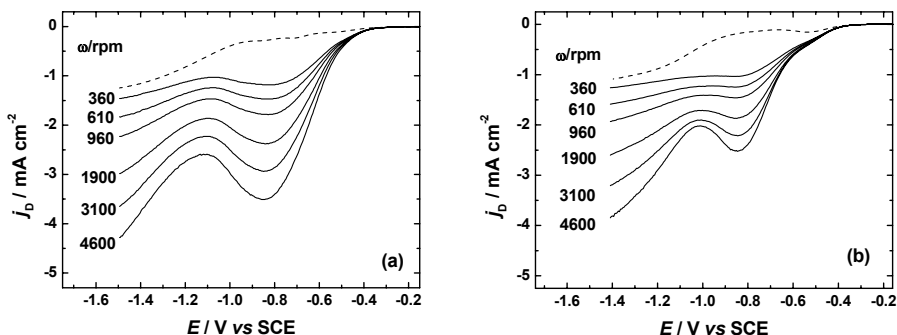
**Figure 6.** Dependence of the yield of peroxide formation ( $\Phi$ ) on potential for: ( $\blacktriangle$ ) GC/AQ, modified in an aqueous solution, ( $\bullet$ ) GC/AQ, modified in acetonitrile and ( $\blacksquare$ ) bare GC.

The number of electrons transferred per O<sub>2</sub> molecule ( $n$ ) was derived from the K-L plots and a value of  $n$  close to 2 was found for GC and GC/AQ electrodes. This is showing the great promise of these materials as electrocatalysts for the production of hydrogen peroxide.

### 6.1.3. Oxygen reduction on AQ- and PQ-modified BDD and HOPG electrodes

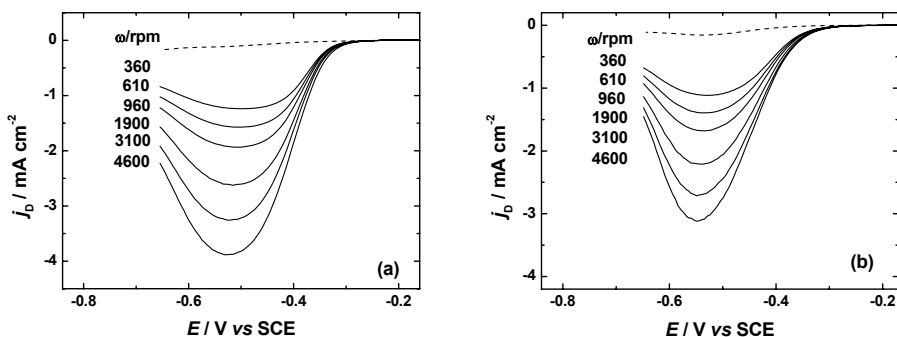
In contrast to glassy carbon, boron-doped diamond and highly oriented pyrolytic graphite are rather inactive towards oxygen reduction in alkaline solutions [II]. It has been proposed that at potentials  $E > -0.7$  V, the reduction of oxygen on GC is mediated by the native quinone-type groups on the GC surface [21]. On HOPG, these functionalities can exist only on defect sites and their surface concentration is very small. There is only a minor current peak seen at *ca*  $-0.55$  V, which is almost independent of rotation rate. It is also apparent that the number of active sites is rather low on polished BDD. As a result, the current of oxygen reduction on BDD and HOPG is very low for  $E > -0.9$  V. The apparent electron transfer rate constant ( $k^0$ ) was found to be  $(4.5 \pm 1.2) \times 10^{-5} \text{ cm s}^{-1}$  and  $(5.7 \pm 0.7) \times 10^{-5} \text{ cm s}^{-1}$  for the bare HOPG and BDD electrodes, respectively. These values of  $k^0$  are more than an order of magnitude lower than that obtained for a bare GC electrode [21]. This behaviour is very convenient for investigating the kinetics of oxygen reduction on surface-bound AQ and PQ without contributions from the electrode substrate and is advantageous over the GC electrodes.

Figure 7 presents the RDE results for oxygen reduction at a BDD/AQ electrode ( $\Gamma_Q = 1.3 \times 10^{-10} \text{ mol cm}^{-2}$ ) and a HOPG/AQ electrode ( $\Gamma_Q = 0.8 \times 10^{-10} \text{ mol cm}^{-2}$ ). A current maximum at *ca*  $-0.83$  V was observed in both cases. The current decreases at more negative potentials, in agreement with the surface redox-catalytic cycle model proposed earlier [21]. It should be noted that such a large current decrease was not observed for GC/AQ electrodes for which only a small hump was observed at *ca*  $-0.8$  V [I]. Therefore, the voltammetric data presented here further confirm the validity of the redox catalytic cycle model of oxygen reduction on quinone-modified electrodes, which predicts a decrease of current at potentials more negative than the redox potential of surface-confined quinones ( $E_r$ ) [21].



**Figure 7.** RDE voltammetry curves for oxygen reduction in  $O_2$ -saturated 0.1 M KOH: (a) BDD/AQ electrode ( $\Gamma_Q = 1.3 \times 10^{-10} \text{ mol cm}^{-2}$ ); (b) HOPG/AQ electrode ( $\Gamma_Q = 8 \times 10^{-11} \text{ mol cm}^{-2}$ ).  $v = 20 \text{ mV s}^{-1}$ . Dashed lines correspond to the  $O_2$  reduction on (a) bare BDD and (b) bare HOPG electrode at 360 rpm.

Figure 8 shows similar results for phenanthrenequinone functionalised BDD/PQ ( $\Gamma_Q = 3.6 \times 10^{-10} \text{ mol cm}^{-2}$ ) and HOPG/PQ ( $\Gamma_Q = 1.3 \times 10^{-10} \text{ mol cm}^{-2}$ ) electrodes. The half-wave potential of  $O_2$  reduction ( $E_{1/2}$ ) on PQ-modified electrodes is much more positive than that of the electrodes modified with AQ [29]. The difference between the  $E_{1/2}$  values of the AQ and PQ modified electrodes is *ca* 0.25 V for both substrates at the same rotation rate and the same surface concentration of quinones. The higher electrocatalytic activity of PQ-modified carbon electrodes is primarily caused by the more positive redox potential of PQ compared to that of surface bound AQ. The number of electrons transferred per  $O_2$  molecule ( $n$ ) in the potential region of maximum electrocatalytic activity by the attached quinone groups, i.e. at the current maximum was calculated from the K-L equation (Equation (25)). The value of  $n$  was found to be close to two in all cases, indicating that the reduction of oxygen stops at peroxide stage.



**Figure 8.** RDE voltammetry curves for oxygen reduction in  $O_2$ -saturated 0.1 M KOH: (a) BDD/PQ electrode ( $\Gamma_Q = 3.6 \times 10^{-10} \text{ mol cm}^{-2}$ ); (b) HOPG/PQ electrode ( $\Gamma_Q = 1.3 \times 10^{-10} \text{ mol cm}^{-2}$ ).  $v = 20 \text{ mV s}^{-1}$ . Dashed lines correspond to the  $O_2$  reduction on (a) bare BDD and (b) bare HOPG electrode at 360 rpm.

The kinetic parameters of O<sub>2</sub> reduction for BDD and HOPG electrodes grafted with quinones were calculated following the surface redox-catalytic cycle model described above. This model was further simplified, because no contribution from the native quinone groups on carbon surface had to be taken into account, allowing more accurate determination of the kinetic parameters for oxygen reduction on quinones. In the case of BDD/PQ and HOPG/PQ electrodes for which the oxygen reduction peak appeared at rather positive potentials (Figure 8), it was assumed that at potentials  $E > -0.65$  V the reduction of O<sub>2</sub> is solely mediated by the surface-bound PQ. Therefore, the term  $2Fc_{O_2}^b k^0 e^{-f\alpha(E-E^0)}$  describing the O<sub>2</sub> reduction on the substrate surface in Equation (23) was considered negligible. However, for AQ-modified electrodes, this term cannot be disregarded, because at more negative potentials ( $E < -1.0$  V) a significant reduction current is observed for both electrode surfaces (Figure 7). The oxygen reduction kinetic parameters were calculated by a non-linear regression (NLR) analysis of the current-potential curves at different rotation rates [21]. From the product  $k_2\Gamma_2$ , the rate constants for the reaction between semiquinone and molecular oxygen ( $k_c$ ) were calculated, using the  $\Gamma_Q$  values determined from the cyclic voltammograms in Ar-saturated solution. Some dependence of the values of the parameters on rotation rate was observed and the averages obtained are listed in Table 2.

**Table 2.** Comparison of the kinetic parameters for oxygen reduction on quinone-modified BDD and HOPG electrodes in 0.1 M KOH.

Electrode	$E_{Q/Q^{2-}}^0$ / V	$\Delta E$ / V	$10^{-8} k_c$ / cm <sup>3</sup> mol <sup>-1</sup> s <sup>-1</sup>
BDD/AQ	$-0.825 \pm 0.008$	$-0.33 \pm 0.02$	$2.7 \pm 0.2$
HOPG/AQ	$-0.833 \pm 0.004$	$-0.26 \pm 0.02$	$1.9 \pm 0.3$
BDD/PQ	$-0.522 \pm 0.003$	$-0.16 \pm 0.01$	$2.2 \pm 0.2$
HOPG/PQ	$-0.537 \pm 0.003$	$-0.16 \pm 0.01$	$2.8 \pm 0.3$

The redox potential of the quinone/hydroquinone couple ( $E_{Q/Q^{2-}}^0$ ) is the main factor that determines the electrocatalytic activity of the quinone-modified electrodes. The  $E_{Q/Q^{2-}}^0$  values obtained for PQ and AQ are somewhat more positive than those obtained on a GC substrate ( $-0.56$  V [29] and  $-0.86$  V [I] for PQ and AQ, respectively). This small shift can be attributed to the different binding sites and/or orientation of the quinone molecules on different substrates. On the other hand, on modified GC electrodes the carbon surface is rather active and the extraction of the parameters of attached quinones is a more complicated task, therefore, the values for quinone-modified GC electrodes may have been determined with less accuracy. The  $E_{Q/Q^{2-}}^0$  values obtained from the NLR analysis are close to the redox potentials determined from the cyclic voltammograms in Ar-saturated solution, which indeed should be the case

according to the redox-catalytic cycle model of oxygen reduction on quinone-modified electrodes [21].

The values of  $k_c$  obtained for surface-bound AQ and PQ on different substrates are all in the order of  $10^8 \text{ cm}^3 \text{ mol}^{-1} \text{ s}^{-1}$ . This indicates that the quinone structure does not have a large influence on the rate constant of the reaction between the semiquinone radical anion and molecular oxygen. The values of  $k_c$  obtained for AQ-grafted HOPG and BDD (Table 2) are somewhat smaller than these of GC/AQ ( $4.7 \times 10^8 \text{ cm}^3 \text{ mol}^{-1} \text{ s}^{-1}$  [I]). The difference is not large and may be related to the different binding sites or orientation of quinone molecules on different substrates. Very high  $k_c$  value was obtained for GC/AQ electrode, as compared to these obtained for various quinones at lower pH-s [26,35,36,42–44]. Surprisingly, even higher  $k_c$  value has been found at pH = 2.5 for AQ covalently attached to multi-walled carbon nanotubes (MWCNTs) ( $k_c = 8.6 \times 10^8 \text{ cm}^3 \text{ mol}^{-1} \text{ s}^{-1}$ ) [49], however, the untreated MWCNTs are rather active towards  $\text{O}_2$  reduction [172] and it is not clear whether their contribution has been eliminated.

Determination of exact values of rate constants for quinones is often complicated by the effect of substrate and the results may depend on the method of analysis used. Nevertheless it is important from the fundamental point of view that the  $k_c$  value has less influence to the  $\text{O}_2$  reduction activity (overpotential) than the redox potential of the quinone couple.

Our results show that the quinones are very active catalysts for  $\text{O}_2$  reduction in alkaline media and catalyse almost exclusively the  $2e^-$  reduction, showing the great promise of these materials as electrocatalysts for the production of hydrogen peroxide.

## **6.2. Oxygen reduction on nanostructured Au electrodes**

The electrochemical reduction of oxygen on vacuum-evaporated thin Au films was studied in acid and alkaline solutions, in order to determine the effect of Au film thickness on the kinetics of  $\text{O}_2$  reduction. Preliminary experiments were carried out in acid media [III]. In the next stage of work, the electrodes were covered with a  $0.5 \text{ }\mu\text{m}$  Nafion film, to provide an environment more similar to a fuel cell cathode compartment [IV].

### **6.2.1. Surface morphology of thin Au films**

The surface morphology of thin Au films was studied using atomic force microscopy (AFM) and transmission electron microscopy (TEM). Complete coverage of the substrate by gold was achieved at a nominal  $10 \text{ nm}$  Au film thickness. The thinner films consisted of separate gold clusters; the island



growth mode observed for Au films deposited on carbon substrates is in agreement with previous observations [93]. Particle size was clearly dependent on the loading of gold. The lowest Au loading ( $h = 0.25$  nm) showed round-shaped particles with a mean particle diameter of  $(2.7 \pm 1.0)$  nm. The particles grow and start to merge into larger agglomerates as the Au loading is increased, however, even for films as thick as 5 nm, a fraction of Au is still present as small clusters, with a particle diameter of  $d < 4$  nm. For example, for the 1 nm Au film, a bidisperse system is formed, where the size of Au nanoclusters is  $(14 \pm 3)$  nm and  $(2.0 \pm 0.6)$  nm.

For comparison, glancing incidence angle X-ray powder diffraction (GIXRD) was used for the estimation of crystallite size of the Au films. The crystallite size calculated from the Scherrer equation increases from  $(4.4 \pm 2)$  nm to  $(16 \pm 6)$  nm with increasing film thickness from 1 to 20 nm. The crystallite size measured by GIXRD is in general smaller than the size of the Au islands revealed by TEM. Since GIXRD actually measures the mean size of coherently diffracting domains, it is not surprising that larger dimensions are observed by TEM since the film is formed by agglomeration of several small crystalline domains with different lattice orientations.

### 6.2.2. Cyclic voltammetry of thin Au films

Prior to  $O_2$  reduction measurements, the thin-film Au electrodes were electrochemically characterised by cyclic voltammetry in Ar-saturated 0.5 M  $H_2SO_4$  (Figure 9). The CV curves were similar for bare [III] and Nafion-coated [IV] thin-film Au electrodes. The CV behaviour of the thin-film Au electrodes was similar to that of bulk polycrystalline gold, but for the thinner films, the first anodic peak at 1.16 V was lower compared with the second peak at 1.33 V. The real surface area of gold ( $A_r$ ) was determined from the CV curves by charge integration under the oxide reduction peak. For Au films thicker than 5 nm,  $A_r$  was approximately twice higher than the geometric area ( $A$ ) of the electrode and the  $A_r/A$  ratio decreased for the thinner films. This ratio was around 0.5 for the thinnest film ( $h = 0.25$  nm).

### 6.2.3. Oxygen reduction on thin Au films in 0.5 M $H_2SO_4$

The ORR electrocatalytic activity of the GC substrate is very low in acid media and therefore, the activity of the thin-film electrodes is due to the deposited Au nanoparticles only. Figure 10 shows representative current-potential curves for oxygen reduction; the background current has been subtracted from these data. Single-wave polarisation curves with no well-defined current plateau were observed for all bare and Nafion-coated thin-film Au electrodes studied as well as for the bulk Au electrode. The RDE data were analysed using the

K-L equation (Equation (25)) and the values for 0.5 M H<sub>2</sub>SO<sub>4</sub>:  $c_{\text{O}_2}^b = 1.13 \times 10^{-6}$  mol cm<sup>-3</sup> [173],  $D_{\text{O}_2} = 1.8 \times 10^{-5}$  cm<sup>2</sup> s<sup>-1</sup> [173] and  $\nu = 0.01$  cm<sup>2</sup> s<sup>-1</sup> [171]. The number of electrons transferred per O<sub>2</sub> molecule ( $n$ ) was calculated at different potentials (see the inset of Figure 11).  $n$  is close to 2 at the foot of the polarisation curve and therefore, H<sub>2</sub>O<sub>2</sub> is the final reduction product. At more negative potentials ( $E < -0.2$  V),  $n$  gradually increases indicating further reduction of H<sub>2</sub>O<sub>2</sub>, in agreement with previous observations [98]. At very negative potentials, the value of  $n$  depends on the Au film thickness, being lower for the thinner films. For the bare thin-film Au electrodes, the value of  $n$  at the negative potentials is slightly higher than for the Nafion-coated electrodes.

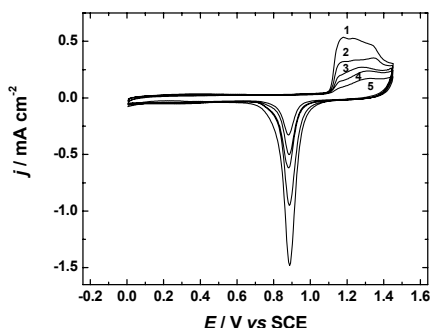


**Figure 9.** Cyclic voltammograms for thin-film Au electrodes (curves 2–5) and bulk Au (curve 1) in Ar-saturated 0.5 M H<sub>2</sub>SO<sub>4</sub>. Au film thickness: (2) 20; (3) 1; (4) 0.5 and (5) 0.25 nm.  $\nu = 100$  mV s<sup>-1</sup>. All the electrodes were covered with 0.5  $\mu$ m Nafion film.

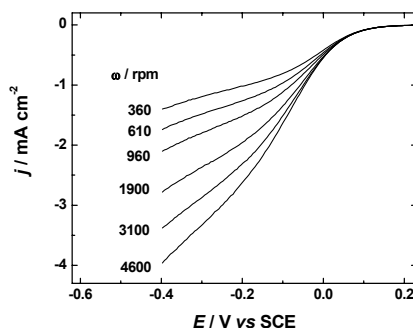


**Figure 10.** RDE voltammetry results for O<sub>2</sub> reduction on 2 nm Au/GC electrode in O<sub>2</sub>-saturated 0.5 M H<sub>2</sub>SO<sub>4</sub>.  $\nu = 10$  mV s<sup>-1</sup>. The electrode was covered with 0.5  $\mu$ m Nafion film.

The polarisation curves of O<sub>2</sub> reduction were similar for all bare and Nafion-coated electrodes, but the apparent catalytic activity of the electrodes decreased with decreasing the film thickness (Figure 11). This is also reflected in the shift of the half-wave potential ( $E_{1/2}$ ) towards more negative values (Table 3). A decrease of the apparent O<sub>2</sub> reduction activity with Au loading would be expected, as the real surface area of Au decreases for the thinner films. To determine the possible effect of the Au film morphology and particle size on the electrocatalytic activity of gold, the specific activity (SA) of thin Au films was calculated:

$$SA = I_k / A_r \quad (26)$$

where  $I_k$  is the kinetic current and  $A_r$  is the real surface area of gold. SA values obtained at  $E = 0.05$  V vs SCE are given in Table 3. It can be concluded that for

bare Au films and for Nafion-coated films of nominal thickness  $h \geq 0.5$  nm the SA is independent of Au loading. However, the average SA value for Nafion-coated films is approximately three times lower compared with bare Au films. This can be attributed to a decrease in the number of reaction sites by Nafion, as proposed by Maruyama et al. who studied the effect of fluorinated alcohols on the kinetics of the ORR on bulk Au electrodes [174,175]. The decrease of the kinetic current has also been observed on Nafion-coated GC electrodes as compared to bare GC and this effect has been related to the lower pH at Nafion-coated GC and/or to blocking by the side chains of the Nafion polymer [176].

**Table 3.** Kinetic parameters for oxygen reduction on bare [III] and Nafion-coated [IV] thin-film Au electrodes in 0.5 M H<sub>2</sub>SO<sub>4</sub>.

Au film thickness	Bare Au films			Nafion-coated Au films		
	Tafel slope (mV dec <sup>-1</sup> )	$E_{1/2}$ (mV)	SA at 0.05 V (mA cm <sup>-2</sup> )	Tafel slope (mV dec <sup>-1</sup> )	$E_{1/2}$ (mV)	SA at 0.05 V (mA cm <sup>-2</sup> )
0.25 nm	-120 ± 4	-163 ± 8	0.43 ± 0.08	-122 ± 6	-256 ± 14	0.08 ± 0.01
0.5 nm	-120 ± 5	-142 ± 12	0.39 ± 0.1	-114 ± 1	-156 ± 18	0.12 ± 0.01
1 nm	-107 ± 2	-89 ± 2	0.37 ± 0.02	-113 ± 1	-127 ± 5	0.13 ± 0.02
2 nm	-109 ± 2	-70 ± 8	0.41 ± 0.03	-106 ± 4	-98 ± 13	0.14 ± 0.02
5 nm	-115 ± 2	-29 ± 3	0.45 ± 0.03	-106 ± 2	-86 ± 9	0.14 ± 0.01
10 nm	-115 ± 2	-28 ± 3	0.41 ± 0.03	-119 ± 1	-112 ± 23	0.12 ± 0.02
20 nm	-107 ± 3	-21 ± 5	0.52 ± 0.03	-110 ± 2	-86 ± 17	0.17 ± 0.01
Bulk Au	-109 ± 2	-13 ± 4	0.40 ± 0.03	-110 ± 5	-70 ± 9	0.21 ± 0.02

The mass-transfer corrected Tafel plots, normalised to Au real surface area were constructed from the RDE data (Figure 12). For bare and Nafion-coated thin-film electrodes, the average Tafel slopes of  $-112 \pm 8$  mV dec<sup>-1</sup> and  $-114 \pm 6$  mV dec<sup>-1</sup>, respectively, were calculated between 0 and 0.2 V and these values were independent of the film thickness (Table 3), indicating that the ORR mechanism does not depend on Au loading or Nafion coating and that the first electron transfer is the rate-determining step.

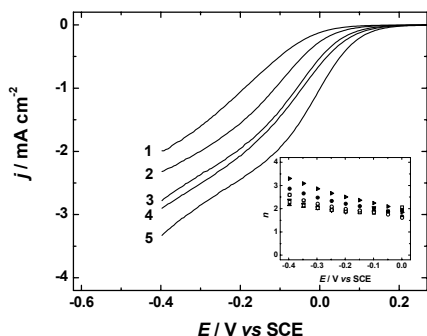


**Figure 11.** RDE voltammetry curves for  $\text{O}_2$  reduction on Au thin films (curves 1–4) and bulk Au (5) in  $\text{O}_2$ -saturated 0.5 M  $\text{H}_2\text{SO}_4$ . Au film thickness: (1) 0.25; (2) 0.5; (3) 2 and (4) 20 nm.  $\omega = 1900$  rpm;  $v = 10$  mV s $^{-1}$ . The inset shows the potential dependence of  $n$  for thin-film and bulk Au electrodes in 0.5 M  $\text{H}_2\text{SO}_4$ . Film thickness: ( $\blacktriangle$ ) 0.25; ( $\blacktriangledown$ ) 0.5; ( $\blacksquare$ ) 1; ( $\blacklozenge$ ) 2; ( $\bullet$ ) 10 and (+) 20 nm V. ( $\blacktriangleright$ ) bulk Au. All the electrodes were covered with 0.5  $\mu\text{m}$  Nafion film.

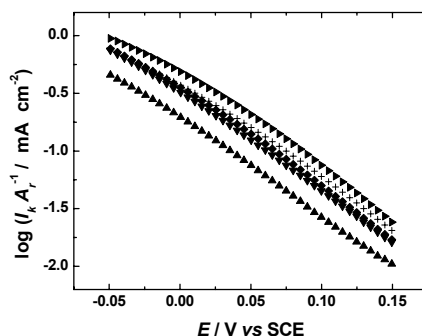


**Figure 12.** Potential dependence of the  $\text{O}_2$  reduction kinetic current density per real Au surface area for thin-film and bulk Au electrodes in 0.5 M  $\text{H}_2\text{SO}_4$ .  $\omega = 1900$  rpm. Film thickness: ( $\blacktriangle$ ) 0.25 nm; ( $\blacktriangledown$ ) 0.5 nm; ( $\blacklozenge$ ) 2 nm; (+) 20 nm. ( $\blacktriangleright$ ) bulk Au. All the electrodes were covered with 0.5  $\mu\text{m}$  Nafion film.

The thinnest Nafion-coated Au film (0.25 nm) has a lower SA value than the thicker films by a factor of two. This may be a particle size effect. The average particle size for this film is less than 4 nm, whereas for the higher loadings, larger clusters dominate. These results are in agreement with the observation by Guerin et al. that the electrocatalytic activity for  $\text{O}_2$  reduction of Au particles smaller than  $d \approx 4$  nm decreases rapidly with size [100]. The origin of these size effects, however, still remains unclear. It may be related to the changes in particle morphology. According to the model of Kinoshita for cubo-octahedral particles [138], the surface fraction of (111) sites increases when the particle size decreases. The adsorption of (bi)sulfate ions that block the adsorption sites for  $\text{O}_2$  is strongest on Au(111) crystal face, whereas the four-fold symmetry of Au(100) is convenient for  $\text{O}_2$  adsorption [56]. Therefore, the purely geometrical considerations can explain the decreased  $\text{O}_2$  reduction activity. On the other hand, the role of the low coordinated Au atoms as the adsorption centres for CO and  $\text{O}_2$  in CO oxidation has been emphasised [101]; most likely the  $\text{O}_2$  adsorption on these centres also influences the electrochemical reduction of  $\text{O}_2$ .

### 6.2.4. Oxygen reduction on thin Au films in 0.1 M KOH

In alkaline solution, the Nafion-coated Au electrodes are rather active catalysts for oxygen reduction; the onset potential of the ORR is *ca*  $-0.1$  V for bulk Au and thicker films. Figure 13 shows representative current-potential curves for the ORR for a 1 nm Au film electrode in  $O_2$ -saturated 0.1 M KOH at several rotation rates and in Figure 14, a comparison for several thin-film Au electrodes with bulk Au and the GC substrate at the same rotation rate is presented. The current-potential characteristics were similar for all electrodes studied and electrodes with thicker films ( $h \geq 5$  nm) showed current maxima at approximately  $-0.4$  V similarly to bulk polycrystalline Au. Extensive studies with Au single crystals have shown that  $HO_2^-$  is predominantly formed at the potentials of the first reduction wave on Au(111) and Au(110).  $HO_2^-$  is further reduced to  $OH^-$  at the second wave [56]. On the Au(100) plane, the  $4e^-$  reduction to  $OH^-$  takes place at relatively low overpotentials and causes the current maximum [56]. Similar  $O_2$  reduction behaviour has also been observed for the reconstructed surface of polycrystalline Au (“(100)-like Au”) [62] and for Au nanoparticles synthesized in water-in-oil microemulsion [78].

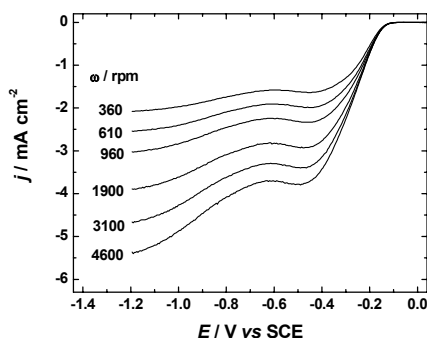


**Figure 13.** RDE voltammetry curves for  $O_2$  reduction on 1 nm Au/GC electrode in  $O_2$ -saturated 0.1 M KOH at different rotation rates.  $v = 10 \text{ mV s}^{-1}$ .

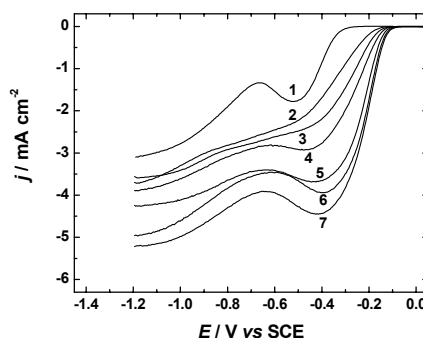


**Figure 14.** RDE voltammetry curves for  $O_2$  reduction on Au thin films (curves 2–6), bulk Au (7) and GC (1) in  $O_2$ -saturated 0.1 M KOH at 1900 rpm. Au film thickness: (2) 0.25; (3) 0.5; (4) 1; (5) 5 and (6) 20 nm.  $\omega = 1900 \text{ rpm}$ ;  $v = 10 \text{ mV s}^{-1}$ .

The number of electrons transferred ( $n$ ) was calculated using Equation (25) and the values for 0.1 M KOH:  $c_{O_2}^b = 1.2 \times 10^{-6} \text{ mol cm}^{-3}$  [170],  $D_{O_2} = 1.9 \times 10^{-5} \text{ cm}^2 \text{ s}^{-1}$  [170] and  $v = 0.01 \text{ cm}^2 \text{ s}^{-1}$  [171]. The  $n$  value depends on potential as well as on Au loading. For high loading,  $n > 3$  at low overpotentials ( $E > -0.4$  V), indicating that  $HO_2^-$  is partially further reduced. At more negative potentials,  $n$  decreases, being close to 2 for electrodes with low Au loading and its value is between 2.5 and 3 for electrodes with higher Au

loading, showing that only a fraction of the  $\text{HO}_2^-$  formed on the surface of nanostructured gold is reduced at these potentials. At  $E < -0.7$  V,  $n$  increases for all the electrodes studied up to the value of four at  $-1.2$  V, corresponding to full reduction to  $\text{OH}^-$ .

The absence of current maxima and lower  $n$  values at low overpotentials observed for the electrodes of smaller Au loading as compared to the thicker films may be related to the differences in particle size and morphology.  $\text{HO}_2^-$  is further reduced at low overpotentials only on Au(100) terraces [69] that are more likely to be present on the surface of larger Au clusters, while the small Au particles have a greater fraction of low coordination surface atoms. In accordance with this, a strong influence of the nanoparticle morphology on  $\text{O}_2$  reduction has been observed by Hernandez et al. [78,79] and El-Deab et al. [83,84,86].

Similarly to the behaviour in acid, the apparent electrocatalytic activity of the electrodes decreases with the nominal film thickness and  $E_{1/2}$  shifts to more negative potentials (Table 4). Figure 15 presents the mass-transfer corrected Tafel plots for  $\text{O}_2$  reduction in 0.1 M KOH, normalised to Au real surface area. The Tafel slope between  $-0.2$  V and  $-0.3$  V was close to  $-120$  mV  $\text{dec}^{-1}$  for all surfaces (Table 4), indicating that the  $\text{O}_2$  reduction mechanism is independent of the Au film thickness.

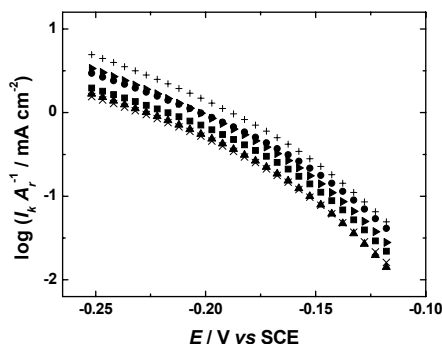


**Figure 15.** Potential dependence of the  $\text{O}_2$  reduction kinetic current density per real Au surface area for thin-film and bulk Au electrodes in 0.1 M KOH.  $\omega = 1900$  rpm. Film thickness: ( $\blacktriangle$ ) 0.25; ( $\times$ ) 0.5; ( $\blacksquare$ ) 1; ( $\blacktriangleright$ ) 5 and (+) 20 nm. ( $\bullet$ ) bulk Au. All the electrodes were covered with  $0.5$   $\mu\text{m}$  Nafion film.

The specific activity of the electrodes was calculated at  $-0.15$  V (Table 4). In contrast to the result in an acid solution, where the  $\text{O}_2$  reduction activity of the GC support is very low, the half-wave potential of this reaction for GC in alkaline solution is approximately 40 mV more negative than for the Au/GC

electrode with the lowest Au loading. Therefore, the reduction on GC has undoubtedly some influence on O<sub>2</sub> reduction at the Au/GC electrodes of lower loading. Nevertheless, at  $E = -0.15$  V where the SA for Au electrodes was determined, the O<sub>2</sub> reduction activity of GC is considered to be negligible.

Analogously to the results in acid solution, where the SA is almost independent of the Au loading, the SA value is only slightly decreased for thinner films in alkaline solutions. A possible explanation might be the relative enrichment of larger Au particles with Au(100) crystal facets, as compared to the small particles. This speculation is supported by the observation that the average number of electrons involved in O<sub>2</sub> reduction increases with the film thickness at low overpotentials. On the other hand, it might be possible that the activity loss is due to some other effect related to particle size. It is evident that the catalytic properties of nanoparticles can be remarkably different from these of bulk metal [5].

Our results show that there is no evidence of strong dependence of Au specific activity on the loading over the range of film thicknesses studied. This is an important finding from the point of view of preparing practical electrocatalysts for fuel cells.

**Table 4.** Kinetic parameters for oxygen reduction on thin-film Au electrodes in 0.1 M KOH [IV]. The electrodes were covered with 0.5  $\mu\text{m}$  Nafion film.

Au film thickness	Tafel slope (mV dec <sup>-1</sup> )	$E_{1/2}$ (mV)	SA at $-0.15$ V (mA cm <sup>-2</sup> )
0.25 nm	$-121 \pm 3$	$-334 \pm 5$	$0.08 \pm 0.02$
0.5 nm	$-122 \pm 4$	$-274 \pm 8$	$0.09 \pm 0.02$
1 nm	$-119 \pm 3$	$-245 \pm 8$	$0.11 \pm 0.01$
2 nm	$-120 \pm 7$	$-273 \pm 14$	$0.05 \pm 0.01$
5 nm	$-102 \pm 5$	$-217 \pm 6$	$0.14 \pm 0.02$
10 nm	$-100 \pm 5$	$-217 \pm 5$	$0.18 \pm 0.01$
20 nm	$-105 \pm 3$	$-210 \pm 4$	$0.24 \pm 0.03$
Bulk Au	$-108 \pm 11$	$-200 \pm 8$	$0.19 \pm 0.03$

### 6.3. Oxygen reduction on nanostructured Pt electrodes

Oxygen reduction on thin Pt films prepared by vacuum-evaporation onto GC [V] and Au [VI] supports was studied in acid solutions. The objective of this part of work was to compare the electrochemical behaviour of Pt nanoislands and thin films in 0.1 M HClO<sub>4</sub> and 0.05 M H<sub>2</sub>SO<sub>4</sub> solutions, in order to evaluate the influence of anion adsorption on nanostructured Pt electrodes to the ORR kinetics and determine the possible effects of the size of Pt islands and the Pt film thickness on the oxygen reduction activity.

### **6.3.1. Surface morphology of thin Pt films**

The morphology of thin Pt films was studied by TEM. The TEM images revealed that the Pt film formation follows an island growth mode. The thinnest films consisted of separate, round-shaped Pt islands; the particle size was  $1.7 \pm 0.2$  nm for 0.25 nm film and increased with the film thickness. For thicker films, a network of Pt islands was formed. For 10 nm film, a continuous film consisting of Pt clusters with the size of  $4.0 \pm 0.7$  nm was observed. Unfortunately, we have no information about the surface morphology of Pt films on Au support. Pedersen et al. have studied deposition of small amounts of Pt to Au(111) substrate by vacuum-evaporation and found that the islands grow layer-by-layer, so that the first monolayer is nearly complete before second layer islands are nucleated [177]. Therefore, Pt islands which are larger in diameter and more flat are expected to form on Au as compared to the small hemispherical particles on carbon substrate for the thinnest films.

### **6.3.2. Cyclic voltammetry of thin Pt films**

Thin-film Pt electrodes were cycled in the Ar-saturated  $\text{HClO}_4$  or  $\text{H}_2\text{SO}_4$  solutions prior to the  $\text{O}_2$  reduction measurements, in order to stabilise and characterise the Pt film. Figure 16 shows the stable cyclic voltammograms of Pt/GC and Pt/Au electrodes of various film thickness in 0.05 M  $\text{H}_2\text{SO}_4$ . For the thin-film Pt electrodes, the CV response showed features characteristic to the polycrystalline Pt in both solutions, the  $\text{H}_{\text{upd}}$  peaks being less pronounced in  $\text{HClO}_4$  [178]. It is most significant that the peak potential of Pt oxide reduction shifted to negative direction for thinner films, the maximum shift being about 50 mV for thinnest films as compared to bulk Pt and thick Pt films. This effect has been attributed to more irreversible adsorption of oxygenated species on smaller Pt particles [114,123,124,139]. The negative shift is experimentally well-established and could be related to lower coordination number of smaller Pt particles, which in turn changes the electronic properties of nanoparticles [124]. The peak potentials of oxide reduction were similar in both solutions. For Pt/Au electrodes, the shift of the oxide reduction peak can also be attributed to the substrate-induced changes of the electronic properties of Pt surface that increase the binding energy of adsorbed oxygen-containing species; this has been observed in earlier studies on the Pt/Au bimetallic systems [152,154,159].



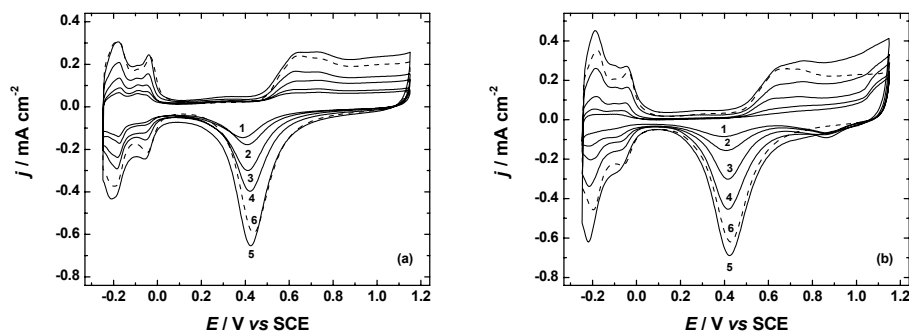


**Figure 16.** Cyclic voltammograms for (a) Pt/GC electrodes and (b) Pt/Au electrodes in Ar-saturated 0.05 M H<sub>2</sub>SO<sub>4</sub>. Film thickness: (a) (1) 0.25; (2) 0.5; (3) 1; (4) 2 and (5) 10 nm; (b) (1) 0.25; (2) 0.5; (3) 2; (4) 5 and (5) 20 nm. The dashed lines (6) correspond to bulk Pt electrode.  $\nu = 100 \text{ mV s}^{-1}$ .

The real surface area ( $A_r$ ) of Pt was determined by charge integration under the hydrogen desorption peaks. It was considerably increasing with the film thickness for thinner films ( $h < 5 \text{ nm}$ ), from approximately  $A_r / A \approx 0.5$  to  $A_r / A \approx 3$  for 0.25 nm and 5 nm Pt/GC films and from  $A_r / A \approx 0.3$  to  $A_r / A \approx 2$  for 0.25 nm and 5 nm Pt/Au films, respectively. For 5 nm and thicker films, there was only a slight increase of the roughness with the film thickness, as the substrate surface was already nearly completely covered by Pt. The smaller real surface area of Pt/Au electrodes as compared to Pt/GC films of the same nominal thickness may be due to different surface morphology of the films, or to the surface alloying and Au segregation that is expected to take place during cycling. Pedersen et al have calculated the surface energy of Pt-Au surface alloy and found it to be larger than that of Pt-Au capped by pure Au “skin”, therefore, Pt atoms tend to diffuse away from the top layer [177].

### 6.3.3. Oxygen reduction on thin Pt films

The electrochemical reduction of oxygen on thin-film Pt electrodes was studied in 0.1 M HClO<sub>4</sub> and 0.05 M H<sub>2</sub>SO<sub>4</sub> solutions using the RDE method. The representative current-potential curves are shown in Figure 17; the background current has been subtracted from these data and only the negative potential sweeps are presented and analysed further. Single-wave polarisation curves with a well-defined current plateau were observed for all the Pt/GC as well as for Pt/Au electrodes studied and the apparent catalytic activity of oxygen reduction increased with the nominal film thickness. It can be seen that in H<sub>2</sub>SO<sub>4</sub> the electrocatalytic activity of Pt films was lower, the half-wave potential of O<sub>2</sub> reduction being approximately 60–70 mV more negative (Tables

5 and 6). This is a well-known phenomenon that the adsorbed (bi)sulfate anions block the sites for O<sub>2</sub> adsorption [103,106–109,142,143, 179] and possibly have a negative electronic effect on the ORR kinetics [109]. The RDE data were analysed using the Koutecky-Levich equation (Equation (25)) and the values for 0.05 M H<sub>2</sub>SO<sub>4</sub>:  $c_{\text{O}_2}^b = 1.22 \times 10^{-6} \text{ mol cm}^{-3}$  [180],  $D_{\text{O}_2} = 1.93 \times 10^{-5} \text{ cm}^2 \text{ s}^{-1}$  [180] and  $\nu = 0.01 \text{ cm}^2 \text{ s}^{-1}$  [171]. The K-L plots were constructed and the number of electrons transferred per O<sub>2</sub> molecule ( $n$ ) was calculated from Equation (25). The value of  $n \approx 4$  was found over the whole range of potentials and Pt film thicknesses studied, both for Pt/GC and Pt/Au electrodes. The 4e<sup>−</sup> pathway of O<sub>2</sub> reduction on Pt has been confirmed in many studies [1,2], however, it is not possible to unequivocally establish whether the reduction of O<sub>2</sub> proceeds through “direct” 4e<sup>−</sup> pathway or through H<sub>2</sub>O<sub>2</sub> intermediate that is immediately reduced further. It has been stated recently that the reduction via adsorbed peroxide is more reasonable [105,108,137].

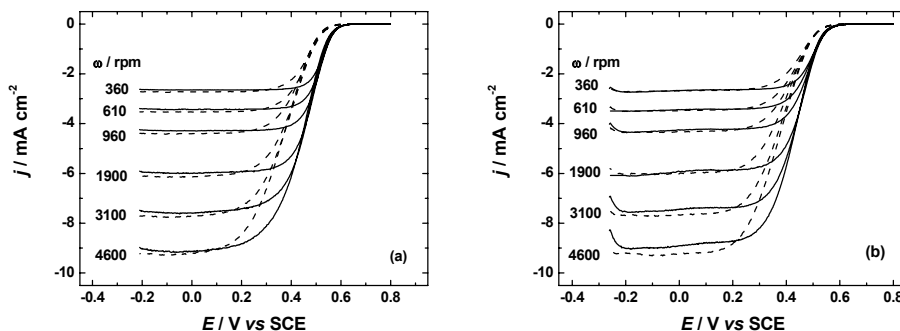


**Figure 17.** RDE voltammetry results for O<sub>2</sub> reduction on (a) 2 nm Pt/GC electrode and (b) 2 nm Pt/Au electrode in O<sub>2</sub>-saturated 0.1 M HClO<sub>4</sub> (solid lines) and 0.05 M H<sub>2</sub>SO<sub>4</sub> (dashed lines).  $\nu = 10 \text{ mV s}^{-1}$ .

The electrocatalytic activity of thin Pt films decreased with decreasing film thickness in both solutions and the half-wave potential shifted in the negative direction (Tables 5 and 6). This activity decrease is mainly caused by the decrease of the real surface area of Pt for the thinner films. The catalytic activity of both GC and Au substrates is very low in acid solutions and therefore the O<sub>2</sub> reduction current at potentials  $E > 0.25 \text{ V}$  is due to the Pt particles only. At more negative potentials, a small quantity of H<sub>2</sub>O<sub>2</sub> can be produced on GC or Au substrate, which is expected to be further reduced on Pt particles, as shown by Antoine and Durand on platinum nanoparticles supported on carbon inside Nafion [122].

To evaluate the percentage of H<sub>2</sub>O<sub>2</sub> formation, the RRDE experiments were carried out on the 0.5 nm Pt/GC and 0.5 nm Pt/Au electrodes. The potential of Pt ring was set to  $E = 0.95 \text{ V}$ , at which the oxidation of H<sub>2</sub>O<sub>2</sub> is diffusion

limited. The fraction of  $\text{H}_2\text{O}_2$  formation on the disk was calculated from Equation (24). The ring current was rather small at the potentials of  $E > -0.1$  V, corresponding to less than 3% of  $\text{H}_2\text{O}_2$  formation on Pt/GC and less than 5% on Pt/Au electrodes. At more negative potentials the  $\text{H}_2\text{O}_2$  production significantly increased and the  $\text{O}_2$  reduction current ( $I_D$ ) decreased accordingly. This has been attributed to the blocking of the sites for dissociative adsorption of oxygen molecules by adsorbed hydrogen atoms [103]. The percentage of  $\text{H}_2\text{O}_2$  formation appears to be independent of electrode substrate and electrolyte solution, only slightly more  $\text{H}_2\text{O}_2$  is produced on Pt/Au electrodes and in the  $\text{H}_2\text{SO}_4$  solution.

Our results are in agreement with the literature data, where only small amounts of  $\text{H}_2\text{O}_2$  produced have been detected on carbon-supported Pt nanoparticles [131] and on Pt nanocubes [140]. Increased  $\text{H}_2\text{O}_2$  production has been observed on Pt/GC electrodes of very low Pt loading and it was proposed that  $\text{H}_2\text{O}_2$  formed on the Pt surface does not necessarily undergo instantaneous further reduction, but that further reduction can occur also after its desorption and subsequent re-adsorption and the probability of latter process decreases with decreasing Pt loading [137]. For Pt/Au systems, small amounts of  $\text{H}_2\text{O}_2$  produced have been found on Pt monolayer on Au [155] and significant formation of  $\text{H}_2\text{O}_2$  on AuPt alloy nanoparticle catalysts [162,163], whereas on Pt-coated Au nanoparticles,  $\text{O}_2$  was completely reduced to  $\text{H}_2\text{O}$  [158].

In Figures 18 and 19, the mass-transfer corrected Tafel plots constructed from the RDE data are presented. Two Tafel regions with the characteristic slopes near to  $-120 \text{ mV dec}^{-1}$  and  $-60 \text{ mV dec}^{-1}$  are clearly distinguished, a transition in slope occurring at potentials between 0.45 and 0.5 V. The value of  $-120 \text{ mV dec}^{-1}$  indicates that the rate determining step is the transfer of the first electron to oxygen molecule. As suggested previously, the change of the slope is not related to the change of the reaction mechanism, but it has been attributed to the potential-dependent coverage of surface oxides that inhibit the adsorption of  $\text{O}_2$  and reaction intermediates [1]. It can be seen that the potential at which the Tafel slope changes shifts negatively for the thinner films, in agreement with the shift of the Pt surface oxide reduction peak (Figure 16). In  $\text{HClO}_4$ , the transition between slopes is more gradual than in  $\text{H}_2\text{SO}_4$  solution. The values of Tafel slopes listed in Tables 5 and 6 do not show a clear dependence on the film thickness and are similar in both solutions, indicating that the mechanism of oxygen reduction on nanostructured Pt is the same as on bulk metal and is not affected by the substrate material.

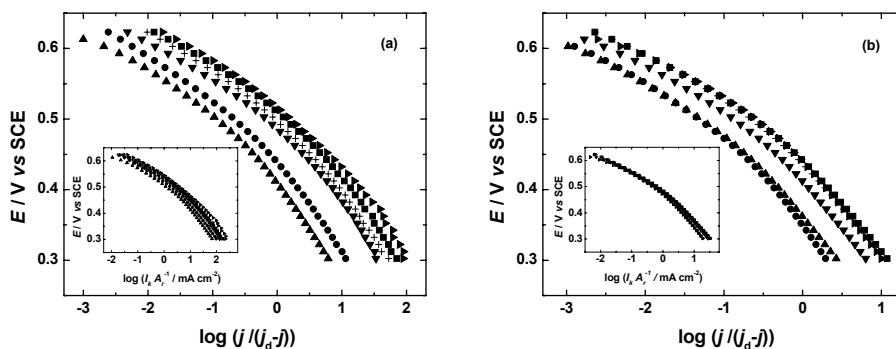


**Figure 18.** Mass-transfer corrected Tafel plots for  $\text{O}_2$  reduction on thin-film and bulk Pt electrodes in (a) 0.1 M  $\text{HClO}_4$  and (b) 0.05 M  $\text{H}_2\text{SO}_4$ .  $\omega = 1900$  rpm. Insets: Potential dependence of  $\text{O}_2$  reduction kinetic current density per real Pt surface area. Film thickness: (▲) 0.25 nm; (●) 0.5 nm; (▼) 2 nm; (+) 5 nm; (■) 10 nm; (►) bulk Pt.

To distinguish the effects of Pt film morphology and particle size on the electrocatalytic activity from the activity decrease due to the decrease of the real surface area of Pt, the kinetic current was normalised to real Pt surface area and the specific activity (SA) of  $\text{O}_2$  reduction was calculated from Equation (26). The SA values obtained at  $E = 0.55$  V vs. SCE in both electrolyte solutions are given in Tables 5 and 6. It is most significant that in  $\text{HClO}_4$  solution, the SA of Pt films on both substrates decreases with decreasing film thickness, whereas in  $\text{H}_2\text{SO}_4$ , the SA value is constant over the whole range of film thicknesses studied. For Pt/GC electrodes, the decrease of the SA with nominal film thickness is apparently related to decreasing the size of Pt particles. The decrease of the  $\text{O}_2$  reduction activity of Pt nanoparticles with the particle size has been observed in many studies [112–124,132], most often, for particle sizes below 3 nm. Therefore, the results obtained in  $\text{HClO}_4$  are in agreement with literature data. The origin of this size effect has most often been attributed to stronger adsorption of OH on smaller Pt particles that hinders the reduction kinetics [114,124]. Adsorbed OH is considered to inhibit the ORR by blocking the surface sites for  $\text{O}_2$  adsorption [108,109] and it also has a negative electronic effect on the ORR kinetics [109]. The more irreversible adsorption of surface oxygenated species is reflected in the shift of oxide reduction peak to lower potential values, as can be seen in Figure 16.

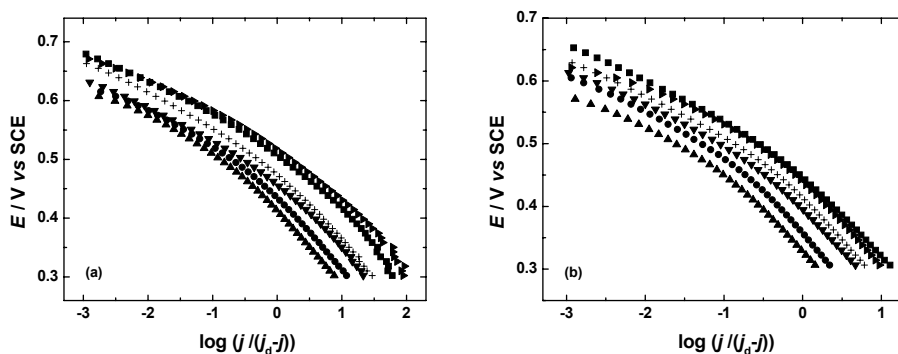


**Figure 19.** Mass-transfer corrected Tafel plots for  $O_2$  reduction on Pt/Au electrodes and bulk Pt in (a) 0.1 M  $HClO_4$  and (b) 0.05 M  $H_2SO_4$ .  $\omega = 1900$  rpm. Film thickness: 0.25 nm ( $\blacktriangle$ ); 0.5 nm ( $\bullet$ ); 2 nm ( $\blacktriangledown$ ); 5 nm (+); 20 nm ( $\blacksquare$ ); bulk Pt ( $\blacktriangleright$ ).

**Table 5.** Kinetic parameters for oxygen reduction on Pt/GC electrodes in 0.1 M  $HClO_4$  and 0.05 M  $H_2SO_4$  at  $\omega = 1900$  rpm.

Elec-trode	0.1 M $HClO_4$				0.05 M $H_2SO_4$			
	Tafel slope (mV dec <sup>-1</sup> )		$E_{1/2}$ (mV)	SA at 0.55 V (mA cm <sup>-2</sup> )	Tafel slope (mV dec <sup>-1</sup> )		$E_{1/2}$ (mV)	SA at 0.55 V (mA cm <sup>-2</sup> )
	I *	II			I	II		
0.25 nm Pt	-62 ± 4	-123 ± 5	419 ± 15	0.26 ± 0.09	-65 ± 3	-127 ± 2	360 ± 3	0.10 ± 0.01
0.5 nm Pt	-65 ± 4	-129 ± 10	427 ± 12	0.28 ± 0.08	-66 ± 2	-138 ± 4	345 ± 10	0.10 ± 0.01
1 nm Pt	-60 ± 4	-110 ± 5	469 ± 4	0.35 ± 0.08	-59 ± 5	-124 ± 2	401 ± 2	0.10 ± 0.01
2 nm Pt	-60 ± 2	-123 ± 9	484 ± 7	0.40 ± 0.08	-63 ± 1	-129 ± 1	410 ± 2	0.10 ± 0.01
5 nm Pt	-66 ± 1	-117 ± 9	493 ± 6	0.45 ± 0.06	-69 ± 2	-127 ± 2	436 ± 1	0.14 ± 0.01
10 nm Pt	-64 ± 2	-123 ± 2	509 ± 2	0.61 ± 0.01	-66 ± 1	-130 ± 4	438 ± 5	0.12 ± 0.01
20 nm Pt	-70 ± 2	-145 ± 4	517 ± 6	0.61 ± 0.04	-65 ± 3	-139 ± 2	440 ± 5	0.10 ± 0.01
Bulk Pt	-63 ± 3	-117 ± 2	513 ± 4	0.79 ± 0.03	-69 ± 7	-140 ± 10	430 ± 12	0.13 ± 0.01

\* Region I corresponds to low current densities and Region II to high current densities.

For Pt/Au electrodes, the stronger adsorption of oxygen-containing intermediates on Pt can be caused by the electronic effect of Au substrate. The theoretical calculations have indicated that in case of Pt monolayer on Au(111), the lattice mismatch induces the expansive strain in Pt and results in a higher

d-band centre energy that leads to a stronger binding of adsorbates to the surface [155,157]. The d-band centre energy of the surface Pt atoms decreases as the number of the Pt layers increases and the Pt–Au interaction decreases. On the other hand, for the Pt-Au surface alloys the d-band centre of the surface Pt atoms decreases as the Pt concentration decreases [181]. This implies that the adsorption energy of O and OH and also the catalytic activity for O<sub>2</sub> reduction is highly dependent on the morphology of the Pt/Au surface and on the Pt loading and that generally a slight decrease of the specific activity of Pt/Au catalysts is expected, as compared to pure Pt. In agreement with this proposition, our results show that thick Pt films on Au are somewhat less active to O<sub>2</sub> reduction than Pt films on GC and bulk Pt. The activity decreases with decreasing film thickness as the influence of Au substrate increases, the same effect has been observed for Pt coated Au nanoparticles [159]. Interestingly, the Pt films of low nominal thickness are slightly more active than the corresponding Pt/GC films. A possible explanation might be the different morphology of Pt nanostructures on Au and GC. Pedersen et al have studied deposition of very small amounts of Pt to Au(111) substrate by vacuum-evaporation and found that the Pt islands grow layer-by-layer, so that the first monolayer is nearly complete before the second layer islands are nucleated [177]. Due to the roughness of the polycrystalline Au substrate used the situation might be somewhat different, but it is still expected that as compared to small hemispherical Pt particles that we observed on carbon substrate, the Pt islands on Au are larger in diameter and more flat. Therefore, the particle size effect to O<sub>2</sub> reduction is small and the decrease of O<sub>2</sub> reduction activity as compared to thicker films is caused only by stronger influence of Au substrate that leads to the more irreversible adsorption of surface oxygenated species. The more irreversible adsorption is evidenced by the shift of Pt oxide reduction peak to a negative direction (Figure 16).

**Table 6.** Kinetic parameters of oxygen reduction on Pt/Au electrodes in 0.1 M HClO<sub>4</sub> and 0.05 M H<sub>2</sub>SO<sub>4</sub> at  $\omega = 1900$  rpm.

Elec-trode	0.1 M HClO <sub>4</sub>				0.05 M H <sub>2</sub> SO <sub>4</sub>			
	Tafel slope (mV dec <sup>-1</sup> )		$E_{1/2}$ (mV)	SA at 0.55 V (mA cm <sup>-2</sup> )	Tafel slope (mV dec <sup>-1</sup> )		$E_{1/2}$ (mV)	SA at 0.55 V (mA cm <sup>-2</sup> )
	I *	II			I	II		
0.25 nm Pt/Au	-65 ± 4	-123 ± 4	398 ± 15	0.31 ± 0.07	-74 ± 5	-135 ± 5	331 ± 8	0.09 ± 0.03
0.5 nm Pt/Au	-66 ± 1	-123 ± 9	429 ± 9	0.34 ± 0.03	-70 ± 2	-132 ± 1	362 ± 4	0.11 ± 0.01
1 nm Pt/Au	-66 ± 5	-122 ± 10	435 ± 14	0.32 ± 0.10	-65 ± 1	-131 ± 1	381 ± 2	0.10 ± 0.01
2 nm Pt/Au	-65 ± 3	-120 ± 15	451 ± 10	0.33 ± 0.02	-65 ± 1	-125 ± 2	397 ± 5	0.10 ± 0.01
5 nm Pt/Au	-62 ± 1	-105 ± 2	475 ± 2	0.34 ± 0.02	-67 ± 3	-113 ± 5	414 ± 2	0.10 ± 0.02
10 nm Pt/Au	-65 ± 5	-116 ± 12	483 ± 9	0.41 ± 0.08	-59 ± 1	-125 ± 1	416 ± 3	0.08 ± 0.01
20 nm Pt/Au	-62 ± 1	-111 ± 2	509 ± 2	0.45 ± 0.04	-64 ± 3	-123 ± 7	445 ± 3	0.10 ± 0.01
Bulk Pt	-63 ± 3	-117 ± 2	513 ± 4	0.79 ± 0.03	-69 ± 7	-140 ± 10	430 ± 12	0.13 ± 0.01

\* Region I corresponds to low current densities and Region II to high current densities.

In H<sub>2</sub>SO<sub>4</sub>, the values of SA are 2.5 to 6 times lower than in HClO<sub>4</sub> (Tables 5 and 6). The adsorbed sulfate ions are known to block the sites for O<sub>2</sub> adsorption and thereby reduce the O<sub>2</sub> reduction activity [103,106–108,142,143,179]. The strongest inhibition has been found on the Pt(111) electrodes, where a bidimensionally ordered adlayer is formed, which is more stable than the disordered adlayers on the other crystal faces [142]. On the contrary to the results obtained in HClO<sub>4</sub>, the SA of thin-film Pt electrodes in H<sub>2</sub>SO<sub>4</sub> appears to be independent of film thickness. It might be due to the different adsorption behaviour of (bi)sulfate ions as compared to adsorbed OH in HClO<sub>4</sub>. In the latter solution, the coverage of OH depends on the potential in the kinetic and mixed kinetic-diffusion region where the SA is determined and varies with the particle size as discussed above, whereas in H<sub>2</sub>SO<sub>4</sub>, the coverage of (bi)sulfate ions is approximately constant in this potential range [109]. These results are not in agreement with those obtained by Markovic et al [106], who have suggested on the basis of their observations on Pt single crystals and using Kinoshita's model of cubo-octahedral Pt particles [138] that the O<sub>2</sub> reduction activity should decrease with decreasing Pt particle size in H<sub>2</sub>SO<sub>4</sub>, as the surface fraction of Pt(111) facets increases. However, Macia et al have shown that stepped surfaces with Pt(111) terraces were considerably more active in H<sub>2</sub>SO<sub>4</sub> than Pt(111) surface and attributed this effect to the formation of

bidimensionally ordered adlayer of (bi)sulfate ions on Pt(111) [142]. In accordance with this, Komanicky et al. have found that on (111)–(100) nanofaceted Pt electrodes with the wedge-to-wedge distance about 12 nm, the activity of Pt(111) and Pt(100) facets is similar. They have proposed that sulfate adsorption is suppressed when the size of the Pt(111) terrace becomes to nanoscale [182]. This is also most likely the case on nanoparticles, therefore, the increase of the surface fraction of Pt(111) as particle size decreases does not necessarily increase the (bi)sulfate adsorption. As a result, the effect of adsorbed sulfate ions on the ORR kinetics is approximately constant over the range of particle sizes studied, whereas the adsorption of OH in HClO<sub>4</sub> solution is stronger on smaller particles and causes the decrease of O<sub>2</sub> reduction activity. Our results are in agreement with those obtained by Tamizhmani et al., who have studied the reduction of O<sub>2</sub> on Pt nanoparticles in HF and H<sub>2</sub>SO<sub>4</sub> solutions and found that the O<sub>2</sub> reduction activity decreased with decreasing particle size in the former and did not change in the latter solution [117].

The effect of particle size on the kinetics of O<sub>2</sub> reduction is of paramount importance from both fundamental and practical point of view. Even though the theoretical modelling of electrocatalytic reactions has seen an enormous progress in recent years, there is still no literature on the calculation of particle size effects for O<sub>2</sub> reduction. Up to now, all knowledge about this has been gained through experimental approaches. Unfortunately, the Pt nanoparticles preparation, characterisation and cleaning procedures differ in different laboratories and for this reason there is a large scatter in the data on the O<sub>2</sub> reduction kinetics. A deep fundamental understanding is needed in order to explain the effect of the Pt particle size in the electrocatalysis of O<sub>2</sub> reduction. These aspects are important for the development of cathode catalysts for low-temperature fuel cells [110].



## 7. SUMMARY

The electrochemical reduction of oxygen on quinone-modified carbon electrodes and on thin gold and platinum films has been studied, using the rotating disk electrode and rotating ring-disk electrode methods. The kinetic parameters for this reaction have been determined.

The covalent attachment of AQ and PQ onto carbon electrodes was achieved by the electrochemical reduction of the corresponding quinone diazonium salt. The reduction of  $O_2$  on quinone-modified electrodes proceeds via  $2e^-$  pathway, yielding hydrogen peroxide quantitatively, as confirmed by the RRDE experiments. The kinetic parameters of oxygen reduction on quinone-modified electrodes were determined, using a surface redox-catalytic cycle model. According to this model, the reduction of  $O_2$  is catalysed by quinone radical anions. For AQ-modified glassy carbon electrodes the surface concentration of quinone was varied and the average value of the rate constant for the chemical reaction between the semiquinone radical anion of AQ and molecular oxygen was determined ( $k_c = (4.7 \pm 0.3) \times 10^8 \text{ cm}^3 \text{ mol}^{-1} \text{ s}^{-1}$ ).

The surface redox-catalytic cycle model was also applied to analyse the kinetics of oxygen reduction on BDD and HOPG electrodes covalently modified with AQ and PQ. The results obtained with these modified electrodes gave further confirmation to the validity of this model. The electrocatalytic activity of PQ-modified electrodes was considerably higher than that of AQ-modified electrodes and this is primarily caused by a more positive redox potential of PQ. The redox potential of the surface-bound quinones is the main factor that determines the electrocatalytic activity of quinone-modified electrodes towards  $O_2$  reduction; the rate constant of the reaction between the semiquinone radical anion and molecular oxygen has a smaller influence.

The reduction of oxygen on vacuum-evaporated thin Au films on GC (nominal film thickness 0.25 to 20 nm) was studied in 0.5 M  $H_2SO_4$  and 0.1 M KOH solutions. The surface morphology examination by TEM revealed that the complete coverage of the substrate by gold was achieved at a nominal 10 nm Au film thickness; the thinner films consisted of separate gold clusters and the cluster size increased with increasing the loading of gold. In acid solution, the  $2e^-$  reduction of  $O_2$  prevailed on all electrodes studied and  $H_2O_2$  was further reduced only at high overpotentials. In alkaline solution, partial reduction of  $HO_2^-$  was observed for thicker films also at low overpotentials. Tafel slopes close to  $-120 \text{ mV dec}^{-1}$  were obtained for all electrodes in both solutions, indicating that the  $O_2$  reduction mechanism is the same for thin-film as for bulk Au electrodes. The specific activity of Au films only slightly decreased with decreasing film thickness in both acid and alkaline media.

The reduction of oxygen on thin Pt films (0.25–20 nm thick) prepared by electron beam evaporation onto GC and Au substrates was studied in 0.1 M  $HClO_4$  and 0.05 M  $H_2SO_4$  solutions. The surface morphology examined by TEM showed that thin Pt films on carbon consist of separate Pt particles; the

particle size increased with the film thickness. The values of Tafel slopes close to  $-120 \text{ mV dec}^{-1}$  in the high current density region and  $-60 \text{ mV dec}^{-1}$  in low current density region were obtained for all electrodes in both solutions, indicating that the mechanism of  $\text{O}_2$  reduction is the same for thin-film electrodes as for bulk Pt. The RRDE experiments revealed that on thin Pt films,  $\text{O}_2$  is predominantly reduced to  $\text{H}_2\text{O}$ . The specific activity of  $\text{O}_2$  reduction in  $\text{HClO}_4$  slightly decreased with decreasing film thickness; this was attributed to the stronger adsorption of surface oxygenated species that hinder the kinetics of  $\text{O}_2$  reduction. In  $\text{H}_2\text{SO}_4$ , the specific activity was lower than in  $\text{HClO}_4$  and appeared to be independent of the Pt loading, this is due to the adsorbed sulfate ions that are known to block the sites for  $\text{O}_2$  adsorption and thereby reduce the  $\text{O}_2$  reduction activity.

## 8. REFERENCES

- [1] R. Adzic, in: J. Lipkowski, P.N. Ross (Eds.), *Electrocatalysis*, Wiley-VCH, New York, 1998, pp. 197–242.
- [2] K. Kinoshita, *Electrochemical Oxygen Technology*, Wiley, New York, 1992.
- [3] E. Yeager, *Electrochim. Acta* 29 (1984) 1527–1537.
- [4] M.R. Tarasevich, A. Sadkowski, E. Yeager, in: B.E. Conway, J.O'M. Bockris, E. Yeager, S.U.M. Khan, R.E. White (Eds.), *Comprehensive Treatise of Electrochemistry*, Plenum Press, New York, 1983, pp. 301–398.
- [5] A. Wieckowski, E.R. Savinova, C.G. Vayenas, *Catalysis and Electrocatalysis at Nanoparticle Surface*, Dekker, New York, 2003.
- [6] N.M. Markovic, P.N. Ross, Jr., in: A. Wieckowski (Ed.), *Interfacial Electrochemistry: Theory, Experiment, and Applications*, Marcel Dekker, New York, 1999, pp. 821–841.
- [7] R. Meyer, C. Lemire, S.K. Shaikhutdinov, H. Freund, *Gold Bull.* 37 (2004) 72–124.
- [8] J.M. Campos-Martin, G. Blanco-Brieva, J.L.G. Fierro, *Angew. Chem. Int. Ed.* 45 (2006) 6962–6984.
- [9] E. Lobontseva, T. Kallio, N. Alexeyeva, K. Tammeveski, K. Kontturi, *Electrochim. Acta* 52 (2007) 7262–7269.
- [10] I. Morcos, E. Yeager, *Electrochim. Acta* 15 (1970) 953–975.
- [11] Z.W. Zhang, D.A. Tryk, E.B. Yeager, in: S. Sarangapani, J.R. Akridge, B. Schumm (Eds.), *Proc. Workshop on the Electrochemistry of Carbon*, Pennington, New Jersey, 1984, pp. 158–178.
- [12] M.S. Hossain, D. Tryk, E. Yeager, *Electrochim. Acta* 34 (1989) 1733–1737.
- [13] R.J. Taylor, A.A. Humffray, *J. Electroanal. Chem.* 64 (1975) 63–84.
- [14] C. Paliteiro, A. Hamnett, J.B. Goodenough, *J. Electroanal. Chem.* 233 (1987) 147–159.
- [15] X. Chu, K. Kinoshita, *Mater. Sci. Eng., B* 49 (1997) 53–60.
- [16] J. Xu, W.H. Huang, R.L. McCreery, *J. Electroanal. Chem.* 410 (1996) 235–242.
- [17] H.H. Yang, R.L. McCreery, *J. Electrochem. Soc.* 147 (2000) 3420–3428.
- [18] B. Sljukic, C.E. Banks, R.G. Compton, *J. Iran. Chem. Soc.* 2 (2005) 1–25.
- [19] D.A. Tryk, C. R. Cabrera, A. Fujishima, N. Spataru, in: J. Prakash, D. Scherson, I. Tae Bae, D. Chu, M. Enayetullah (Eds.), *Fundamental Understanding of Electrode Processes in Memory of Professor Ernest B. Yeager*, The Electrochemical Society Proceedings, PV 2003–30, Pennington, New Jersey, 2005, pp. 45–57.
- [20] K. Vaik, D.J. Schiffrin, K. Tammeveski, *Electrochem. Commun.* 6 (2004) 1–5.
- [21] K. Tammeveski, K. Kontturi, R.J. Nichols, R.J. Potter, D.J. Schiffrin, *J. Electroanal. Chem.* 515 (2001) 101–112.
- [22] E. Yeager, *J. Mol. Catal.* 38 (1986) 5–25.
- [23] G.S. Calabrese, R.M. Buchanan, M.S. Wrighton, *J. Am. Chem. Soc.* 105 (1983) 5594–5600.
- [24] T. Nagaoka, T. Sakai, K. Ogura, T. Yoshino, *Anal. Chem.* 58 (1986) 1953–1955.
- [25] A. Salimi, M.F. Mousavi, H. Sharghi, M. Shamsipur, *Bull. Chem. Soc. Jpn.* 72 (1999) 2121–2127.
- [26] A. Salimi, C.E. Banks, R.G. Compton, *Phys. Chem. Chem. Phys.* 5 (2003) 3988–3993.
- [27] S.M. Golabi, J.B. Raoof, *J. Electroanal. Chem.* 416 (1996) 75–82.

- [28] J.B. Raoof, S.M. Golabi, *Bull. Chem. Soc. Jpn.* 68 (1995) 2253–2261.
- [29] K. Vaik, A. Sarapuu, K. Tammeveski, F. Mirkhalaf, D.J. Schiffrin, *J. Electroanal. Chem.* 564 (2004) 159–166.
- [30] F. Mirkhalaf, K. Tammeveski, D.J. Schiffrin, *Phys. Chem. Chem. Phys.* 6 (2004) 1321–1327.
- [31] K. Vaik, U. Mäeorg, F.C. Maschion, G. Maia, D.J. Schiffrin, K. Tammeveski, *Electrochim. Acta* 50 (2005) 5126–5131.
- [32] G.S. Calabrese, R.M. Buchanan, M.S. Wrighton, *J. Am. Chem. Soc.* 104 (1982) 5786–5788.
- [33] T. Nagaoka, T. Sakai, K. Ogura, T. Yoshino, *J. Chem. Soc., Faraday Trans. I* 83 (1987) 1823–1833.
- [34] A. Salimi, H. Eshghi, H. Sharghi, S.M. Golabi, M. Shamsipur, *Electroanalysis* 11 (1999) 114–119.
- [35] B. Sljukic, C.E. Banks, R.G. Compton, *Electroanalysis* 17 (2005) 1025–1034.
- [36] B. Sljukic, C.E. Banks, S. Mentus, R.G. Compton, *Phys. Chem. Chem. Phys.* 6 (2004) 992–997.
- [37] G. Maia, F.C. Maschion, S.T. Tanimoto, K. Vaik, U. Mäeorg, K. Tammeveski, *J. Solid State Electrochem.* 11 (2007) 1411–1420.
- [38] G. Jürmann, D.J. Schiffrin, K. Tammeveski, *Electrochim. Acta* 53 (2007) 390–399.
- [39] J.S. Foord, W. Hao, S. Hurst, *Diamond Relat. Mater.* 16 (2007) 877–880.
- [40] P. Allongue, M. Delamar, B. Desbat, O. Fagebaume, R. Hitmi, J. Pinson, J.M. Saveant, *J. Am. Chem. Soc.* 119 (1997) 201–207.
- [41] J. Pinson, F. Podvorica, *Chem. Soc. Rev.* 34 (2005) 429–439.
- [42] P. Manisankar, A. Gomathi, *Electroanalysis* 17 (2005) 1051–1057.
- [43] P. Manisankar, A. Gomathi, *Bull. Chem. Soc. Jpn.* 78 (2005) 1783–1790.
- [44] P. Manisankar, A. Gomathi, D. Velayutham, *J. Solid State Electrochem.* 9 (2005) 601–608.
- [45] C. Degrand, *J. Electroanal. Chem.* 169 (1984) 259–268.
- [46] J.R.T.J. Wass, E. Ahlberg, I. Panas, D.J. Schiffrin, *J. Phys. Chem. A* 110 (2006) 2005–2020.
- [47] J.R.T.J. Wass, E. Ahlberg, I. Panas, D.J. Schiffrin, *Phys. Chem. Chem. Phys.* 8 (2006) 4189–4199.
- [48] M. Kullapere, G. Jürmann, T.T. Tenno, J.J. Paprotny, F. Mirkhalaf, K. Tammeveski, *J. Electroanal. Chem.* 599 (2007) 183–193.
- [49] C.E. Banks, G.G. Wildgoose, C.G.R. Heald, R.G. Compton, *J. Iran. Chem. Soc.* 2 (2005) 60–64.
- [50] T. Yano, D.A. Tryk, K. Hashimoto, A. Fujishima, *J. Electrochem. Soc.* 145 (1998) 1870–1876.
- [51] M.A. Genshaw, A. Damjanovic, J.O'M. Bockris, *J. Electroanal. Chem.* 15 (1967) 163–172.
- [52] M. Alvarez-Rizatti, K. Jüttner, *J. Electroanal. Chem.* 144 (1983) 351–363.
- [53] S. Strbac, R.R. Adzic, *J. Serb. Chem. Soc.* 57 (1992) 835–848.
- [54] S. Strbac, R.R. Adzic, *Electrochim. Acta* 41 (1996) 2903–2908.
- [55] V. Torma, G. Lang, *Magy. Kem. Foly.* 104 (1998) 265–276.
- [56] R.R. Adzic, S. Strbac, N. Anastasijevic, *Mater. Chem. Phys.* 22 (1989) 349–375.
- [57] R.W. Zurilla, R.K. Sen, E.B. Yeager, *J. Electrochem. Soc.* 125 (1978) 1103–1109.

- [58] H.S. Wroblowa, Y.C. Pan, G. Razumney, *J. Electroanal. Chem.* 69 (1976) 195–201.
- [59] N.R.K. Vilambi, E.J. Taylor, *J. Electroanal. Chem.* 270 (1989) 61–77.
- [60] M.R. Tarasevich, K.A. Radyushkina, V.Yu. Filinovskii, R.K. Burshtein, *Elektrokhimiya* 6 (1970) 1522–1525.
- [61] A. Damjanovic, M.A. Genshaw, J.O'M. Bockris, *J. Electroanal. Chem.* 15 (1967) 173–181.
- [62] C. Paliteiro, *Electrochim. Acta* 39 (1994) 1633–1639.
- [63] R.R. Adzic, N.M. Markovic, V.B. Vesovic, *J. Electroanal. Chem.* 165 (1984) 105–120.
- [64] N.M. Markovic, R.R. Adzic, V.B. Vesovic, *J. Electroanal. Chem.* 165 (1984) 121–133.
- [65] T.J. Schmidt, V. Stamenkovic, M. Arenz, N.M. Markovic, P.N. Ross, *Electrochim. Acta* 47 (2002) 3765–3776.
- [66] E.J. Taylor, N.R.K. Vilambi, A. Gelb, *J. Electrochem. Soc.* 136 (1989) 1939–1944.
- [67] A. Prieto, J. Hernandez, E. Herrero, J.M. Feliu, *J. Solid State Electrochem.* 7 (2003) 599–606.
- [68] B.B. Blizanac, C.A. Lucas, M.E. Gallagher, M. Arenz, P.N. Ross, N.M. Markovic, *J. Phys. Chem. B* 108 (2004) 625–634.
- [69] S. Strbac, R.R. Adzic, *J. Electroanal. Chem.* 403 (1996) 169–181.
- [70] N.M. Markovic, I.M. Tidswell, P.N. Ross, *Langmuir* 10 (1994) 1–4.
- [71] C. Paliteiro, A. Hamnett, J.B. Goodenough, *J. Electroanal. Chem.* 234 (1987) 193–211.
- [72] S. Strbac, N.A. Anastasijevic, R.R. Adzic, *J. Electroanal. Chem.* 323 (1992) 179–195.
- [73] M.H. Shao, R.R. Adzic, *J. Phys. Chem. B* 109 (2005) 16563–16566.
- [74] J.W. Kim, A.A. Gewirth, *J. Phys. Chem. B* 110 (2006) 2565–2571.
- [75] P. Vassilev, M.T.M. Koper, *J. Phys. Chem. C* 111 (2007) 2607–2613.
- [76] J.D.E. McIntyre, W.F. Peck, in: J.D.E. McIntyre, M.J. Weaver, E. Yeager (Eds.), *The Physics and Chemistry of Electrocatalysis*, The Electrochemical Society, Pennington, New Jersey, 1984, pp. 102–129.
- [77] A. Kuzume, E. Herrero, J.M. Feliu, E. Ahlberg, R.J. Nichols, D.J. Schiffrin, *Phys. Chem. Chem. Phys.* 7 (2005) 1293–1299.
- [78] J. Hernandez, J. Solla-Gullon, E. Herrero, *J. Electroanal. Chem.* 574 (2004) 185–196.
- [79] J. Hernandez, J. Solla-Gullon, E. Herrero, A. Aldaz, J.M. Feliu, *J. Phys. Chem. B* 109 (2005) 12651–12654.
- [80] J. Hernandez, J. Solla-Gullon, E. Herrero, A. Aldaz, J.M. Feliu, *J. Phys. Chem. C* 111 (2007) 14078–14083.
- [81] A.I. Gopalan, K.P. Lee, K.M. Manesh, P. Santhosh, J.H. Kim, *J. Mol. Catal. A: Chem.* 256 (2006) 335–345.
- [82] M.S. El Deab, T. Okajima, T. Ohsaka, *J. Electrochem. Soc.* 150 (2003) A851–A857.
- [83] M.S. El Deab, T. Sotomura, T. Ohsaka, *J. Electrochem. Soc.* 152 (2005) C1–C6.
- [84] M.S. El Deab, T. Sotomura, T. Ohsaka, *Electrochem. Commun.* 7 (2005) 29–34.
- [85] F.F. Gao, M.S. El Deab, T. Okajima, T. Ohsaka, *J. Electrochem. Soc.* 152 (2005) A1226–A1232.
- [86] M.S. El Deab, T. Sotomura, T. Ohsaka, *Electrochim. Acta* 52 (2006) 1792–1798.

- [87] M.S. El Deab, T. Sotomura, T. Ohsaka, *J. Electrochem. Soc.* 152 (2005) C730–C737.
- [88] Y. Zhang, V. Suryanarayanan, I. Nakazawa, S. Yoshihara, T. Shirakashi, *Electrochim. Acta* 49 (2004) 5235–5240.
- [89] Y.R. Zhang, S. Asahina, S. Yoshihara, T. Shirakashi, *Electrochim. Acta* 48 (2003) 741–747.
- [90] G. Sine, I. Duo, B. El Roustom, G. Foti, C. Comninellis, *J. Appl. Electrochem.* 36 (2006) 847–862.
- [91] I. Yagi, T. Ishida, K. Uosaki, *Electrochem. Commun.* 6 (2004) 773–779.
- [92] S. Szunerits, M. Manesse, P. Actis, B. Marcus, G. Denuault, C. Jama, R. Boukherroub, *Electrochem. Solid-State Lett.* 10 (2007) G43–G46.
- [93] S. Guerin, B.E. Hayden, D. Pletcher, M.E. Rendall, J.P. Suchsland, L.J. Williams, *J. Comb. Chem.* 8 (2006) 791–798.
- [94] C.R. Raj, A.I. Abdelrahman, T. Ohsaka, *Electrochem. Commun.* 7 (2005) 888–893.
- [95] A.I. Abdelrahman, A.M. Mohammad, T. Okajima, T. Ohsaka, *J. Phys. Chem. B* 110 (2006) 2798–2803.
- [96] N. Alexeyeva, T. Laaksonen, K. Kontturi, F. Mirkhalaf, D.J. Schiffrin, K. Tammeveski, *Electrochem. Commun.* 8 (2006) 1475–1480.
- [97] M.S. El Deab, T. Ohsaka, *Electrochem. Commun.* 4 (2002) 288–292.
- [98] M.S. El Deab, T. Ohsaka, *Electrochim. Acta* 47 (2002) 4255–4261.
- [99] A. Tegou, S. Papadimitriou, E. Pavlidou, G. Kokkinidis, S. Sotiropoulos, *J. Electroanal. Chem.* 608 (2007) 67–77.
- [100] S. Guerin, B.E. Hayden, D. Pletcher, M.E. Rendall, J.P. Suchsland, *J. Comb. Chem.* 8 (2006) 679–686.
- [101] T.V.W. Janssens, B.S. Clausen, B. Hvolbaek, H. Falsig, C.H. Christensen, T. Bligaard, J.K. Norskov, *Top. Catal.* 44 (2007) 15–26.
- [102] N.M. Markovic, R.R. Adzic, B.D. Cahan, E.B. Yeager, *J. Electroanal. Chem.* 377 (1994) 249–259.
- [103] N.M. Markovic, H.A. Gasteiger, P.N. Ross, *J. Phys. Chem.* 99 (1995) 3411–3415.
- [104] V. Stamenkovic, N.M. Markovic, P.N. Ross, *J. Electroanal. Chem.* 500 (2001) 44–51.
- [105] N.M. Markovic, H.A. Gasteiger, B.N. Grgur, P.N. Ross, *J. Electroanal. Chem.* 467 (1999) 157–163.
- [106] N. Markovic, H. Gasteiger, P.N. Ross, *J. Electrochem. Soc.* 144 (1997) 1591–1597.
- [107] J. Perez, H.M. Villullas, E.R. Gonzalez, *J. Electroanal. Chem.* 435 (1997) 179–187.
- [108] N.M. Markovic, P.N. Ross, *Surf. Sci. Rep.* 45 (2002) 121–229.
- [109] J.X. Wang, N.M. Markovic, R.R. Adzic, *J. Phys. Chem. B* 108 (2004) 4127–4133.
- [110] H.A. Gasteiger, S.S. Kocha, B. Sompalli, F.T. Wagner, *Appl. Catal. B* 56 (2005) 9–35.
- [111] J. Bett, J. Lundquist, E. Washington, P. Stonehart, *Electrochim. Acta* 18 (1973) 343–348.
- [112] K.F. Blurton, P. Greenberg, H.G. Oswin, D.R. Rutt, *J. Electrochem. Soc.* 119 (1972) 559–564.
- [113] L.J. Bregoli, *Electrochim. Acta* 23 (1978) 489–492.

- [114] M. Peuckert, T. Yoneda, R.A. Dalla Betta, M. Boudart, *J. Electrochem. Soc.* 133 (1986) 944–947.
- [115] M.L. Sattler, P.N. Ross, *Ultramicroscopy* 20 (1986) 21–28.
- [116] N. Giordano, E. Passalacqua, L. Pino, A.S. Arico, V. Antonucci, M. Vivaldi, K. Kinoshita, *Electrochim. Acta* 36 (1991) 1979–1984.
- [117] G. Tamizhmani, J.P. Dodelet, D. Guay, *J. Electrochem. Soc.* 143 (1996) 18–23.
- [118] S.L. Gojkovic, S.K. Zecevic, R.F. Savinell, *J. Electrochem. Soc.* 145 (1998) 3713–3720.
- [119] M.K. Min, J.H. Cho, K.W. Cho, H. Kim, *Electrochim. Acta* 45 (2000) 4211–4217.
- [120] F. Maillard, M. Martin, F. Gloaguen, J.M. Leger, *Electrochim. Acta* 47 (2002) 3431–3440.
- [121] O. Antoine, R. Durand, *J. Appl. Electrochem.* 30 (2000) 839–844.
- [122] O. Antoine, Y. Bultel, R. Durand, *J. Electroanal. Chem.* 499 (2001) 85–94.
- [123] S. Guerin, B.E. Hayden, C.E. Lee, C. Mormiche, J.R. Owen, A.E. Russell, B. Theobald, D. Thompsett, *J. Comb. Chem.* 6 (2004) 149–158.
- [124] K.J.J. Mayrhofer, B.B. Blizanac, M. Arenz, V.R. Stamenkovic, P.N. Ross, N.M. Markovic, *J. Phys. Chem. B* 109 (2005) 14433–14440.
- [125] M. Watanabe, H. Sei, P. Stonehart, *J. Electroanal. Chem.* 261 (1989) 375–387.
- [126] H. Yano, J. Inukai, H. Uchida, M. Watanabe, P.K. Babu, T. Kobayashi, J.H. Chung, E. Oldfield, A. Wieckowski, *Phys. Chem. Chem. Phys.* 8 (2006) 4932–4939.
- [127] K. Wikander, H. Ekström, A.E.C. Palmqvist, G. Lindbergh, *Electrochim. Acta* 52 (2007) 6848–6855.
- [128] F. Gloaguen, F. Andolfatto, R. Durand, P. Ozil, *J. Appl. Electrochem.* 24 (1994) 863–869.
- [129] F. Gloaguen, P. Convert, S. Gamburzev, O.A. Velez, S. Srinivasan, *Electrochim. Acta* 43 (1998) 3767–3772.
- [130] T.J. Schmidt, H.A. Gasteiger, G.D. Stab, P.M. Urban, D.M. Kolb, R.J. Behm, *J. Electrochem. Soc.* 145 (1998) 2354–2358.
- [131] U.A. Paulus, T.J. Schmidt, H.A. Gasteiger, R.J. Behm, *J. Electroanal. Chem.* 495 (2001) 134–145.
- [132] Y. Takasu, N. Ohashi, X.G. Zhang, Y. Murakami, H. Minagawa, S. Sato, K. Yahikozawa, *Electrochim. Acta* 41 (1996) 2595–2600.
- [133] J.A. Poirier, G.E. Stoner, *J. Electrochem. Soc.* 141 (1994) 425–430.
- [134] K. Tammeveski, T. Tenno, J. Claret, C. Ferrater, *Electrochim. Acta* 42 (1997) 893–897.
- [135] H. Ye, J.A. Crooks, R.M. Crooks, *Langmuir* 23 (2007) 11901–11906.
- [136] S. Kumar, S.Z. Zou, *Electrochem. Commun.* 8 (2006) 1151–1157.
- [137] A. Schneider, L. Colmenares, Y.E. Seidel, Z. Jusys, B. Wickman, B. Kasemo, R.J. Behm, *Phys. Chem. Chem. Phys.* 10 (2008) 1931–1943.
- [138] K. Kinoshita, *J. Electrochem. Soc.* 137 (1990) 845–848.
- [139] S. Mukerjee, J. McBreen, *J. Electroanal. Chem.* 448 (1998) 163–171.
- [140] M. Inaba, M. Ando, A. Hatanaka, A. Nomoto, K. Matsuzawa, A. Tasaka, T. Kinumoto, Y. Iriyama, Z. Ogumi, *Electrochim. Acta* 52 (2006) 1632–1638.
- [141] C. Wang, H. Daimon, Y. Lee, J. Kim, S. Sun, *J. Am. Chem. Soc.* 129 (2007) 6974–6975.
- [142] M.D. Macia, J.M. Campina, E. Herrero, J.M. Feliu, *J. Electroanal. Chem.* 564 (2004) 141–150.

- [143] A. Kuzume, E. Herrero, J.M. Feliu, *J. Electroanal. Chem.* 599 (2007) 333–343.
- [144] S.L. Chen, A. Kucernak, *J. Phys. Chem. B* 108 (2004) 3262–3276.
- [145] J. Zhang, F.H.B. Lima, M.H. Shao, K. Sasaki, J.X. Wang, J. Hanson, R.R. Adzic, *J. Phys. Chem. B* 109 (2005) 22701–22704.
- [146] J. Zhang, Y. Mo, M.B. Vukmirovic, R. Klie, K. Sasaki, R.R. Adzic, *J. Phys. Chem. B* 108 (2004) 10955–10964.
- [147] R.R. Adzic, J. Zhang, K. Sasaki, M.B. Vukmirovic, M. Shao, J.X. Wang, A.U. Nilekar, M. Mavrikakis, J.A. Valerio, F. Uribe, *Top. Catal.* 46 (2007) 249–262.
- [148] H. Yano, M. Kataoka, H. Yamashita, H. Uchida, M. Watanabe, *Langmuir* 23 (2007) 6438–6445.
- [149] V.R. Stamenkovic, B.S. Mun, M. Arenz, K.J.J. Mayrhofer, C.A. Lucas, G.F. Wang, P.N. Ross, N.M. Markovic, *Nat. Mater.* 6 (2007) 241–247.
- [150] M. Van Brussel, G. Kokkinidis, I. Vandendael, C. Buess-Herman, *Electrochem. Commun.* 4 (2002) 808–813.
- [151] M. Van Brussel, G. Kokkinidis, A. Hubin, C. Buess-Herman, *Electrochim. Acta* 48 (2003) 3909–3919.
- [152] M. Desic, M.M. Popovic, M.D. Obradovic, L.M. Vracar, B.N. Grgur, *J. Serb. Chem. Soc.* 70 (2005) 231–242.
- [153] M.I. Awad, M.S. El Deab, T. Ohsaka, *J. Electrochem. Soc.* 154 (2007) B810–B816.
- [154] A. Kongkanand, S. Kuwabata, *J. Phys. Chem. B* 109 (2005) 23190–23195.
- [155] J.L. Zhang, M.B. Vukmirovic, Y. Xu, M. Mavrikakis, R.R. Adzic, *Angew. Chem. Int. Ed.* 44 (2005) 2132–2135.
- [156] K. Sasaki, Y. Mo, J.X. Wang, M. Balasubramanian, F. Uribe, J. McBreen, R.R. Adzic, *Electrochim. Acta* 48 (2003) 3841–3849.
- [157] A.U. Nilekar, Y. Xu, J. Zhang, M.B. Vukmirovic, K. Sasaki, R.R. Adzic, M. Mavrikakis, *Top. Catal.* 46 (2007) 276–284.
- [158] Y.D. Jin, Y. Shen, S.J. Dong, *J. Phys. Chem. B* 108 (2004) 8142–8147.
- [159] J.F. Zhai, M.H. Huang, S.J. Dong, *Electroanalysis* 19 (2007) 506–509.
- [160] B. El Roustom, G. Sine, G. Foti, C. Comninellis, *J. Appl. Electrochem.* 37 (2007) 1227–1236.
- [161] R. Zeis, A. Mathur, G. Fritz, J. Lee, J. Erlebacher, *J. Power Sources* 165 (2007) 65–72.
- [162] J. Luo, P.N. Njoki, Y. Lin, L. Wang, C.J. Zhong, *Electrochem. Commun.* 8 (2006) 581–587.
- [163] M.M. Maye, N.N. Kariuki, J. Luo, L. Han, P. Njoki, L.Y. Wang, Y. Lin, H.R. Naslund, C.J. Zhong, *Gold Bull.* 37 (2004) 217–223.
- [164] P. Hernandez-Fernandez, S. Rojas, P. Ocon, J.L.G. de la Fuente, J.S. Fabian, J. Sanza, M.A. Pena, F.J. Garcia-Garcia, P. Terreros, J.L.G. Fierro, *J. Phys. Chem. C* 111 (2007) 2913–2923.
- [165] J. Zhang, K. Sasaki, E. Sutter, R.R. Adzic, *Science* 315 (2007) 220–222.
- [166] J.K. Norskov, J. Rossmeisl, A. Logadottir, L. Lindqvist, J.R. Kitchin, T. Bligaard, H. Jonsson, *J. Phys. Chem. B* 108 (2004) 17886–17892.
- [167] M.P. Hyman, J.W. Medlin, *J. Phys. Chem. C* 111 (2007) 17052–17060.
- [168] K.J.J. Mayrhofer, D. Strmcnik, B.B. Bliznac, V. Stamenkovic, M. Arenz, N.M. Markovic, *Electrochim. Acta* 53 (2008) 3181–3188.
- [169] M.F.W. Dunker, E.B. Starkey, G.L. Jenkins, *J. Am. Chem. Soc.* 58 (1936) 2308–2309.
- [170] R.E. Davis, G.L. Horvath, C.W. Tobias, *Electrochim. Acta* 12 (1967) 287–297.



- [171] D.R. Lide (Ed.), *CRC Handbook of Chemistry and Physics*, 82<sup>nd</sup> Ed., CRC Press, Boca Raton, 2001.
- [172] N. Alexeyeva, K. Tammeveski, *Electrochem. Solid-State Lett.* 10 (2007) F18–F21.
- [173] S. Gottesfeld, I.D. Raistrick, S. Srinivasan, *J. Electrochem. Soc.* 134 (1987) 1455–1462.
- [174] J. Maruyama, M. Inaba, Z. Ogumi, *Electrochim. Acta* 45 (1999) 415–422.
- [175] J. Maruyama, M. Inaba, T. Morita, Z. Ogumi, *J. Electroanal. Chem.* 504 (2001) 208–216.
- [176] J. Maruyama, I. Abe, *J. Electroanal. Chem.* 527 (2002) 65–70.
- [177] M.O. Pedersen, S. Helveg, A. Ruban, I. Stensgaard, E. Laegsgaard, J.K. Norskov, F. Besenbacher, *Surf. Sci.* 426 (1999) 395–409.
- [178] H. Angerstein-Kozłowska, B.E. Conway, B. Barnett, J. Mozota, *J. Electroanal. Chem.* 100 (1979) 417–446.
- [179] T.J. Schmidt, U.A. Paulus, H.A. Gasteiger, R.J. Behm, *J. Electroanal. Chem.* 508 (2001) 41–47.
- [180] R.R. Adzic, J. Wang, B.M. Ocko, *Electrochim. Acta* 40 (1995) 83–89.
- [181] Y. Gohda, A. Gross, *J. Electroanal. Chem.* 607 (2007) 47–53.
- [182] V. Komanicky, A. Menzel, H. You, *J. Phys. Chem. B* 109 (2005) 23550–23557.

## 9. KOKKUVÕTE

### Hapniku elektrokeemiline redutseerumine kinoonidega modifitseeritud süsinikelektroodidel ning õhukestel plaatina- ja kuldkatetel

Doktoritöös uuriti hapniku elektrokeemilist redutseerumist kinoonidega modifitseeritud süsinikelektroodidel ning õhukestel kuld- ja platinakiledel, kasutades pöörleva ketaselektroodi ja pöörlev ketaselektrood rõngaga meetodeid. Saadud andmete põhjal määrati hapniku redutseerumisreaktsiooni kineetilised parameetrid nendel elektroodidel.

Töö esimeses osas uuriti hapniku redutseerumist kinoonidega modifitseeritud süsinikelektroodidel 0,1 M KOH lahuses. Antrakinoon ja fenantreenkinoon seondati kovalentselt elektroodide pinnale, kasutades diasooniumisoola redutseerumise meetodit. Kinoonidega modifitseeritud elektroodidel toimub hapniku kaheelktroniline redutseerumine ja tekib vesinikperoksiid, mis edasi ei redutseeru; seda kinnitasid ka pöörlev ketaselektrood rõngaga meetodil läbi viidud eksperimendid. Hapniku redutseerumise kineetiliste parameetrite määramiseks kinoonidega modifitseeritud elektroodidel kasutati pinnal toimuva redoks-katalüütilise tsükli mudelit, mille kohaselt on O<sub>2</sub> redutseerumisel katalüütiliselt aktiivsed kinooni radikaalanioonid. Antrakinooniga modifitseeritud klaassüsinikelektroodidel varieeriti eksperimentide käigus kinooni pindkontsentratsiooni ning leiti, et kinooni radikaalaniooni ja hapniku vahelise reaktsiooni kiirus on võrdeline kinooni pindkontsentratsiooniga. Selle reaktsiooni kiiruskonstandi keskmiseks väärtuseks saadi  $k_c = (4,7 \pm 0,3) \times 10^8 \text{ cm}^3 \text{ mol}^{-1} \text{ s}^{-1}$ .

Järgnevalt uuriti hapniku redutseerumise kineetikat antrakinooni ja fenantreenkinooniga kovalentselt modifitseeritud booriga dopeeritud teemant-elektroodil ja kõrgorienteeritud pürolüütilisest grafiidist elektroodil. Andmete analüüsimisel kasutati taas pinnal toimuva redokskatalüütilise tsükli mudelit ning saadud tulemused kinnitasid, et mudel kehtib erinevate substraatide korral. Fenantreenkinooniga modifitseeritud elektroodide elektrokatalüütiline aktiivsus oli oluliselt kõrgem kui antrakinooniga modifitseeritud elektroodidel ja see on tingitud peamiselt fenantreenkinooni positiivsemast redokspotentsiaalst. Kinooni redokspotentsiaal on kõige olulisem parameeter, mis määrab modifitseeritud elektroodide elektrokatalüütilise aktiivsuse; kinooni radikaalaniooni ja molekulaarse hapniku vahelise reaktsiooni kiiruskonstant avaldab väiksemat mõju.

Töö teises osas uuriti hapniku redutseerumist klaassüsinikule vaakumaurustatud õhukestel kuldkatetel nominaalse paksusega 0,25 kuni 20 nm 0,5 M H<sub>2</sub>SO<sub>4</sub> ja 0,1 M KOH lahustes. Pinna morfoloogia iseloomustamiseks kasutati läbistuselektronmikroskoopiat. Pind oli täielikult kullaga kaetud 10 nm ja paksemate katete korral, õhemad katted olid saarelise struktuuriga ja saarekese suurus vähenes Au kattepaksuse kahanedes. Happelises lahuses

toimus kuldelektroodidel valdavalt kaheellektroniline redutseerumine ja moodustuv vesinikperoksiid redutseerus edasi vaid kõrgetel ülepingetel. Leeliselises lahuses esines  $\text{HO}_2^-$  edasine redutseerumine paksemate Au katete korral ka madalatel ülepingetel. Tafeli tõusu väärtuseks saadi  $-120 \text{ mV dec}^{-1}$  kõigi uuritud elektroodide korral mõlemas lahuses ja see annab tunnistust, et reaktsioonimehhanism õhukesekilelistel elektroodidel on sama, mis kompaktsel kuldelektroodil. Au kilede eriaktiivsus vähesel määral langes kattepaksuse kahanedes nii happelises kui ka leeliselises lahuses.

Hapniku redutseerumist uuriti ka klaassüsinikule ja kuldalusele vaakumaurustatud õhukestel platinakiledel  $0,1 \text{ M HClO}_4$  ja  $0,05 \text{ M H}_2\text{SO}_4$  lahustes. Pinna morfoloogia uurimine läbistuselektronmikroskoobi abil näitas, et õhukesed Pt kiled koosnevad Pt osakestest ning osakese suurus kasvab Pt katte paksenedes. Tafeli tõusu väärtused olid uuritud elektroodidel mõlemas lahuses ligikaudu  $-120 \text{ mV dec}^{-1}$  kõrge voolutihedusega alas ja  $-60 \text{ mV dec}^{-1}$  madala voolutihedusega alas, mis annab tunnistust, et reaktsioonimehhanism ei sõltu katte paksusest ja on sama, mis kompaktsel Pt elektroodil. Pöörlev ketas-elektrood rõngaga meetodil läbi viidud eksperimendid kinnitasid, et hapniku redutseerumine õhukesekilelistel plaatinaelektroodidel kulgeb peamiselt vee tekkeni. Hapniku elektrookeemilise redutseerumise eriaktiivsus  $\text{HClO}_4$  lahuses mõnevõrra vähenes Pt katte õhenedes ja selle põhjuseks võib olla hapnikkusisaldavate (vahe)ühendite tugevam adsorptsioon väiksematel Pt osakestel. Need ühendid blokeerivad  $\text{O}_2$  adsorptsioonitsentrid ja pärsivad seega  $\text{O}_2$  redutseerumise kineetikat.  $\text{H}_2\text{SO}_4$  lahuses oli eriaktiivsus madalam kui  $\text{HClO}_4$ -s ja ei sõltunud Pt kattepaksusest ning selle põhjuseks on pinna tsentrite blokeerimine adsorbeerunud sulfaatioonide poolt.

## 10. ACKNOWLEDGEMENTS

First, I would like to express my sincere gratitude to my doctoral advisor Dr. Kaido Tammeveski for his invaluable assistance, scientific guidance and encouragement through the years of my studies.

I am very grateful to Prof. David J. Schiffrin for sharing his ideas and expertise that led to our fruitful collaboration.

I would like to thank the staff at the Institute of Physics, especially Aarne Kasikov and Dr. Arnold Rosental for preparing thin metal films, Dr. Leonard Matisen for the XPS measurements, Dr. Hugo Mändar for GIXRD studies and Prof. Väino Sammelselg for AFM studies and helpful discussions.

I also thank Prof. Kyösti Kontturi and Dr. Timo Laaksonen at the Helsinki University of Technology for performing the TEM measurements.

I wish to express my sincere appreciation to Prof. Toomas Tenno and my colleagues at the Chair of Colloid and Environmental Chemistry for collaboration, encouragement and good company.

My warmest thanks go to my husband, children and parents for their continuous support, patience and understanding.

The financial support from the Estonian Science Foundation (Grants Nos. 4623, 5831 and 7546), European Union Framework V Growth program, CLETEPEG project (contract no. G5RD-CT-2001-00463) and European Union Framework VI program, NENA Project (contract No. NMP3-CT-2004-505906) is gratefully acknowledged.

## **II. PUBLICATIONS**





A. Sarapuu, K. Vaik, D.J. Schiffrin, K. Tammeveski,  
Electrochemical reduction of oxygen on anthraquinone-modified glassy carbon  
electrodes in alkaline solution, *Journal of Electroanalytical Chemistry*  
541 (2003) 23–29.

Reprinted with permission from Elsevier, Copyright (2002).



## II

**A. Sarapuu**, K. Helstein, D.J. Schiffrin, K. Tammeveski,  
Kinetics of Oxygen Reduction on Quinone-Modified HOPG and BDD Electrodes  
in Alkaline Solution, *Electrochemical and Solid State Letters* 8 (2005) E30–E33.

Reproduced by permission of ECS – The Electrochemical Society.



**A. Sarapu**, K. Tammeveski, T.T. Tenno, V. Sammelselg, K. Kontturi, D.J. Schiffrin,  
Electrochemical reduction of oxygen on thin-film Au electrodes in acid solution,  
*Electrochemistry Communications* 3 (2001) 446–450.

Reprinted with permission from Elsevier, Copyright (2001).



**A. Sarapuu**, M. Nurmik, H. Mändar, A. Rosental, T. Laaksonen, K. Kontturi, D.J. Schiffrin, K. Tammeveski, Electrochemical reduction of oxygen on nanostructured gold electrodes, *Journal of Electroanalytical Chemistry* 612 (2008) 78–86.

Reprinted with permission from Elsevier, Copyright (2007).

v

**A. Sarapuu**, A. Kasikov, T. Laaksonen, K. Kontturi, K. Tammeveski, Electrochemical reduction of oxygen on thin-film Pt electrodes in acid solutions, *Electrochimica Acta* (2008, in press) (doi:10.1016/j.electacta.2008.04.003).

Reprinted with permission from Elsevier, Copyright (2008).



**A. Sarapu**, A. Kasikov, L. Matisen, K. Tammeveski, Electroreduction of oxygen on gold-supported thin Pt films in acid solutions, *Journal of Electroanalytical Chemistry*, submitted (JELECHEM-D-08-00120)

# Electroreduction of oxygen on gold-supported thin Pt films in acid solutions

Ave Sarapuu<sup>a</sup>, Aarne Kasikov<sup>b</sup>, Leonard Matisen<sup>b</sup>, Kaido Tammeveski<sup>a,1</sup>

<sup>a</sup>*Institute of Chemistry, University of Tartu, Jakobi 2, 51014 Tartu, Estonia*

<sup>b</sup>*Institute of Physics, University of Tartu, Riia 142, 51014 Tartu, Estonia*

## ABSTRACT

The electrochemical reduction of oxygen was studied on vacuum evaporated thin Pt films (0.25–20 nm thick) on polycrystalline Au substrate (Pt/Au) in 0.1 M HClO<sub>4</sub> and 0.05 M H<sub>2</sub>SO<sub>4</sub> solutions using the rotating disk electrode (RDE) method. The O<sub>2</sub> reduction specific activity of Pt films increased with increasing the film thickness in HClO<sub>4</sub>, but was lower than that of bulk Pt even for the thickest films. In H<sub>2</sub>SO<sub>4</sub>, the specific activity showed no significant dependence on the platinum loading and was lower than in HClO<sub>4</sub>. The Tafel slope values characteristic to polycrystalline Pt (–120 mV dec<sup>–1</sup> and –60 mV dec<sup>–1</sup>) were found for all electrodes. The RRDE studies of 0.5 nm Pt/Au electrode revealed that O<sub>2</sub> reduction predominantly proceeds through 4e<sup>–</sup> pathway and H<sub>2</sub>O<sub>2</sub> is produced in low quantities.

**Keywords:** Oxygen reduction; Electrocatalysis; Kinetic parameters; Gold support; Pt film

## 1. INTRODUCTION

The oxygen reduction reaction (ORR) on platinum-based catalysts has been widely studied due to their technical application in fuel cell cathodes [1,2]. Considerable efforts have been directed towards improving the catalyst efficiency of energy conversion and lowering the content of costly Pt in electrocatalysts [3]. For this purpose, numerous investigations have been carried out using Pt nanoparticles supported on porous carbon [3–7]. However, it has been found that the specific activity (SA) of oxygen reduction decreases with

---

<sup>1</sup> Corresponding author. Tel.: +372 7375168; fax: +372 7375181.  
E-mail address: kaido@chem.ut.ee (K. Tammeveski).

decreasing particle size [3–6]. A promising way to further reduce the Pt content in ORR electrocatalysts without losing activity involves using Pt alloys with other metals or very thin Pt layers supported on metal nanoparticles [8,9]. In such bimetallic systems, the activity of Pt can be changed through electronic and/or geometric effects [8–10].

Due to its inertness, gold is a metal of choice to be used in combination with Pt. There are several reports on O<sub>2</sub> reduction studies for Pt catalysts supported on various forms of gold: bulk polycrystalline Au [11–14], Au(111) monocrystal [15–18], Au nanoparticles [17,19,20] and Au sputtered onto BDD [21]. Bare gold is much less active electrocatalyst than platinum for ORR in acid media [22–25]. However, in some cases it has been found that the activity of gold-supported Pt is higher than that of bulk platinum. Van Brussel et al have studied O<sub>2</sub> reduction on polycrystalline gold electrodes modified by Pt and noted that the electrocatalytic activity of the electrodes was lower than that of the bulk Pt electrode in the negative potential scan, but significantly higher in the positive scan [11,12]. Desic et al have also found that in the high current density region, Au–Pt electrodes showed higher O<sub>2</sub> reduction activities than pure platinum [13]. On the other hand, Pt monolayer [15,16,18] and Pt islands [15] on Au(111) appeared to be less active than bulk Pt. The activity of Au/Pt core-shell nanoparticles increased with increasing the thickness of the Pt shell [20]. In addition, O<sub>2</sub> reduction has also been studied on Pt-Au alloy nanoparticles and their activity increased with increasing the Pt content in alloy in acid media [26,27]. The activity of Pt-Au alloy nanoparticles depends on the preparation method and may be almost equal to the activity of Pt particles [28]. It has recently been demonstrated that modifying Pt nanoparticles with Au clusters considerably stabilizes these catalysts during prolonged potential cycling [29].

The change of the Pt reactivity in the Pt-Au bimetallic systems has also been a subject of theoretical modelling. These calculations have indicated that the oxygen reduction activity of transition metal catalysts is primarily determined by changes in the oxygen binding energy, however, the OH bonding energy is also important [30]. Zhang et al have found that ORR electrocatalytic activity of platinum monolayers supported on other metal monocrystals show a volcano-type dependence on the d-band centre of the platinum monolayer structures [16]. Recently, it was shown using DFT calculations that the adsorption energy of oxygenated intermediates does not depend solely on the d-band centre of the surface, but also on the electron density near the Fermi level. The relationship between electronic structure and adsorption energies of the O<sub>2</sub> reduction intermediates (O, OH, OOH, O<sub>2</sub>, and H<sub>2</sub>O) was modelled for modified Pt surfaces, including Pt-Au systems. It was found that for instance, Pt pseudomorphic overlayer on Au(111) binds both O and OH more strongly than Pt(111) [31].

Adsorbed OH on Pt is known to inhibit the ORR by the site-blocking and electronic effects [32,33]. In bimetallic systems, the coverage of Pt by OH may

be lower due to the lateral repulsion, in case OH binds on the neighbouring metal more strongly. Au, however, is known to bind OH more weakly, therefore, the O<sub>2</sub> reduction currents were lower on Pt-Au monolayer on Pd(111) than these on Pt monolayer [34].

Besides the adsorption of oxygenated species, the O<sub>2</sub> reduction activity of Pt is highly affected by the adsorption of other ions, like (bi)sulfate and halide anions [35]. In H<sub>2</sub>SO<sub>4</sub> solution, the greatest decrease in O<sub>2</sub> reduction activity has been observed on Pt(111) plane due to the formation of an ordered adlayer of specifically adsorbed anions [33,36–41].

The aim of this work was to study the electrochemical reduction of O<sub>2</sub> on vacuum-evaporated thin Pt films on gold support in 0.1 M HClO<sub>4</sub> and 0.05 M H<sub>2</sub>SO<sub>4</sub> solutions in order to determine the effects of anion adsorption and Pt film thickness on the kinetics of oxygen reduction.

## 2. EXPERIMENTAL

Bulk polycrystalline gold and platinum electrodes were prepared by mounting Au and Pt disks into Teflon holders. The geometrical area of the electrodes (*A*) was 0.2 cm<sup>2</sup>. Surface of the electrodes was polished to a mirror finish with 1.0 μm, 0.3 μm and 0.05 μm alumina powder (Buehler). After polishing, the electrodes were ultrasonically cleaned in Milli-Q (Millipore, Inc.) water for 5 minutes.

Thin films of Pt having a nominal thickness (*h*) of 0.25 to 20 nm were prepared on the Au substrates by electron beam evaporation. The nominal film thickness represents the catalyst loading and both terms are used throughout the manuscript. The evaporation was made from a graphite crucible using Vacuum Service OY evaporation device at a base pressure of around  $2 \times 10^{-6}$  Torr. For X-ray photoelectron spectroscopy (XPS) studies, the Pt films were evaporated onto Gold arrandee<sup>TM</sup> specimen (250 ± 50 nm thick gold film with a pre-layer of 2.5 ± 1.5 nm of chromium on a borosilicate glass slides, 11 × 11 mm<sup>2</sup>). The XPS experiments were carried out with a SCIENTA SES-100 spectrometer using an unmonochromated Mg K $\alpha$  X-ray source (incident energy = 1253.6 eV), electron take-off angle of 90° and a source power of 400 W. The pressure in the analysis chamber was below 10<sup>-9</sup> Torr. While collecting the high resolution scan, the following parameters were used: energy range = 95–60 eV, pass energy = 200 eV and step size = 0.1 eV.

Oxygen reduction was studied in 0.1 M HClO<sub>4</sub> and 0.05 M H<sub>2</sub>SO<sub>4</sub> using the rotating disk electrode (RDE) and rotating ring-disk electrode (RRDE) methods. A saturated calomel electrode (SCE) was employed as a reference and all the potentials are referred to this electrode. The counter electrode compartment of the three-electrode cell was separated by a glass frit from the main cell compartment, Pt wire served as a counter electrode. The potential was applied with an Autolab potentiostat PGSTAT30 (Eco Chemie B.V., The Netherlands)

and the experiments were controlled with General Purpose Electrochemical System (GPES) software. The solutions were prepared from 70% HClO<sub>4</sub> (Suprapur, Merck) and 96% H<sub>2</sub>SO<sub>4</sub> (Suprapur, Merck) and Milli-Q (Millipore, Inc) water; these were saturated with pure O<sub>2</sub> (99.999%, AGA) or deaerated with Ar gas (99.999%, AGA). An EDI101 rotator and a CTV101 speed control unit (Radiometer, Copenhagen) were used for the RDE experiments. The rotating ring-disk electrode (RRDE) experiments were carried out on an Au disk-Pt ring electrode (Pine Instruments,  $A = 0.164 \text{ cm}^2$ ) with the collection efficiency of  $N = 0.22$ . A Pine Instrument Company (Grove City, PA, USA) AFMSRX rotator and MSRX speed controller were used for the RRDE measurements. The Pt ring electrode potential for detecting peroxide was set to 0.95 V. All experiments were carried out at room temperature ( $23 \pm 1^\circ\text{C}$ ).

Prior to the O<sub>2</sub> reduction measurements, the electrodes were electrochemically pre-treated in 0.1 M HClO<sub>4</sub> or 0.05 M H<sub>2</sub>SO<sub>4</sub> by scanning the potential between  $-0.25$  and  $1.15 \text{ V}$  at  $100 \text{ mV s}^{-1}$  until a stable CV response was obtained (10–30 cycles). To study the effect of electrochemical treatment on Pt films, the Pt films evaporated onto Gold arrandee<sup>TM</sup> samples were treated by scanning the potential between  $-0.25$  and  $1.15 \text{ V}$  at  $100 \text{ mV s}^{-1}$  for 30 cycles and the XPS spectra were acquired after that.

The real surface area ( $A_r$ ) of Pt was determined by charge integration under the hydrogen desorption peaks, assuming a charge of  $210 \mu\text{C cm}^{-2}$  for the electroactive Pt surface [42]. After potential cycling the electrodes were immediately transferred to an O<sub>2</sub>-saturated solution in another cell in order to avoid surface contamination in air. For O<sub>2</sub> reduction measurements, the potential was held at  $0.8 \text{ V}$  for 5 s and scanned between  $0.8$  and  $-0.2 \text{ V}$  at  $10 \text{ mV s}^{-1}$ .

### 3. RESULTS AND DISCUSSION

#### 3.1 XPS analysis

The X-ray photoelectron spectroscopy (XPS) measurements were conducted on as-prepared and electrochemically treated 0.25 nm, 0.5 nm and 5 nm Pt films on Au substrate in order to evaluate the possible loss of Pt during potential cycling (Figure 1). The survey spectra (not presented) showed the peaks of Au, Pt, O and C, originating from Au substrate, Pt film, oxygen containing adsorbates and carbon containing contaminants, respectively. High resolution spectra of Pt4f region showed doublet with peaks at about  $71.0 \text{ eV}$  (Pt4f<sub>7/2</sub>) and  $74.3 \text{ eV}$  (Pt4f<sub>5/2</sub>) (Figure 1), these values are characteristic to bulk Pt [43,44]. Au4f<sub>7/2</sub> and Au4f<sub>5/2</sub> peaks are located at  $83.8 \text{ eV}$  and  $87.5 \text{ eV}$ , respectively, and Au satellite peaks at  $75.5$  and  $79 \text{ eV}$ , the former appearing as a shoulder on Pt4f<sub>5/2</sub> peak. In addition, the slightly asymmetrical shape of Pt4f peaks may be due to the

overlapping Pt(II) peaks corresponding to PtO that appear at higher binding energy than Pt(0) [43], or the effect of Pt-Au interface.

Comparing the areas under Pt4f<sub>7/2</sub> peaks before and after potential cycling reveals that the amount of Pt has slightly decreased. This is not unexpected, as it has been noted before that nanostructured Pt may dissolve during cycling [45]. For as-prepared 5 nm Pt/Au film, the intensity of Au peaks was very low, but it was increased about two times for the cycled sample, indicating possible diffusion of Au atoms into the overlying Pt film.

### 3.2 Cyclic voltammetry (CV)

In order to achieve the stable Pt films or islands on gold, the electrodes were cycled in the Ar-saturated HClO<sub>4</sub> or H<sub>2</sub>SO<sub>4</sub> solutions prior to the O<sub>2</sub> reduction measurements. The representative cyclic voltammograms of Pt/Au electrodes after repeated potential cycling in 0.1 M HClO<sub>4</sub> and 0.05 M H<sub>2</sub>SO<sub>4</sub> are shown in Figure 2. The CV responses of the Pt/Au electrodes were in general similar to that of the polycrystalline Pt, but the current peaks related to Au surface oxide formation (at  $E > 0.9$  V in HClO<sub>4</sub> and  $E > 1$  V in H<sub>2</sub>SO<sub>4</sub>) and reduction (around 0.87 V) are in evidence even for relatively thick Pt films ( $h = 5$  nm). For thinner films these peaks slightly increased during potential cycling, indicating the change of the morphology of the electrodes and possible diffusion of Au onto the surface of Pt. For thick Pt films the residual Au peaks are apparently related to a small leakage of the electrolyte to the side area of Au disks. This side surface does not give any contribution to the oxygen reduction current in the potential range of interest. The peak potential of the reduction of Pt surface oxides was more negative for Pt/Au electrodes as compared to bulk Pt and it shifted negatively with decreasing the film thickness. The negative shift of the oxide reduction peak of Pt/Au bimetallic systems has been observed before and it has been attributed to the changes in the electronic properties of the surface that increase the binding energy of adsorbed oxygen containing species [13,15,20]. In addition to the electronic effects caused by the Au substrate, the electronic properties of Pt nanoparticles may change as the particle size decreases, because the coordination number of the surface atoms decreases [6].

The real surface area ( $A_r$ ) of Pt was determined by charge integration under the H<sub>upd</sub> desorption peaks. During the initial potential cycling, some decrease in  $A_r$  was observed, especially for the thinner films, where the decrease was up to 20%. This can be attributed to the change of surface morphology, possibly the diffusion of subsurface Au atoms onto the Pt surface. The final  $A_r$  value was considerably increasing with the Pt loading for thinner films ( $h < 5$  nm), from approximately  $A_r / A \approx 0.3$  to  $A_r / A \approx 2$  for 0.25 nm and 5 nm films, respectively. It should be noted that the real surface area of Pt for thinner Pt films is smaller for Pt/Au electrodes than for Pt/GC electrodes of the same nominal film thickness [46]. It may be due to different morphology of the films,

or to the surface alloying and Au segregation that is expected to take place during cycling. Pedersen et al have calculated the surface energy of Pt-Au surface alloy and found it to be larger than that of Pt-Au capped by pure Au “skin”, therefore, Pt atoms tend to diffuse away from the top layer [47].

### 3.3 Oxygen reduction

The electrochemical reduction of O<sub>2</sub> on Pt/Au electrodes was studied in 0.1 M HClO<sub>4</sub> and 0.05 M H<sub>2</sub>SO<sub>4</sub> solutions using the RDE method. In Figure 3, the representative *I-E* curves (cathodic sweeps only) are depicted at various rotation rates; the background current has been subtracted from these data. The single-wave polarisation curves for O<sub>2</sub> reduction similar to polycrystalline Pt were observed for all electrodes in both solutions, but in H<sub>2</sub>SO<sub>4</sub> the electrocatalytic activity was lower, the half-wave potential being about 60 mV more negative (Table 1). The decrease in the O<sub>2</sub> reduction activity of Pt in solutions containing ions that show specific adsorption, such as (bi)sulfate, is well known and it has been attributed to the blocking the O<sub>2</sub> adsorption centres [33,36–40] and possible negative electronic effect on the ORR kinetics [33].

The number of electrons transferred per O<sub>2</sub> molecule (*n*) was calculated from the RDE data using the Koutecky-Levich (K-L) equation:

$$\frac{1}{j} = \frac{1}{j_k} + \frac{1}{j_d} = -\frac{1}{nFkC_{O_2}^b} - \frac{1}{0.62nFD_{O_2}^{2/3}\nu^{-1/6}C_{O_2}^b\omega^{1/2}} \quad (1)$$

where *j* is the measured current density, *j<sub>k</sub>* and *j<sub>d</sub>* are the kinetic and diffusion-limited current densities, respectively, *k* is the rate constant for O<sub>2</sub> reduction, *F* is the Faraday constant (96485 C mol<sup>-1</sup>), *ω* is the rotation rate, *C<sub>O<sub>2</sub></sub><sup>b</sup>* is the concentration of oxygen in the bulk (1.22 × 10<sup>-6</sup> mol cm<sup>-3</sup>) [48], *D<sub>O<sub>2</sub></sub>* is the diffusion coefficient of oxygen (1.93 × 10<sup>-5</sup> cm<sup>2</sup> s<sup>-1</sup>) [48] and *ν* is the kinematic viscosity of the solution (0.01 cm<sup>2</sup> s<sup>-1</sup>) [49].

For all Pt/Au electrodes studied, the average value of *n* = 3.9 ± 0.1 was obtained and there was no clear dependence on the Pt loading. This is an indication that O<sub>2</sub> reduction predominantly follows the 4e<sup>-</sup> pathway. Production of small amount of H<sub>2</sub>O<sub>2</sub> is possible on thinner films, since there is a significant amount of free Au substrate that supports partial 2e<sup>-</sup> reduction of O<sub>2</sub> at potentials *E* < 0.25 V. However, part of the H<sub>2</sub>O<sub>2</sub> produced on Au sites is expected to be further reduced to water at nearby Pt islands.

In order to evaluate the fraction of H<sub>2</sub>O<sub>2</sub> formation, the RRDE experiments were carried out on the 0.5 nm Pt/Au electrode (Figure 4). The potential of Pt ring was set to *E* = 0.95 V, at which the oxidation of H<sub>2</sub>O<sub>2</sub> is diffusion limited. The fraction of H<sub>2</sub>O<sub>2</sub> formation on the disk was calculated from [50]:

$$X_{H_2O_2} = \frac{200I_R/N}{I_D + I_R/N} \quad (2)$$

where  $I_R$  is the ring current,  $I_D$  is the disk current and  $N$  is the collection efficiency ( $N = 0.22$ ). The ring current was rather small at the potentials of  $E > -0.1$  V, corresponding to less than 5% of  $H_2O_2$  formation. At more negative potentials the  $H_2O_2$  production significantly increased and the  $O_2$  reduction current ( $I_D$ ) decreased accordingly. This has been attributed to the blocking of the sites for dissociative adsorption of oxygen molecules by adsorbed hydrogen atoms [36]. There are no remarkable differences between the  $H_2O_2$  formation in  $HClO_4$  and  $H_2SO_4$ , only slightly more  $H_2O_2$  is produced in the latter solution.

Small amounts of  $H_2O_2$  produced have been found for Pt monolayers on Au [16] and significant formation of  $H_2O_2$  for AuPt alloy nanoparticle catalysts [26,27], whereas on Pt-coated Au nanoparticles,  $O_2$  was completely reduced to  $H_2O$  [19].

The mass-transfer corrected Tafel plots were constructed from the RDE data (Figure 5). It is evident that the Tafel slope gradually changes between  $0.45 < E < 0.5$  V, from  $-60 \text{ mV dec}^{-1}$  at low current density region to  $-120 \text{ mV dec}^{-1}$  at high current density region (Table 1). These values are typical for polycrystalline platinum [1,2], therefore, it may be concluded that the ORR mechanism is not modified by the presence of the Au substrate. The slope of  $-120 \text{ mV dec}^{-1}$  indicates that the transfer of the first electron to  $O_2$  molecule is the rate determining step. The change of the slope has been previously attributed to potential-dependent coverage of surface oxides that inhibit the adsorption of  $O_2$  and reaction intermediates [41,51]. The values of Tafel slopes appeared to be independent of the Pt film thickness and were similar in  $HClO_4$  and  $H_2SO_4$ . These results are in accordance of the slope values of  $-122 \text{ mV dec}^{-1}$  and  $-64 \text{ mV dec}^{-1}$  obtained for PtAu alloy nanoparticles [28]. Single Tafel slopes near to  $-120 \text{ mV dec}^{-1}$  have been observed for Pt monolayers on Au nanoparticles and Au(111) [17] and  $-86 \text{ mV dec}^{-1}$  for Pt monolayer on Au(111) [15], this was attributed to reduced coverage of adsorbed OH on the Pt/Au catalysts in comparison with pure Pt.

It can be seen in Figure 5 that the electrocatalytic activity of the Pt/Au electrodes decreases with decreasing film thickness in both solutions; this is mainly caused by the decrease of the real surface area of Pt. The half-wave potential ( $E_{1/2}$ ) of  $O_2$  reduction for the electrode of lowest Pt loading is about 100 mV more negative than that of the highest loadings and bulk Pt (Table 1). The onset of  $O_2$  reduction wave on bulk Au in acid solution is around 0.25 V vs SCE (data not shown). Therefore, at more positive potentials all electrode activity is due to the Pt islands. The decrease of  $O_2$  reduction activity with decreasing Pt loading is expected, as the real surface area of Pt decreases. To differentiate the possible effect of Au substrate to Pt films of various thickness,



the specific activities (SA) of O<sub>2</sub> reduction for the electrodes at 0.55 V vs SCE were calculated by dividing the kinetic current at this potential ( $I_k$ ) to the real surface area of Pt ( $A_r$ ). The SA values are given in Table 1 (these correspond to the negative-going potential scan).

A slight decrease of SA in HClO<sub>4</sub> with decreasing Pt loading was observed, whereas in H<sub>2</sub>SO<sub>4</sub>, the SA value was almost independent of the Pt loading. Theoretical calculations [16,18] as well as experimental data [16–18] have indicated that Pt-Au bimetallic systems are less active catalysts for ORR than bulk Pt. The reactivity of bimetallic systems has been described previously using the d-band centre model [52]. In case of Pt monolayer on Au(111), the lattice mismatch induces the expansive strain in Pt and results in higher d-band centre energy that leads to a stronger binding of adsorbates to the surface [16,18]. Therefore, the Pt<sub>ML</sub>/Au(111) surface binds atomic O more strongly than bulk Pt and thereby facilitates the O–O bond breaking, but due to slow O or OH hydrogenation rates the surface O or OH coverage increases and blocks the centres of further O<sub>2</sub> adsorption, thereby inhibiting the ORR [16,18]. For a good ORR electrocatalyst, both O–O bond breaking and OH hydrogenation rates should be high. Theoretical calculations have shown that for the pseudomorphic Pt overlayers on Au, the d-band centre of the surface Pt atoms decreases as the number of the Pt layers increases and the Pt–Au interaction decreases. On the other hand, for the Pt-Au surface alloys the d-band centre of the surface Pt atoms decreases as the Pt concentration decreases [53]. In addition, for small supported Pt clusters a decrease in the d-band centre is expected due to the reduction of interatomic distances of the cluster surface, as modelled for Pd/Au system [54]. This implies that the adsorption energy of O and OH and also the catalytic activity for O<sub>2</sub> reduction is highly dependent on the morphology of the Pt/Au surface, not only on the Pt loading; but generally a slight decrease of the specific activity of Pt/Au catalysts is expected, as compared to pure Pt. In agreement with this, our results show that thick Pt films on Au are somewhat less active for O<sub>2</sub> reduction than Pt films on GC and bulk Pt [46]. The activity decreases with decreasing film thickness as the influence of Au substrate increases, the same effect has been observed for Pt coated Au nanoparticles [20]. Interestingly, the Pt films of low nominal thickness are slightly more active than the corresponding Pt/GC films [46]. A possible explanation might be the different morphology of Pt nanostructures on Au and GC. Pedersen et al have studied deposition of very small amounts of Pt to Au(111) substrate by vacuum-evaporation and found that the islands grow layer-by-layer, so that the first monolayer is nearly complete before second layer islands are nucleated [47]. Due to the roughness of the polycrystalline Au substrate used the situation might be somewhat different, but it is still expected that as compared to small hemispherical particles that we observed on carbon substrate [46], the Pt islands on Au are larger in diameter and more flat. Therefore, the particle size effect to O<sub>2</sub> reduction is small and the decrease of O<sub>2</sub> reduction activity as compared to thicker films is caused only by stronger influence of Au substrate that leads to

the more irreversible adsorption of surface oxygenated species. The more irreversible adsorption is evidenced by the shift of Pt oxide reduction peak to negative direction (Figure 2).

In  $\text{H}_2\text{SO}_4$ , the SA of Pt/Au electrodes is about 3–4 times lower than in  $\text{HClO}_4$  and appears to be independent of the Pt loading (Table 1). It has been well-established that the adsorbed (bi)sulfate ions are blocking  $\text{O}_2$  adsorption sites and thereby hindering the ORR [33,36–40]. At  $E = 0.55$  V vs. SCE where the SA is determined, the coverage of (bi)sulfate is near to its maximum and does not change considerably with potential. In  $\text{HClO}_4$ , on the contrary, the coverage of OH depends on the potential in the kinetic or mixed kinetic-diffusion controlled region where the SA is determined and varies for different Pt loadings as the influence of Au substrate changes. This is a possible explanation to the observation that the SA depends on the film thickness in  $\text{HClO}_4$  solution, but does not depend in  $\text{H}_2\text{SO}_4$ .

The development of new electrocatalysts for oxygen reduction is a challenging problem to improve the performance of fuel cells. Considerable research efforts have been undertaken to design nanostructured Pt catalysts on foreign metal supports. A promising approach is to use combinatorial screening methods in order to extract information about the electrocatalytic properties of these materials. The results obtained in the present work using Pt/Au catalysts provide a set of kinetic parameters to be compared with those of the other electrocatalysts for  $\text{O}_2$  reduction.

## CONCLUSIONS

The  $\text{O}_2$  reduction studies on Pt/Au electrodes revealed that the specific  $\text{O}_2$  reduction activity in  $\text{HClO}_4$  solution slightly decreases with decreasing Au film thickness. This effect was attributed to increasing influence of Au substrate that leads to stronger adsorption of surface oxygenated species and blocking of the centres for further  $\text{O}_2$  adsorption that hinders oxygen reduction. In  $\text{H}_2\text{SO}_4$  solution, in contrast, the  $\text{O}_2$  reduction activity was lower and almost independent on Pt film thickness, this is presumably due to the adsorption of site-blocking (bi)sulfate ions.

The Tafel slopes close to  $-120 \text{ mV dec}^{-1}$  in high current density range and  $-60 \text{ mV dec}^{-1}$  in low current density range were obtained for all electrodes in both solutions, indicating that the mechanism of  $\text{O}_2$  reduction is the same for Pt/Au electrodes as for bulk Pt. The analysis of the RRDE data showed that the main product of  $\text{O}_2$  reduction is water and only small amounts of  $\text{H}_2\text{O}_2$  (less than 5%) are produced.

## ACKNOWLEDGEMENTS

Support from the European Union Framework VI programme, NENA project Contract No. NMP3-CT-2004-505906, is gratefully acknowledged. This research was also supported by the Estonian Science Foundation (Grant No. 7546).

## REFERENCES

1. K. Kinoshita, *Electrochemical Oxygen Technology*, Wiley, New York, 1992.
2. R. Adzic, in: J. Lipkowski, P.N. Ross (Eds.), *Electrocatalysis*, Wiley-VCH, New York, 1998, pp. 197–242.
3. H.A. Gasteiger, S.S. Kocha, B. Sompalli, F.T. Wagner, *Appl. Catal. B* 56 (2005) 9–35.
4. O. Antoine, Y. Bultel, R. Durand, *J. Electroanal. Chem.* 499 (2001) 85–94.
5. S. Guerin, B.E. Hayden, C.E. Lee, C. Mormiche, J.R. Owen, A.E. Russell, B. Theobald, D. Thompsett, *J. Comb. Chem.* 6 (2004) 149–158.
6. K.J.J. Mayrhofer, B.B. Blizanac, M. Arenz, V.R. Stamenkovic, P.N. Ross, N.M. Markovic, *J. Phys. Chem. B* 109 (2005) 14433–14440.
7. H. Yano, J. Inukai, H. Uchida, M. Watanabe, P.K. Babu, T. Kobayashi, J.H. Chung, E. Oldfield, A. Wieckowski, *Phys. Chem. Chem. Phys.* 8 (2006) 4932–4939.
8. J. Zhang, F.H.B. Lima, M.H. Shao, K. Sasaki, J.X. Wang, J. Hanson, R.R. Adzic, *J. Phys. Chem. B* 109 (2005) 22701–22704.
9. J. Zhang, Y. Mo, M.B. Vukmirovic, R. Klie, K. Sasaki, R.R. Adzic, *J. Phys. Chem. B* 108 (2004) 10955–10964.
10. R.R. Adzic, J. Zhang, K. Sasaki, M.B. Vukmirovic, M. Shao, J.X. Wang, A.U. Nilekar, M. Mavrikakis, J.A. Valerio, F. Uribe, *Top. Catal.* 46 (2007) 249–262.
11. M. Van Brussel, G. Kokkinidis, I. Vandendael, C. Buess-Herman, *Electrochem. Commun.* 4 (2002) 808–813.
12. M. Van Brussel, G. Kokkinidis, A. Hubin, C. Buess-Herman, *Electrochim. Acta* 48 (2003) 3909–3919.
13. M. Desic, M.M. Popovic, M.D. Obradovic, L.M. Vracar, B.N. Grgur, *J. Serb. Chem. Soc.* 70 (2005) 231–242.
14. M.I. Awad, M.S. El Deab, T. Ohsaka, *J. Electrochem. Soc.* 154 (2007) B810–B816.
15. A. Kongkanand, S. Kuwabata, *J. Phys. Chem. B* 109 (2005) 23190–23195.
16. J.L. Zhang, M.B. Vukmirovic, Y. Xu, M. Mavrikakis, R.R. Adzic, *Angew. Chem. Int. Ed.* 44 (2005) 2132–2135.
17. K. Sasaki, Y. Mo, J.X. Wang, M. Balasubramanian, F. Uribe, J. McBreen, R.R. Adzic, *Electrochim. Acta* 48 (2003) 3841–3849.
18. A.U. Nilekar, Y. Xu, J. Zhang, M.B. Vukmirovic, K. Sasaki, R.R. Adzic, M. Mavrikakis, *Top. Catal.* 46 (2007) 276–284.
19. Y.D. Jin, Y. Shen, S.J. Dong, *J. Phys. Chem. B* 108 (2004) 8142–8147.
20. J.F. Zhai, M.H. Huang, S.J. Dong, *Electroanalysis* 19 (2007) 506–509.
21. B. El Roustom, G. Sine, G. Foti, Ch. Comninellis, *J. Appl. Electrochem.* 37 (2007) 1227–1236.
22. S. Strbac, R.R. Adzic, *J. Serb. Chem. Soc.* 57 (1992) 835–848.
23. S. Strbac, R.R. Adzic, *Electrochim. Acta* 41 (1996) 2903–2908.

24. A. Sarapuu, K. Tammeveski, T.T. Tenno, V. Sammelselg, K. Kontturi, D.J. Schiffrin, *Electrochem. Commun.* 3 (2001) 446–450.
25. A. Sarapuu, M. Nurmik, H. Mändar, A. Rosental, T. Laaksonen, K. Kontturi, D.J. Schiffrin, K. Tammeveski, *J. Electroanal. Chem.* 612 (2008) 78–86.
26. J. Luo, P.N. Njoki, Y. Lin, L. Wang, C.J. Zhong, *Electrochem. Commun.* 8 (2006) 581–587.
27. M.M. Maye, N.N. Kariuki, J. Luo, L. Han, P. Njoki, L.Y. Wang, Y. Lin, H.R. Naslund, C.J. Zhong, *Gold Bull.* 37 (2004) 217–223.
28. P. Hernandez-Fernandez, S. Rojas, P. Ocon, J.L.G. de la Fuente, J.S. Fabian, J. Sanza, M.A. Pena, F.J. Garcia-Garcia, P. Terreros, J.L.G. Fierro, *J. Phys. Chem. C* 111 (2007) 2913–2923.
29. J. Zhang, K. Sasaki, E. Sutter, R.R. Adzic, *Science* 315 (2007) 220–222.
30. J.K. Norskov, J. Rossmeisl, A. Logadottir, L. Lindqvist, J.R. Kitchin, T. Bligaard, H. Jonsson, *J. Phys. Chem. B* 108 (2004) 17886–17892.
31. M.P. Hyman, J.W. Medlin, *J. Phys. Chem. C* 111 (2007) 17052–17060.
32. N.M. Markovic, H.A. Gasteiger, B.N. Grgur, P.N. Ross, *J. Electroanal. Chem.* 467 (1999) 157–163.
33. J.X. Wang, N.M. Markovic, R.R. Adzic, *J. Phys. Chem. B* 108 (2004) 4127–4133.
34. M.B. Vukmirovic, J. Zhang, K. Sasaki, A.U. Nilekar, F. Uribe, M. Mavrikakis, R.R. Adzic, *Electrochim. Acta* 52 (2007) 2257–2263.
35. N.M. Markovic, P.N. Ross, *Surf. Sci. Rep.* 45 (2002) 117–229.
36. N.M. Markovic, H.A. Gasteiger, P.N. Ross, *J. Phys. Chem.* 99 (1995) 3411–3415.
37. N. Markovic, H. Gasteiger, P.N. Ross, *J. Electrochem. Soc.* 144 (1997) 1591–1597.
38. M.D. Macia, J.M. Campina, E. Herrero, J.M. Feliu, *J. Electroanal. Chem.* 564 (2004) 141–150.
39. A. Kuzume, E. Herrero, J.M. Feliu, *J. Electroanal. Chem.* 599 (2007) 333–343.
40. T.J. Schmidt, U.A. Paulus, H.A. Gasteiger, R.J. Behm, *J. Electroanal. Chem.* 508 (2001) 41–47.
41. J. Perez, H.M. Villullas, E.R. Gonzalez, *J. Electroanal. Chem.* 435 (1997) 179–187.
42. H. Angerstein-Kozłowska, in: E. Yeager, J. O'M. Bockris, B. E. Conway, S. Sarangapani (Eds.), *Comprehensive Treatise of Electrochemistry*, vol. 9, Plenum Press, New York, 1984, pp. 15–59.
43. A. Sun, J. Franc, D.D. Macdonald, *J. Electrochem. Soc.* 153 (2006) B260–B277.
44. R. Giorgi, P. Ascarelli, S. Turtu, V. Contini, *App. Surf. Sci.* 178 (2001) 149–155.
45. R. Borup, J. Meyers, B. Pivovar, Y.S. Kim, R. Mukundan, N. Garland, D. Myers, M. Wilson, F. Garzon, D. Wood, P. Zelenay, K. More, K. Stroh, T. Zawodzinski, J. Boncella, J.E. McGrath, M. Inaba, K. Miyatake, M. Hori, K. Ota, Z. Ogumi, S. Miyata, A. Nishikata, Z. Siroma, Y. Uchimoto, K. Yasuda, K.I. Kimijima, N. Iwashita, *Chem. Rev.* 107 (2007) 3904–3951.
46. A. Sarapuu, A. Kasikov, T. Laaksonen, K. Kontturi, K. Tammeveski, *Electrochim. Acta*, submitted.
47. M.O. Pedersen, S. Helveg, A. Ruban, I. Stensgaard, E. Laegsgaard, J.K. Norskov, F. Besenbacher, *Surf. Sci.* 426 (1999) 395–409.
48. R.R. Adzic, J. Wang, B.M. Ocko, *Electrochim. Acta* 40 (1995) 83–89.
49. D.R. Lide (Ed.), *CRC Handbook of Chemistry and Physics*, 82nd ed., CRC Press, Boca Raton, 2001.
50. U.A. Paulus, T.J. Schmidt, H.A. Gasteiger, R.J. Behm, *J. Electroanal. Chem.* 495 (2001) 134–145.

51. N.M. Markovic, R.R. Adzic, B.D. Cahan, E.B. Yeager, *J. Electroanal. Chem.* 377 (1994) 249–259.
52. J. Greeley, J.K. Norskov, *Surf. Sci.* 592 (2005) 104–111.
53. Y. Gohda, A. Gross, *J. Electroanal. Chem.* 607 (2007) 47–53.
54. A. Gross, *Top. Catal.* 37 (2006) 29–39.

**Table 1.** Kinetic parameters of oxygen reduction on Pt/Au electrodes in 0.1 M HClO<sub>4</sub> and 0.05 M H<sub>2</sub>SO<sub>4</sub> at  $\omega = 1900$  rpm.

Electrode	0.1 M HClO <sub>4</sub>				0.05 M H <sub>2</sub> SO <sub>4</sub>			
	Tafel slope (mV dec <sup>-1</sup> )	Tafel slope (mV dec <sup>-1</sup> )	$E_{1/2}$ (mV vs. SCE)	SA at 0.55 V (mA cm <sup>-2</sup> )	Tafel slope (mV dec <sup>-1</sup> )	Tafel slope (mV dec <sup>-1</sup> )	$E_{1/2}$ (mV vs. SCE)	SA at 0.55 V (mA cm <sup>-2</sup> )
	I region*	II region*			I region*	II region*		
0.25 nm Pt/Au	-65±4	-123±4	398±15	0.31±0.07	-74±5	-135±5	331±8	0.09±0.03
0.5 nm Pt/Au	-66±1	-123±9	429±9	0.34±0.03	-70±2	-132±1	362±4	0.11±0.01
1 nm Pt/Au	-66±5	-122±10	435±14	0.32±0.10	-65±1	-131±1	381±2	0.10±0.01
2 nm Pt/Au	-65±3	-120±15	451±10	0.33±0.02	-65±1	-125±2	397±5	0.10±0.01
5 nm Pt/Au	-62±1	-105±2	475±2	0.34±0.02	-67±3	-113±5	414±2	0.10±0.02
10 nm Pt/Au	-65±5	-116±12	483±9	0.41±0.08	-59±1	-125±1	416±3	0.08±0.01
20 nm Pt/Au	-62±1	-111±2	509±2	0.45±0.04	-64±3	-123±7	445±3	0.10±0.01
Bulk Pt	-63±3	-117±2	513±4	0.79±0.03	-69±7	-140±10	430±12	0.13±0.01

\* Region I corresponds to low current densities and Region II to high current densities.

## FIGURE

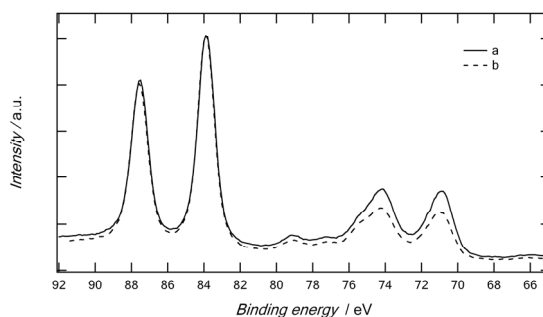


**Figure 1.** XPS spectra of 0.5 nm Pt films on Au substrate, normalized to Au peak height. (a) as-prepared sample, (b) electrochemically treated sample.

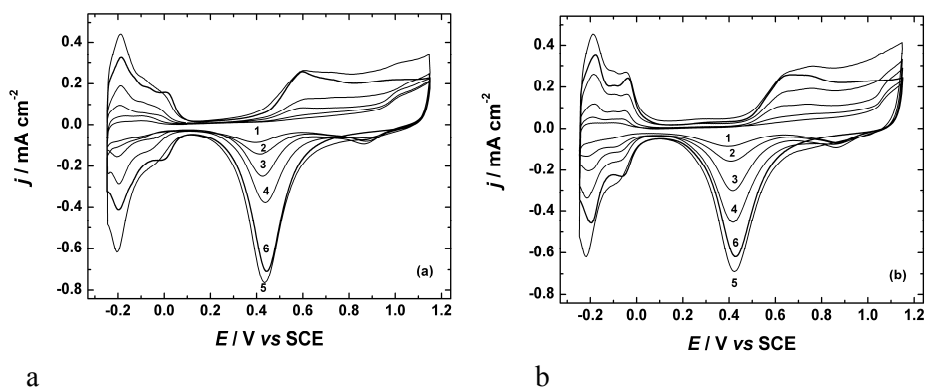


**Figure 2.** Cyclic voltammograms for Pt/Au electrodes (curves 1-5) and bulk Pt (curve 6) in (a) Ar-saturated 0.1 M  $\text{HClO}_4$  and (b) 0.05 M  $\text{H}_2\text{SO}_4$ . Pt film thickness: (1) 0.25; (2) 0.5; (3) 2; (4) 5 and (5) 20 nm.  $\nu = 100 \text{ mV s}^{-1}$ .

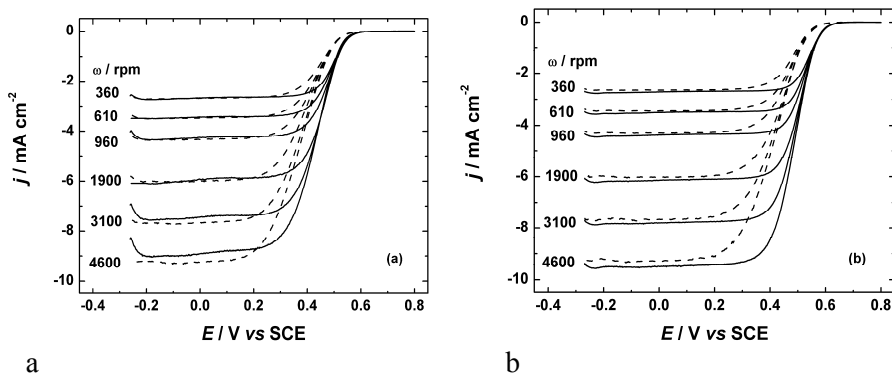


**Figure 3.** RDE voltammetry curves for  $\text{O}_2$  reduction on: (a) 2 nm Pt/Au and (b) 20 nm Pt/Au electrode in  $\text{O}_2$ -saturated 0.1 M  $\text{HClO}_4$  (solid lines) and 0.05 M  $\text{H}_2\text{SO}_4$  (dashed lines).  $\nu = 10 \text{ mV s}^{-1}$ .

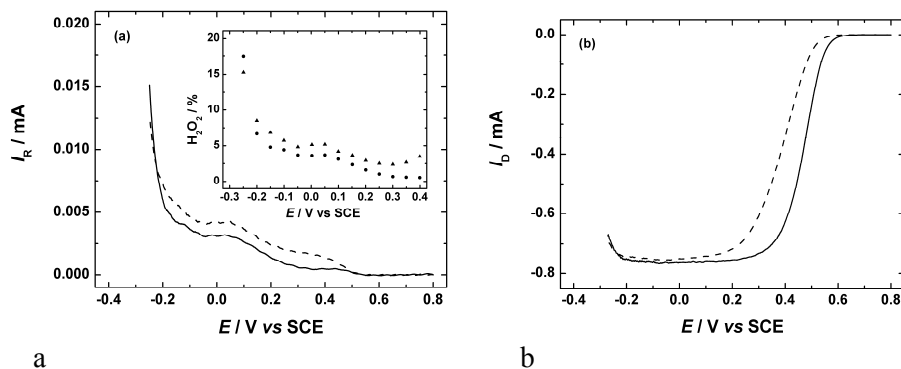


**Figure 4.** Oxygen reduction and hydrogen peroxide oxidation on a 0.5 nm Pt/Au disk-Pt ring electrode in  $\text{O}_2$ -saturated 0.1 M  $\text{HClO}_4$  (solid lines) and 0.05 M  $\text{H}_2\text{SO}_4$  (dashed lines). (a) ring and (b) disk currents.  $\nu = 10 \text{ mV s}^{-1}$ ,  $\omega = 960 \text{ rpm}$ ,  $E_R = 0.95 \text{ V}$ . The inset shows the potential dependence of the fraction of peroxide formation in 0.1 M  $\text{HClO}_4$  (●) and 0.05 M  $\text{H}_2\text{SO}_4$  (▲).



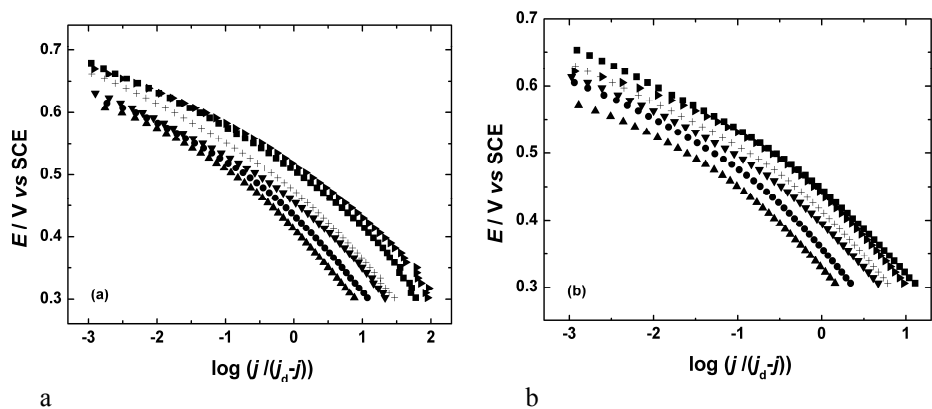


**Figure 5.** Mass-transfer corrected Tafel plots for  $\text{O}_2$  reduction on Pt/Au electrodes and bulk Pt in (a) 0.1 M  $\text{HClO}_4$  and (b) 0.05 M  $\text{H}_2\text{SO}_4$ .  $\omega = 1900$  rpm. Film thickness: 0.25 nm (▲); 0.5 nm (●); 2 nm (▼); 5 nm (+); 20 nm (■); bulk Pt (►).

# CURRICULUM VITAE

## Ave Sarapuu

Born: December 21, 1975, Viljandi, Estonia  
Citizenship: Estonian  
Marital status: married, 2 children  
Address: Pärna 29–60, 50604 Tartu, Estonia  
Phone: +372 7 375 277; +372 52 95430  
E-mail: [aves@chem.ut.ee](mailto:aves@chem.ut.ee)

## Education

2001–2007 PhD student, Department of Chemistry, University of Tartu, Estonia; doctoral advisor Kaido Tammeveski  
1998–2001 graduate student, Department of Chemistry, University of Tartu, Estonia, *M.Sc.* 2001  
1994–1998 undergraduate student, Department of Chemistry, University of Tartu, Estonia, *B.Sc.* 1998.  
1991–1994 Nõo Secondary Science School

## Professional employment

2005– University of Tartu, Institute of Chemistry, researcher  
2004–2005 University of Tartu, Institute of Physical Chemistry, extraordinary researcher  
1999–2001 University of Tartu, Institute of Physical Chemistry, chemist

### Main scientific publications

1. A. Sarapuu, K. Tammeveski, T.T. Tenno, V. Sammelselg, K. Kontturi, D.J. Schiffrin, Electrochemical reduction of oxygen on thin-film Au electrodes in acid solution, *Electrochemistry Communications* 3 (2001) 446–450.
2. A. Sarapuu, K. Vaik, D.J. Schiffrin, K. Tammeveski, Electrochemical reduction of oxygen on anthraquinone-modified glassy carbon electrodes in alkaline solution, *Journal of Electroanalytical Chemistry* 541 (2003) 23–29.
3. K. Vaik, A. Sarapuu, K. Tammeveski, F. Mirkhalaf, D.J. Schiffrin, Oxygen reduction on phenanthrenequinone-modified glassy carbon electrodes in 0.1 M KOH, *Journal of Electroanalytical Chemistry* 564 (2004) 159–166.
4. A. Sarapuu, K. Helstein, D.J. Schiffrin, K. Tammeveski, Kinetics of Oxygen Reduction on Quinone-Modified HOPG and BDD Electrodes in Alkaline Solution, *Electrochemical and Solid State Letters* 8 (2005) E30–E33.
5. A. Sarapuu, M. Nurmik, H. Mändar, A. Rosental, T. Laaksonen, K. Kontturi, D.J. Schiffrin, K. Tammeveski, Electrochemical reduction of oxygen on nanostructured gold electrodes, *Journal of Electroanalytical Chemistry* 612 (2008) 78–86.
6. A. Sarapuu, A. Kasikov, T. Laaksonen, K. Kontturi, K. Tammeveski, Electrochemical reduction of oxygen on thin-film Pt electrodes in acid solutions, *Electrochimica Acta* (2008, in press) (doi:10.1016/j.electacta.2008.04.003).
7. A. Sarapuu, A. Kasikov, L. Matisen, K. Tammeveski, Electroreduction of oxygen on gold-supported thin Pt films in acid solutions, *Journal of Electroanalytical Chemistry*, submitted (JELECHEM-D-08-00120)

# ELULOOKIRJELDUS

## Ave Sarapuu

Sündinud: 21.12.1975, Viljandi  
Kodakondsus: Eesti  
Perekonnaseis: abielus, 2 last  
Aadress: 50604 Tartu, Pärna 29–60  
Telefon: +372 7 375 277; +372 52 95430  
E-mail: [aves@chem.ut.ee](mailto:aves@chem.ut.ee)

## Haridus

2001–2007 Doktoriõpe TÜ keemiaosakonna füüsikalise keemia instituudi juures, juhendaja Kaido Tammeveski  
1998–2001 Magistriõpe TÜ keemiaosakonna füüsikalise keemia instituudi juures, *M.Sc.* 2001.  
1994–1998 Bakalaureuseõpe TÜ keemiaosakonnas, *B.Sc.* 1998.  
1991–1994 Nõo Reaalgümnaasium

## Teenistuskäik

2005– Tartu Ülikool, Keemia instituut, kolloid- ja keskkonnakeemia teadur  
2004–2005 Tartu Ülikool, Füüsikalise keemia instituut, erakorraline teadur  
1999–2001 Tartu Ülikool, Füüsikalise keemia instituut, keemik

### Tähtsamad teaduspublikatsioonid

1. A. Sarapuu, K. Tammeveski, T.T. Tenno, V. Sammelselg, K. Kontturi, D.J. Schiffrin, Electrochemical reduction of oxygen on thin-film Au electrodes in acid solution, *Electrochemistry Communications* 3 (2001) 446–450.
2. A. Sarapuu, K. Vaik, D.J. Schiffrin, K. Tammeveski, Electrochemical reduction of oxygen on anthraquinone-modified glassy carbon electrodes in alkaline solution, *Journal of Electroanalytical Chemistry* 541 (2003) 23–29.
3. K. Vaik, A. Sarapuu, K. Tammeveski, F. Mirkhalaf, D.J. Schiffrin, Oxygen reduction on phenanthrenequinone-modified glassy carbon electrodes in 0.1 M KOH, *Journal of Electroanalytical Chemistry* 564 (2004) 159–166.
4. A. Sarapuu, K. Helstein, D.J. Schiffrin, K. Tammeveski, Kinetics of Oxygen Reduction on Quinone-Modified HOPG and BDD Electrodes in Alkaline Solution, *Electrochemical and Solid State Letters* 8 (2005) E30–E33.
5. A. Sarapuu, M. Nurmik, H. Mändar, A. Rosental, T. Laaksonen, K. Kontturi, D.J. Schiffrin, K. Tammeveski, Electrochemical reduction of oxygen on nanostructured gold electrodes, *Journal of Electroanalytical Chemistry* 612 (2008) 78–86.
6. A. Sarapuu, A. Kasikov, T. Laaksonen, K. Kontturi, K. Tammeveski, Electrochemical reduction of oxygen on thin-film Pt electrodes in acid solutions, *Electrochimica Acta* (2008, in press) (doi:10.1016/j.electacta.2008.04.003).
7. A. Sarapuu, A. Kasikov, L. Matisen, K. Tammeveski, Electroreduction of oxygen on gold-supported thin Pt films in acid solutions, *Journal of Electroanalytical Chemistry*, submitted (JELECHEM-D-08-00120)

## DISSERTATIONES CHIMICAE UNIVERSITATIS TARTUENSIS

1. **Toomas Tamm.** Quantum-chemical simulation of solvent effects. Tartu, 1993, 110 p.
2. **Peeter Burk.** Theoretical study of gas-phase acid-base equilibria. Tartu, 1994, 96 p.
3. **Victor Lobanov.** Quantitative structure-property relationships in large descriptor spaces. Tartu, 1995, 135 p.
4. **Vahur Mäemets.** The  $^{17}\text{O}$  and  $^1\text{H}$  nuclear magnetic resonance study of  $\text{H}_2\text{O}$  in individual solvents and its charged clusters in aqueous solutions of electrolytes. Tartu, 1997, 140 p.
5. **Andrus Metsala.** Microcanonical rate constant in nonequilibrium distribution of vibrational energy and in restricted intramolecular vibrational energy redistribution on the basis of Slater's theory of unimolecular reactions. Tartu, 1997, 150 p.
6. **Uko Maran.** Quantum-mechanical study of potential energy surfaces in different environments. Tartu, 1997, 137 p.
7. **Alar Jänes.** Adsorption of organic compounds on antimony, bismuth and cadmium electrodes. Tartu, 1998, 219 p.
8. **Kaido Tammeveski.** Oxygen electroreduction on thin platinum films and the electrochemical detection of superoxide anion. Tartu, 1998, 139 p.
9. **Ivo Leito.** Studies of Brønsted acid-base equilibria in water and non-aqueous media. Tartu, 1998, 101 p.
10. **Jaak Leis.** Conformational dynamics and equilibria in amides. Tartu, 1998, 131 p.
11. **Toonika Rinken.** The modelling of amperometric biosensors based on oxidoreductases. Tartu, 2000, 108 p.
12. **Dmitri Panov.** Partially solvated Grignard reagents. Tartu, 2000, 64 p.
13. **Kaja Orupõld.** Treatment and analysis of phenolic wastewater with microorganisms. Tartu, 2000, 123 p.
14. **Jüri Ivask.** Ion Chromatographic determination of major anions and cations in polar ice core. Tartu, 2000, 85 p.
15. **Lauri Vares.** Stereoselective Synthesis of Tetrahydrofuran and Tetrahydropyran Derivatives by Use of Asymmetric Horner-Wadsworth-Emmons and Ring Closure Reactions. Tartu, 2000, 184 p.
16. **Martin Lepiku.** Kinetic aspects of dopamine  $\text{D}_2$  receptor interactions with specific ligands. Tartu, 2000, 81 p.
17. **Katrin Sak.** Some aspects of ligand specificity of  $\text{P2Y}$  receptors. Tartu, 2000, 106 p.
18. **Vello Pällin.** The role of solvation in the formation of iotsitch complexes. Tartu, 2001, 95 p.

19. **Katrin Kollist.** Interactions between polycyclic aromatic compounds and humic substances. Tartu, 2001, 93 p.
20. **Ivar Koppel.** Quantum chemical study of acidity of strong and superstrong Brønsted acids. Tartu, 2001, 104 p.
21. **Viljar Pihl.** The study of the substituent and solvent effects on the acidity of OH and CH acids. Tartu, 2001, 132 p.
22. **Natalia Palm.** Specification of the minimum, sufficient and significant set of descriptors for general description of solvent effects. Tartu, 2001, 134 p.
23. **Sulev Sild.** QSPR/QSAR approaches for complex molecular systems. Tartu, 2001, 134 p.
24. **Ruslan Petrukhin.** Industrial applications of the quantitative structure-property relationships. Tartu, 2001, 162 p.
25. **Boris V. Rogovoy.** Synthesis of (benzotriazolyl)carboximidamides and their application in relations with *N*- and *S*-nucleophiles. Tartu, 2002, 84 p.
26. **Koit Herodes.** Solvent effects on UV-vis absorption spectra of some solvatochromic substances in binary solvent mixtures: the preferential solvation model. Tartu, 2002, 102 p.
27. **Anti Perkson.** Synthesis and characterisation of nanostructured carbon. Tartu, 2002, 152 p.
28. **Ivari Kaljurand.** Self-consistent acidity scales of neutral and cationic Brønsted acids in acetonitrile and tetrahydrofuran. Tartu, 2003, 108 p.
29. **Karmen Lust.** Adsorption of anions on bismuth single crystal electrodes. Tartu, 2003, 128 p.
30. **Mare Piirsalu.** Substituent, temperature and solvent effects on the alkaline hydrolysis of substituted phenyl and alkyl esters of benzoic acid. Tartu, 2003, 156 p.
31. **Meeri Sassian.** Reactions of partially solvated Grignard reagents. Tartu, 2003, 78 p.
32. **Tarmo Tamm.** Quantum chemical modelling of polypyrrole. Tartu, 2003. 100 p.
33. **Erik Teinemaa.** The environmental fate of the particulate matter and organic pollutants from an oil shale power plant. Tartu, 2003. 102 p.
34. **Jaana Tammiku-Taul.** Quantum chemical study of the properties of Grignard reagents. Tartu, 2003. 120 p.
35. **Andre Lomaka.** Biomedical applications of predictive computational chemistry. Tartu, 2003. 132 p.
36. **Kostyantyn Kirichenko.** Benzotriazole — Mediated Carbon–Carbon Bond Formation. Tartu, 2003. 132 p.
37. **Gunnar Nurk.** Adsorption kinetics of some organic compounds on bismuth single crystal electrodes. Tartu, 2003, 170 p.
38. **Mati Arulepp.** Electrochemical characteristics of porous carbon materials and electrical double layer capacitors. Tartu, 2003, 196 p.

39. **Dan Cornel Fara.** QSPR modeling of complexation and distribution of organic compounds. Tartu, 2004, 126 p.
40. **Riina Mahlapuu.** Signalling of galanin and amyloid precursor protein through adenylate cyclase. Tartu, 2004, 124 p.
41. **Mihkel Kerikmäe.** Some luminescent materials for dosimetric applications and physical research. Tartu, 2004, 143 p.
42. **Jaanus Kruusma.** Determination of some important trace metal ions in human blood. Tartu, 2004, 115 p.
43. **Urmas Johanson.** Investigations of the electrochemical properties of polypyrrole modified electrodes. Tartu, 2004, 91 p.
44. **Kaido Sillar.** Computational study of the acid sites in zeolite ZSM-5. Tartu, 2004, 80 p.
45. **Aldo Oras.** Kinetic aspects of dATP $\alpha$ S interaction with P2Y<sub>1</sub> receptor. Tartu, 2004, 75 p.
46. **Erik Mölder.** Measurement of the oxygen mass transfer through the air-water interface. Tartu, 2005, 73 p.
47. **Thomas Thomberg.** The kinetics of electroreduction of peroxodisulfate anion on cadmium (0001) single crystal electrode. Tartu, 2005, 95 p.
48. **Olavi Loog.** Aspects of condensations of carbonyl compounds and their imine analogues. Tartu, 2005, 83 p.
49. **Siim Salmar.** Effect of ultrasound on ester hydrolysis in aqueous ethanol. Tartu, 2006, 73 p.
50. **Ain Uustare.** Modulation of signal transduction of heptahelical receptors by other receptors and G proteins. Tartu, 2006, 121 p.
51. **Sergei Yurchenko.** Determination of some carcinogenic contaminants in food. Tartu, 2006, 143 p.
52. **Kaido Tamm.** QSPR modeling of some properties of organic compounds. Tartu, 2006, 67 p.
53. **Olga Tšubrik.** New methods in the synthesis of multisubstituted hydrazines. Tartu, 2006, 183 p.
54. **Lilli Sooväli.** Spectrophotometric measurements and their uncertainty in chemical analysis and dissociation constant measurements. Tartu, 2006, 125 p.
55. **Eve Koort.** Uncertainty estimation of potentiometrically measured pH and pK<sub>a</sub> values. Tartu, 2006, 139 p.
56. **Sergei Kopanchuk.** Regulation of ligand binding to melanocortin receptor subtypes. Tartu, 2006, 119 p.
57. **Silvar Kallip.** Surface structure of some bismuth and antimony single crystal electrodes. Tartu, 2006, 107 p.
58. **Kristjan Saal.** Surface silanization and its application in biomolecule coupling. Tartu, 2006, 77 p.
59. **Tanel Tätte.** High viscosity Sn(OBu)<sub>4</sub> oligomeric concentrates and their applications in technology. Tartu, 2006, 91 p.



60. **Dimitar Atanasov Dobchev.** Robust QSAR methods for the prediction of properties from molecular structure. Tartu, 2006, 118 p.
61. **Hannes Hagu.** Impact of ultrasound on hydrophobic interactions in solutions. Tartu, 2007, 81 p.
62. **Rutha Jäger.** Electroreduction of peroxodisulfate anion on bismuth electrodes. Tartu, 2007, 142 p.
63. **Kaido Viht.** Immobilizable bisubstrate-analogue inhibitors of basophilic protein kinases: development and application in biosensors. Tartu, 2007, 88 p.
64. **Eva-Ingrid Rõõm.** Acid-base equilibria in nonpolar media. Tartu, 2007, 156 p.
65. **Sven Tamp.** DFT study of the cesium cation containing complexes relevant to the cesium cation binding by the humic acids. Tartu, 2007, 102 p.
66. **Jaak Nerut.** Electroreduction of hexacyanoferrate(III) anion on Cadmium (0001) single crystal electrode. Tartu, 2007, 180 p.
67. **Lauri Jalukse.** Measurement uncertainty estimation in amperometric dissolved oxygen concentration measurement. Tartu, 2007, 112 p.
68. **Aime Lust.** Charge state of dopants and ordered clusters formation in  $\text{CaF}_2\text{:Mn}$  and  $\text{CaF}_2\text{:Eu}$  luminophors. Tartu, 2007, 100 p.
69. **Iiris Kahn.** Quantitative Structure-Activity Relationships of environmentally relevant properties. Tartu, 2007, 98 p.
70. **Mari Reinik.** Nitrates, nitrites, N-nitrosamines and polycyclic aromatic hydrocarbons in food: analytical methods, occurrence and dietary intake. Tartu, 2007, 172 p.
71. **Heili Kasuk.** Thermodynamic parameters and adsorption kinetics of organic compounds forming the compact adsorption layer at Bi single crystal electrodes. Tartu, 2007, 212 p.
72. **Erki Enkvist.** Synthesis of adenosine-peptide conjugates for biological applications. Tartu, 2007, 114 p.
73. **Svetoslav Hristov Slavov.** Biomedical applications of the QSAR approach. Tartu, 2007, 146 p.
74. **Eneli Härk.** Electroreduction of complex cations on electrochemically polished Bi(*hkl*) single crystal electrodes. Tartu, 2008, 158 p.
75. **Priit Möller.** Electrochemical characteristics of some cathodes for medium temperature solid oxide fuel cells, synthesized by solid state reaction technique. Tartu, 2008, 90 p.
76. **Signe Viggor.** Impact of biochemical parameters of genetically different pseudomonads at the degradation of phenolic compounds. Tartu, 2008, 122 p.